POLITECNICO DI TORINO

Master of Science Degree in Aerospace Engineering

Academic Year 2023/2024

Master degree's thesis

Methodology and tool to support the conceptual design of a reusable HTHL TSTO vehicle and cost assessment

Supervisors:

Dott.ssa Roberta Fusaro

Prof.ssa Nicole Viola

Candidate:

Luca Pasqualin

December 2024

Abstract

A great deal of well-established and cutting-edge practices and reliable tools have been developed over the last decades to support hypersonic aircraft conceptual and preliminary design.
Among these, the Hypersonic Convergence sizing approach for transonic to hypersonic vehicle applications first developed at formerly McDonnell Aircraft Company between 1970 and 1990, represents one of the most common in the field. An innovative approach to a such consolidated sizing methodology with relevant modifications is presented as main topic of this thesis.
In particular, the integration of the Multiple Matching Chart Analysis tool, implemented in the last years by the Aerospace Engineering Department of Politecnico di Torino, to the classical procedure widely described in literature enables an important refinement of the design point searching algorithm, when the objective is to size SSTO (Single-Stage-To-Orbit) or TSTO (Two-Stage-To-Orbit) HTHL (Horizontal Take-off and Landing) vehicles. The modularity, through the utilization of multiple functions, and a more user-friendly customization of the tool with respect to previous works are two of the main achievements illustrated in the thesis.
Moreover, considerable insight about potential improvements of the methodology as well as new and derived formulas concerning the Kuchemann correlation for subsonic carriers, the concept of effective efficiency in Breguet's formula and the correction of the mass ratio for first stages subjected to separation events are the major aim of this work.
A statistical analysis about both existing and aborted TSTO HTHL projects and concepts is preliminarily conducted to depict the framework and the field of applicability of the methodology.
Eventually, the results of the validation of the updated methodology and tool and a preliminary cost assessment based on the economical TransCost Model are reported, using as case study the Sänger II vehicle configuration, a TSTO HTHL design concept elaborated in Germany during the 80s.

Acknowledgments

Here is where the story comes to an end. As a matter of fact, this is the beginning of the end, but I've realized it is a lie. There's something special about any 24-year ordinary student on the verge of getting the final degree: this is the end of the beginning instead.

When I started seeking a thesis topic in March, I was quite sure I would have ended up to carry out an internship in a well-known aerospace company. Apparently, I was wrong, because for different reasons, each time I had an interview, I did not feel completely satisfied, either by the topic itself, or by organizational aspects and future perspectives. After several changes of mind, I opted for contacting Dott.ssa Fusaro, since I was immediately interested in her topic of research: hypersonic vehicles design. Two years ago I thought space was my field, then in Erasmus I realized aeronautics was actually my vocation. In the end, according to a Hegel-like decision logic, my *synthesis* has been a blend of the two worlds, overcoming both *thesis* (space) and *anti-thesis* (aeronautics).
It took me three months of search to run into the hypersonic field, simply because I was trying to find an optimized solution in a too restricted domain, and that was always on the border: as soon as I widened my view, by enlarging the domain, I discovered the thing I was looking for and I found a maximum, exactly as for math functions. By rephrasing the famous British writer Simon Sinek, I think this topic is capable of fulfilling my *why*, rather than simply a *what*, and that makes it fitting. I don't know if I will work on that again in the future, but of one thing I am sure: this is the type of comprehensive and multidisciplinary topic I have always wanted to end with my academic experience at Politecnico.

I want to dedicate this work to my parents first, Roberta and Stefano, because they have always supported me, financially and emotively, and celebrated every success I achieved as if it was the first one. They represented my certainty, my safe harbour, no matter what happened.
I want to thank my closest friends, with who I spent most of my leisure time and tackled the stress of the most challenging moments over these last five years.
I want to thank all the people I met, even randomly and even for a few instants, during my university career, both at Politecnico and at Carlos III de Madrid, who contributed, in different ways and entity, to make me the person I am now.

I want to thank Alta Scuola Politecnica, because I learnt useful knowledge about soft skills and it gave me the opportunity to meet incredible people to work with at project MOSS.
I want to thank PACE Aerospace, because after winning the Future Innovators Award 2023 for the best preliminary aircraft design project with my trusted university colleagues, it contributed to pave my way to the design field.
I want to thank my thesis supervisors Dott.ssa Roberta Fusaro and Prof.ssa Nicole Viola for the support provided during the last recent six months and the entire Department of Aerospace Engineering DIMEAS at Politecnico di Torino.
I want to thank myself, for being here, for never giving up, for having lived any moment of this journey with passion and dedication, for being consistent despite all the obstacles.
And finally, I would like to dedicate this entire work to a person who has always loved me, unconditionally, since I was born and until her last breath: my grandmother, Lia.
"May you now live on the brightest star of the sky and drive me in life from now on. Maybe, on board of a hypersonic vehicle, I will visit you from time to time".

Italian version

Non sembra vero ma, guardando fuori dal finestrino, mi rendo conto che sono giunto al capolinea di questo incredibile viaggio. Questo è l'inizio della conclusione ma ho recentemente scoperto essere una menzogna. C'è qualcosa di speciale nella vita di un qualunque studente di 24 anni sul punto di laurearsi dopo 5 anni di studio: questa è invece la conclusione dell'inizio.

Quando a marzo 2024 ho cominciato a cercare un argomento di tesi, credevo che sarei finito a svolgere un tirocinio in un'azienda di carattere aeronautico e questo era il mio obiettivo. Per diverse ragioni, poi, legate a volte alla tipologia di mansione, altre a ostacoli di natura organizzativa o associate a prospettive di lavoro futuro lontane dalla mia persona, mi sono trovato a dover ammettere di aver sbagliato nella ricerca. Dopo aver cambiato idea molte volte, mi sono imbattuto nel progetto di ricerca della Dott.ssa Fusaro, il quale ha subito catturato la mia attenzione: il design di veicoli ipersonici. Due anni fa ritenevo che lo spazio fosse il mio mondo, poi grazie all'esperienza Erasmus a Madrid mi sono reso conto che l'aeronautica fosse al contrario la mia vocazione. Alla fine, così come Hegel ci ricorda, la mia *sintesi* sarà data dalla combinazione della *tesi*, ossia lo spazio, e dell'*antitesi*, ovvero l'aeronautica, e ciò mi rende molto fiero. Mi ci sono voluti tre mesi di ricerca per imbattermi in questa tipologia di campo su cui sviluppare la tesi, ossia l'aeronautica ipersonica, semplicemente perchè mi ostinavo a cercare la soluzione ottimale in un dominio troppo ristretto, la quale naturalmente andava a giacere sempre sul bordo, ovunque guardassi. Non appena ho allargato i miei orizzonti, espandendo il dominio come per una funzione matematica, ho compreso di aver trovato il massimo

che cercavo. Parafrasando il famoso scrittore britannico Simon Sinek, credo che questo argomento di tesi soddisfi non solo il mio *"che cosa"*, ma anche il mio *"perchè"*, come coronamento di un viaggio di conoscenza. Non so se in futuro lavorerò in quest'ambito, tuttavia di una cosa sono certo: questo è il tipo di argomento, nella sua eterogeneità e completezza, con cui ho sempre desiderato concludere il mio percorso accademico al Politecnico di Torino.

Vorrei dedicare questo lavoro ai miei genitori *in primis*, Roberta e Stefano, per il supporto emotivo ed economico che mi hanno dato in questi cinque anni, festeggiando con me ogni successo, anche piccolo, come se fosse il primo. Hanno rappresentato la mia sicurezza, il mio porto sicuro, nonostante tutto il resto intorno.
Vorrei ringraziare le persone e gli amici più stretti, che mi hanno aiutato a combattere i momenti più stressanti con una risata o una semplice chiacchierata, mantenendo vivo l'animo bambino dentro me.
Vorrei ringraziare tutte le persone che ho incontrato durante la mia carriera universitaria, dai colleghi a coloro con cui ho interagito per caso o anche solo per pochi minuti, sia al Politecnico di Torino che alla Universidad Carlos III de Madrid, contribuendo a rendermi, chi più, chi meno, la persona che sono ora.
Vorrei ringraziare l'Alta Scuola Politecnica, perchè mi ha permesso di apprendere concetti illuminanti in tema di soft skills e mi ha dato l'opportunità di incontrare persone meravigliose con cui lavorare al progetto MOSS.
Vorrei ringraziare PACE Aerospace, perchè la vittoria del contest Future Innovators Awards 2023 a Berlino con un gruppo di fidati colleghi universitari ha indirizzato la mia strada verso il mondo dell'*aircraft preliminary design.*
Vorrei ringraziare le mie relatrici di tesi, la Dott.ssa Roberta Fusaro e la Prof.ssa Nicole Viola, per il supporto fornitomi durante gli ultimi sei mesi e tutto il Dipartimento di Ingegneria Aerospaziale del Politecnico, il DIMEAS.
Vorrei ringraziare me stesso, per essere arrivato qui, per non aver mai mollato, per aver vissuto ogni momento di questo viaggio con passione e dedizione, per essere stato costante e aver perseverato, nonostante gli innumerevoli ostacoli. E in ultimo, vorrei dedicare questo lavoro a una persona, che mi ha voluto bene, incondizionatamente, sin dal giorno in cui sono nato e fino al suo ultimo respiro: mia nonna, Lia. *"Spero che tu possa vivere sulla stella più luminosa del cielo profondo e guidarmi d'ora in avanti nella vita. Forse un giorno, a bordo di un aereo ipersonico, verrò a trovarti".*

Contents

List of Figures

List of Tables

List of acronyms and main symbols

SSTO Single-Stage-To-Orbit

TSTO Two-Stage-To-Orbit

HTHL Horizontal Takeoff and Horizontal Landing

VLO Vertical Lift-off

CAV Cruise and Acceleration Vehicle

HST High-Speed Transportation

EHTV (European Hypersonic Transport vehicle

RLV Reusable Launch Vehicle

SABRE Synergetic Air Breathing Rocket Engine

RBCC Rocket Based Combined cycle

TBCC Turbine Based Combined Cycle

LOX Liquid Oxygen

SFC Specific Fuel Consumption

NASA National Aeronautics and Space Administration

ICI Industrial Capability Index

ELVs Expendable Launch Vehicles

TC TransCost Model

CERs Cost Estimated Relations

RDTE Research, Development, Test and Evaluation

TFU Theoretical First Unit

DOC Direct Operations Cost

RSC Refurbishment and Spares Cost

IOC Indirect Operations Cost

WYr Work-Year

LCC Life Cycle Cost

UHTCs Ultra-High Temperature Ceramics

LEO Low Earth Orbit

MC Matching Chart

MMCs Multiple Matching Charts

MCA Matching Chart Analysis

T/W Thrust-to-Weight Ratio

W/S Wing Loading

$MTOM$ Maximum Takeoff Mass

m_s Structural Mass (for statistical analysis)

m_{dry} Structural Mass (for economical computations)

m_{ppl} Propellant Mass

m_{pay} Payload Mass

m_{OE} Operative Empty Mass

m_{TO} Takeoff Mass

m_G Gross Mass

m_{tot} Total Mass (for design purposes)

E_{eff} Effective Efficiency

MF Margin Factor

AR Aspect Ratio

TOP Takeoff Parameter

OEI One Engine Inoperative

Chapter 1

Introduction on hypersonic vehicles

1.1 Main challenges of hypersonic flight

The term "hypersonic flight" refers to a flight regime typically not encountered by most of aircraft. It describes speed conditions over Mach 5-7, only reached by suitably designed vehicles. It is noteworthy to stress that a tangible hypersonic speed barrier does not exist, thus the transition generally occurs within that Mach range, when high-temperature phenomena begin getting impactful. Hypersonic vehicles fall into three main categories:

- Spacecraft, including launchers, reentry capsules, probes...;
- Technological demonstrators, consisting mainly of cruise and acceleration vehicles (CAVs), used to prove the feasibility as well as the reliability of a new technology;
- Military aircraft, developed to enhance combat or recognition performances.

Whatever is the purpose, a hypersonic vehicle demands for stringent requirements to be fulfilled, since it operates in extreme conditions. This is true especially for spacecraft, due to the fact they experience all flight and flow conditions, from subsonic to hypersonic, from continuum regime to vacuum. As a matter of fact, in design phases, lots of aspects need to be considered and the most relevant are illustrated hereafter.

- **Viscous interaction**: it is defined as the mutual interaction occurring between the boundary layer in contact with the body subjected to a stream and the outer inviscid flow. In the boundary layer, the viscous effect becomes preponderant. One of the most dangerous types of viscous interactions is called shock wave/boundary layer interaction and may occur in various parts of a hypersonic vehicle, such as at wings or stabilizers, at a control surface or at the cowl lip of an inlet. Where a strong shock wave encounters the boundary layer, localized accelerated flow can be found in proximity of the wall, causing localized intense pressure and heat flux peaks, potentially destructive. Therefore, this kind of interaction has to be avoided, by studying a suitable design preliminarily. In Figure 1.1, a representation of shock wave/ boundary layer interaction is illustrated.

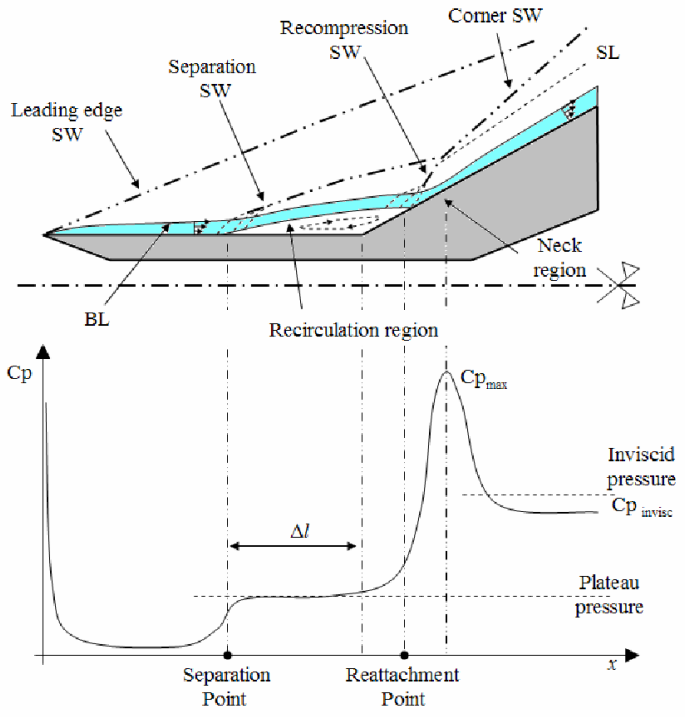

Figure 1.1: Schematic view of shock wave/boundary layer interaction. It is clear how the area in which the interaction is stronger is characterized by a peak in pressure as well.

- **Thermochemical effects**: if the local temperature reaches and exceeds 2000 K, and this is the case, chemical dissociation reactions of O_2, N_2 and NO begin covering a crucial role, being the most numerous species present in air. In fact, their interaction with the surface of the vehicle may be either negligible or consistent, depending on the type of wall, namely catalytic, non-catalytic and partially catalytic and the chemical status into the boundary layer, that is in equilibrium or non-equilibrium. When the boundary layer is in chemical equilibrium, recombination of atoms occurs before they can impact on the wall and, being the reaction exothermic, heat is released, causing the local temperature and consequently the heat flux towards the wall to increase. On the other hand, when the boundary layer is in non-chemical equilibrium, atomic dissociated species can reach the wall, where they totally recombine if the wall is fully catalytic, they partially recombine if it is partially catalytic or they bounce without recombination if it is non-catalytic [1]. According to the case, peaks of heat exchange might be reached: being the recombination process exothermic, the fully catalytic case is the most stressed.

- **Heating of surface**: it is one of the most important quantities to assess, since it affects the design and manufacture of the thermal protection system, crucial for reentry vehicles but still important for cruise and accelerating vehicles. Heating is given by the summation of two main contributions, namely the convective heating,

coming from the particles collision with the structure and the radiative heating, due to photons emission caused by de-excitation of energetic particles. The convective heating at surface is composed by a conduction component, driven by temperature gradient ∇T and a diffusive component, driven by mole fraction gradient ∇x_i. The stagnation point on the nose of a hypersonic vehicle typically shows the most severe temperature conditions. It was demonstrated that by applying the newtonian theory to the Fay-Riddel equations, in the stagnation point the following proportionality is valid:

$$q_w \propto \sqrt{\left(\frac{dV_e}{dx}\right)_s} \propto \frac{1}{\sqrt{R}} \tag{1.1}$$

where q_w stands for the convective heating at wall, $\left(\frac{dV_e}{dx}\right)_s$ is the flow velocity gradient outside the boundary layer at stagnation point along a curvilinear axis on the nose profile and R is the curvature radius of the nose [1]. This reveals why a design feature of reentry vehicles is normally having low curvatures: the higher the radius, the lower the thermal stress. On the other hand, the radiative heating presents an opposite behaviour, being $q_r \propto R$. This results in the necessity of defining the best trade-off to minimize both the convective and the radiative heat fluxes, being dominated by opposing laws in relation to the blunted nose curvature.

As regards atmospheric vehicles, like military fighters or technological demonstrators, the nose is typically sharp, with hugely high curvatures, and their shape is slender. These opposite design features with respect to reentry vehicles are due to their different purpose: a reentry vehicle must decelerate while accessing the atmosphere from the outer space, thus an increase in drag is pursued; on the other hand, CAVs require high performances, thus low angles of attack and thinner profiles are mandatory to reduce the wave drag (Figure 1.2 and Figure 1.3).

High temperature resistant materials are employed to cover the more stressed portions of the frame.

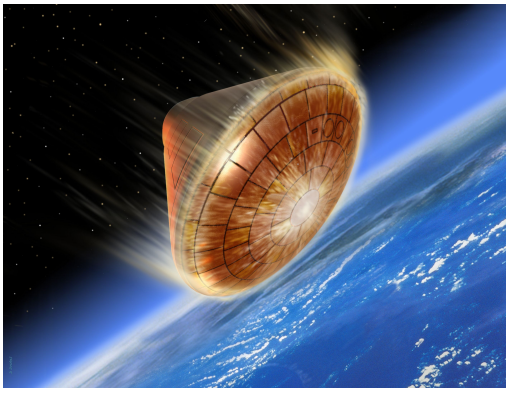

Figure 1.2: Example of capsule for reentry.

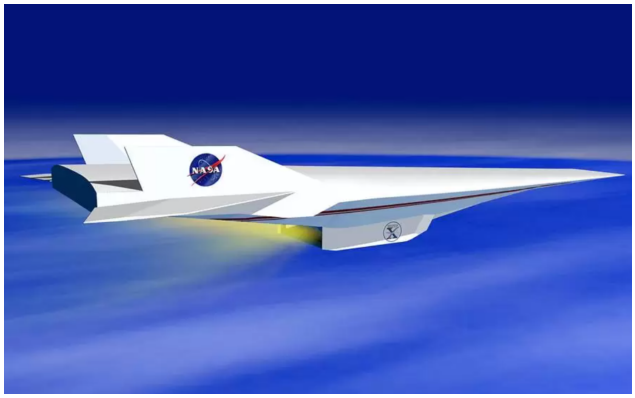

Figure 1.3: Example of cruise and acceleration vehicle.

- **Adequate propulsion systems**: the two main classes of propulsion configuration systems are vehicle-integrated rocket propulsion and vehicle-integrated airbreathing propulsion. Moreover, synergical hybrid solutions also exist, in order to overcome the issues of both and converge to an optimized multi-environment architecture, such as the SABRE engine (Synergetic Airbreathing and Rocket Engine). The choice of the propulsion system is dictated by the requirements fulfillment and can affect the entire vehicle concept. For example, an aircraft that is a hypersonic glider exits the atmosphere on either rocket boosters or a first stage of a two-stage-to-orbit aircraft. It is crucial that the vehicle is controlled in flight such that its attitude and direction are within tight limits set by aerothermodynamics, thus the thrust vectoring is asked to ensure a high level of reliability.
  An aircraft that uses airbreathing propulsion needs to capture atmospheric air to generate thrust by chemical combustion during the ascent phase, thus it requires an integrated propulsion system that produces more thrust than drag, in addition to also producing lift. For the air-breathing propulsion system to function efficiently, the dynamic pressure and air mass flow per unit area must be higher than in a rocket exit (ascent) trajectory, as it is the airflow that enables the propulsion system to produce thrust in excess of drag for the vehicle to accelerate. The correct transition between turbojet, ramjet and scramjet functioning of the engine represents another source of complexity, as well as keeping combustion stability: maintaining stable combustion at hypersonic speeds is difficult due to the high-speed airflow, which can cause flameouts and other issues.

- **Structural integrity:** the high speeds and temperatures result in significant mechanical stress and vibration, which can affect the structural integrity of the vehicle. Secondly, an appropriate distribution of aerodynamic and thermal loads is paramount to prevent structural failures, that has to be accurately predicted in the preliminary and advanced design phases. Excessive angles of attack could increase the dynamic pressure resulting in fatal configurations, so a constant attitude monitoring system must be correctly implemented. The role covered by the used materials is extremely important: conventional aerospace materials are inadequate for hypersonic conditions. Cutting-edge materials, such as ultra-high-temperature ceramics (UHTCs) or carbon-carbon composites, represent a valid option instead, but further studies and a more intensive development are required.

- **Economical impact**: most of the projects involving hypersonic vehicles design developed throughout the last decades, especially the ones related to reusable spaceplanes, were cancelled due to the high cost to be sustained, combined with the uncertainty about the actual advantages. As a matter of fact, the need for advanced materials, complex and specific design processes, rigorous testing and operational maintenance discouraged governments which they usually decided to address funds

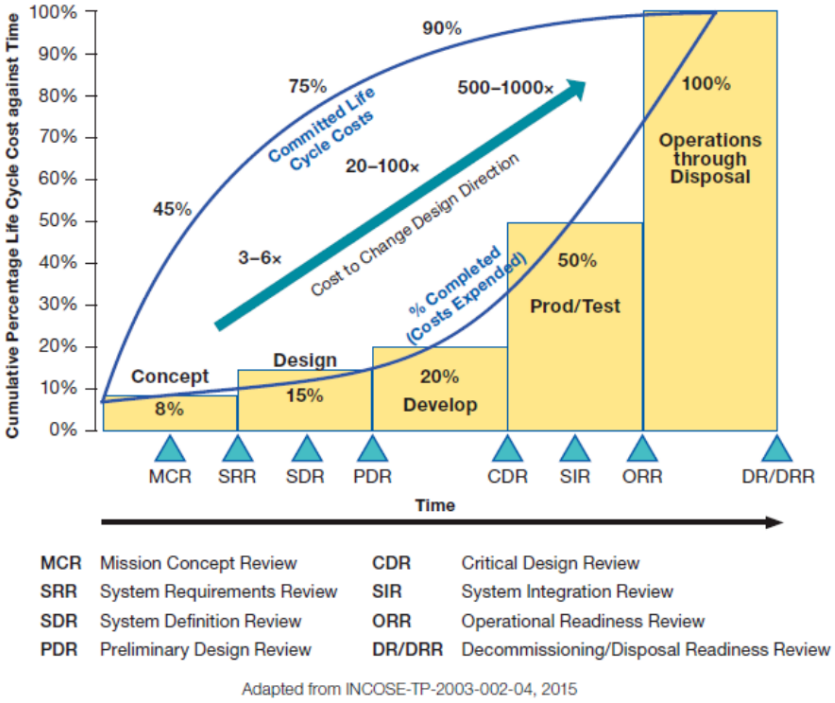

Figure 1.4: Life-Cycle Cost Impacts from Early Phase Decision-Making (Hirshorn et al., 2017).

to other safer projects instead. Moreover, dealing with such a multidisciplinary problem requires greater technical expertise in aerothermodynamics, propulsion, control systems and structural science, representing an additional cost. Typically, the overall cost of a hypersonic vehicle is assessed through a LCC analysis (Life-Cycle Cost), where the main phases are represented by concept definition, design, development, production and test, operations and disposal, as illustrated in Figure 1.4. The figure shows that the capability to predict committed costs since the very beginning of design process may be beneficial for the success of the overall project. Indeed, the early identification and solution of issues related to system development, production and operations can avoid sudden changes in design direction and prevent from costly re-design and verification activities later in the life cycle, thus leading to consistent cost savings [2].

1.2 Vertical vs horizontal takeoff: a comparison

Depending on the target altitude to achieve, takeoff and landing can be performed in different ways. For a hypersonic cruiser aircraft, which is not designed to reach exo-atmospheric altitudes, the takeoff mode is not an issue: both takeoff and landing can be done horizontally, on a runway. On the other hand, if the hypersonic vehicle is designed to reach the space, as for a space launcher, the issue is not so immediate to address. Since

mass ratios for launchers could be more than two times higher, due to the greater request of fuel to carry onboard, the required takeoff speed may be impractical to reach on any existing runway. In fact, horizontal takeoff is possible when the lift generated by the wing at takeoff speed limit is enough to leave the ground, and that requires a minimum wing loading as well as a minimum coefficient of lift at takeoff. Despite additional problems could be faced, horizontal takeoff and landing vehicles bring some advantages:

- **Conventional runways** already existing over the world can be used for both phases, making the launch process faster and cheaper, since more locations are available with respect to the few vertical launch sites present at the moment.
- **less amount of propellant** is required onboard, due to the fact that the oxidizer, namely the air, comes from outside in an airbreathing configuration, and there is no need to store it inside, like happens for classical vertical launchers. However, this statement must not be misinterpreted: this is true to a certain extent, indeed the smoother climbing profile requires more time to achieve the target altitude, thus more propellant could be consumed. This would discern missions in which horizontal takeoff is still convenient and other where it is not, especially when space is the target.
- they encourage **reusability**. Independently on the number of stages considered, each of them, or most of them, can be employed several times before disposal. As result of that, they aim at being more economically sustainable as regards operational life [3].

Throughout the decades of research, three main solutions have been investigated about the achievement of a reduced take off speed for hypersonic vehicles with horizontal configuration, usable also for space purposes and they are illustrated hereafter.

- The introduction of a **switchblade wing**. For high sweep delta planforms, such as that of the FDL-7MC and Model 176, the only high-lift device available are the switchblade wing and a retractable canard near the nose of the vehicle. The correct utilisation of these deployable devices at take off enables to decrease the takeoff speed and make it approximately equal to the landing speed. Since the deployment of the wing increases the lift generated, it seems useful both at the beginning of the flight, to provide a reasonable takeoff speed, and at the end of it, to cause the landing speed to decrease further, in case it is needed, even at lower values when compared with most civil transport and military aircraft [4].
- The use of a large **gimbaled rocket motor**. This solution consisted of a motor rotating upward, with the aim of making the entire aircraft to turn as well, encouraging the nose wheel detachment from ground at lower speeds. In other words, this was a sort of thrust-supported takeoff, but it was never applied to real systems [4].

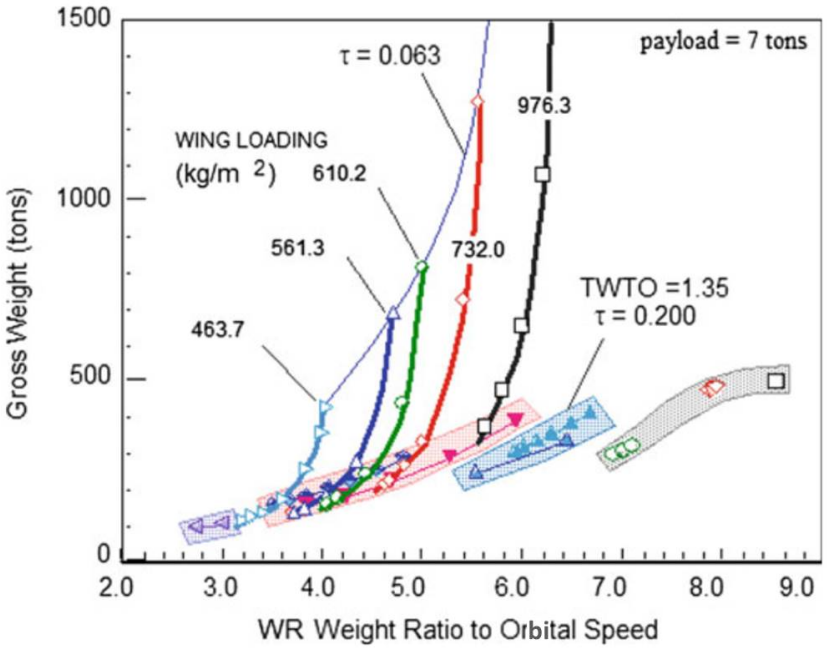

Figure 1.5: Chart showing takeoff gross mass as a function of mass ratio.

- The installation of a **larger wing planform**. If the takeoff speed is too high for the propulsion system chosen, due to high mass ratio values, then the only way to decrease the takeoff speed is to increase the planform area. If S_{pln} grows up, then τ, a crucial parameter for hypersonic vehicles, defined as $V_{tot}/S_{pln}^{1.5}$ (dimensionless, volume to planform area powered to 1.5 ratio), has to drop. As consequence of that, a chain reaction leads to higher values in the mass breakdown, with an exponential rise of takeoff gross weight. For this reason, this option is viable in moderate proportions, unless it generates unfeasible design solutions [4].

A comparison between vertical and horizontal takeoff vehicles is illustrated in Figure 1.5 [4]. They refer to a SSTO vehicle, in either configuration, although the reasoning may be extended to multi-stage vehicles with appropriate modifications. The chart correlates the gross mass at takeoff to the mass ratio required to orbit. The shaded areas at the bottom of the figure express vertical takeoff converged solutions, meaning that the mission requirements are fulfilled and the mass and volume of each solution have converged. Each area shows a different propulsion mode, passing from air-breathing systems, on the left, to all-rocket systems on the right and they have all been obtained by fixing τ at 0.2 and the thrust to weight at takeoff equal to 1.35. On the other hand, the horizontal takeoff converged solutions are reported as curves, each for a specific wing loading W/S, where τ decreases from 0.2 to 0.063 by sweeping them from the bottom to the top. Indeed, as previously stated, if W/S is fixed and the gross mass increases, so the wing area does, causing τ to fall. The point, given a certain W/S for horizontal takeoff, where the curve meets the shaded areas defines the upper mass ratio limit which makes

horizontal takeoff a reasonable option. In other words, that point identifies the same gross weight for both takeoff configurations, thus it represents the maximum mass ratio for which there is no penalty for choosing horizontal takeoff.

For air-breathing-rocket propulsion configuration, a mass ratio of 5.0 is clearly achievable. That results in a gross weight of about 230 tonnes if we refer to the shadowed area solutions space, that is the one for vertical takeoff. This is less than half the 480 tonnes for an all-rocket case, so it demonstrates the benefits coming from the adoption of an air-breathing-rocket configuration. However, if a horizontal takeoff requirement is imposed, the lowest wing loading for which a practical solution exists is 610.2 kg/m^2 . At that point, the gross weight for the horizontal takeoff solution is about 800 tonnes, almost twice the vertical all-rocket value. A possible conclusion might be that the problem relies on the choice of the propulsion system, if no comparison with vertical takeoff is conducted, but that is a mistake. Actually, the same wing loading with the same propulsion system becomes a viable option for HTHL when the mass ratio does not exceed 4.5. The use of air-breathing-rocket technology is possible for a mass ratio of 5, but it gets non-competitive in case horizontal takeoff is chosen instead of vertical.

To conclude, when the weight ratio is greater than 4.5, the best vehicle configuration seems to be either a pure rocket vertical takeoff or an air-breathing-rocket propulsion advanced configuration. In case the mass ratio is inferior, then air-breathing horizontal takeoff appears as a more convenient option in terms of gross weight required, as illustrated in Figure 1.6 [4]. However, the choice of the takeoff mode is a result of engineering decisions, thus it is not an arbitrary selection: it is important to let the features of the converged solution themselves determine the takeoff and landing modes, if the lowest gross weight and smallest size vehicle are the project goals.
The thesis will focus on horizontal takeoff and landing hypersonic vehicles, since they could represent the most interesting configuration for reusability.

1.3 Review of existing projects HTHL TSTO

In the design process of a hypersonic vehicle, the choice related to the number of stages is crucial and dictated by the mission requirements as well as the technological feasibility. It is generally believed that SSTO designs are more technically challenging, more performance sensitive and lead to larger take-off weights with respect to TSTO of equivalent payload capability [5]. This statement justifies the purpose of this work, investigating design methodologies for HTHL TSTO vehicles, but it is only partially true. If further comparative analysis regarding development, recurring costs, operability, and reliability of a launch fleet are conducted, the trade space between SSTO and TSTO design approaches gets complicated and not trivial to understand. In fact, some studies demonstrated that the SSTO vehicles are economically superior to any TSTO system for LEO missions and for reaching the International Space Station, whilst they result approxi-

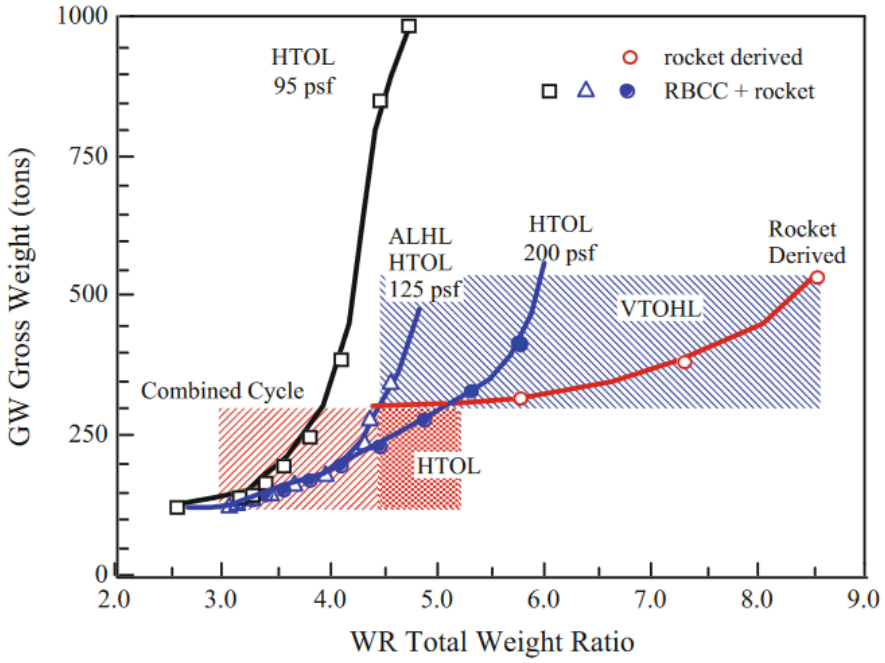

Figure 1.6: Chart summarizing how to discern between horizontal and vertical configuration.

mately equally expensive for polar orbit missions [6]. Moreover, more redundancies and reliability are required for a TSTO vehicle, since dealing with two separate units and a separation phase increase complexity.
The HTHL TSTO vehicles illustrated and briefly described in the next pages include several different configurations. In order to fully understand the concept of 2 stages, all the vehicles presented are characterized by the following features:

- The lower stage takes off horizontally and deploys the upper stage, which is normally external, at a specific altitude and speed;
- The lower stage can be either a carrier mothership or a complementary part of the whole vehicle;
- The upper stage can be either a waverider, a winged-body, a blended-body or a rocket-based vehicle, according to the specific design employed.

TSTO vehicles are typically Rocket-Based-Combined-Cycle (RBCC): the first stage, typically the carrier aircraft, is used to accelerate the second stage up to a speed where its ramjet engine can start working efficiently. After separation, the second stage remains powered by its ramjet mode, until supersonic combustion occurs and it switches to scramjet. Once the external density becomes too low for an appropriate functioning, the engine reverts to a pure rocket mode and propels the vehicle into orbit or into the desired altitude.

Another possible architecture is given by Turbine-Based-Combined-Cycle vehicles (TBCC): in this case, the carrier itself is capable of switching from a turbojet mode, at low speed, to a ramjet mode, where the second stage can be separated, powered by a rocket motor. The transition is a delicate phase, since the same engine is used to meet different requirements [7].
Other examples reported, especially technological demonstrators, present even a different configuration: due to the fact they are not required to reach orbital altitudes, no rocket motor is installed. It means that the first stage releases the second stage, typically a small demonstrator vehicle, so as it can work as a ramjet and sometimes, also as a scramjet, for reduced time ranges.

1.3.1 B52-A / X15

The Boeing B52 Stratofortress is an American long-range, subsonic, jet-powered strategic bomber. Due to its high mission-capable rate, large payload, long range, persistence and ability to employ both nuclear and conventional precision standoff weapons, B52 is still in service today [8].
B52-A represented the first variant built and put in commerce in the 50s, although only three vehicles were produced and employed for testing activities. The first production B52-A differed from previous prototypes in having a redesigned forward fuselage. The bubble canopy and tandem seating was replaced by a side-by-side arrangement and a slight nose extension accommodated more avionics and up to six crew members [9]. The B-52A models were equipped with 8 Pratt & Whitney J57-P-1W turbojets, providing a dry thrust of 44 kN [10].
The B52-A was used as carrier in the joint X-15 hypersonic research program that NASA conducted with the U.S. Air Force, the Navy, and North American Aviation Inc. in the 60s. The aircraft flew during a period of nearly 10 years and set the world's unofficial speed and altitude records of Mach 6.7 and 354,200 feet in a program to investigate all aspects of piloted hypersonic flight [11]. Because of the large fuel consumption of its rocket engine, the X-15 was air launched from a B-52 aircraft at about 45,000 feet and speeds upward of 500 mph. Depending on the mission, the XLR-99 rocket engine provided thrust for the first 80 to 120 seconds of flight. The remainder of the normal 8- to 12-minute flight was without power and ended in a 200-mph glide landing [11]. Among the accomplishments achieved through the several flights performed, a better knowledge of high aerodynamic heating rates, stability and control, physiological phenomena, and other problems relating to hypersonic flight was acquired. In Figure 1.7, the release of X15 from B52-A is depicted.

Figure 1.7: B52-A / X15.

Figure 1.8: B52-B / Pegasus.

1.3.2 B52-B / Pegasus

The B52 was used for other transportation missions in the later years. In particular, the B-52B was the first version to enter service with the USAF in 1955 with other purposes than just testing [12]. This version included minor changes with respect to the previous model, especially concerning the engines and avionics. Moreover, it was equipped with 8 Pratt & Whitney J57-P-29W series engines, all rated at 47 kN, with a slight increase in the dry thrust provided.
The B52-B was employed in the early 2000s to carry Pegasus, a winged, three-stage, solid rocket booster used typically to deploy small satellites weighing up to 1,000 pounds (453.59 kg) into low-Earth orbit [13]. Nevertheless, in this case, Pegasus's purpose was to release the demonstrator vehicle X43 at supersonic speed. Pegasus, carrying the X43, was released from a B52-B at about 11,900 m and Mach 0.82 and free-fell five seconds before igniting its first stage rocket motor. The booster lifted the research vehicle to its unique test altitude and speed, so as to test dual-mode ramjet/scramjet propulsion system at speeds from Mach 7 up to Mach 10 [14]. Three successful flights were performed: once reached the detachment conditions, the X43 vehicle was separated from the booster rocket by two small pistons and its scramjet engine operated for about ten seconds obtaining large amounts of unique flight data for an airframe-integrated scramjet [15]. The X43 flights were the first actual flight tests of an aircraft powered by a revolutionary scramjet engine capable of operating at hypersonic speeds. The 12-foot, unpiloted research vehicle was developed and built by MicroCraft Inc., Tullahoma, TN, under NASA contract. Though this could be actually categorized as a Three-Stage-To-Orbit vehicle, the combination Pegasus/X43 was considered to be an unique assembly. In Figure 1.8, both Pegasus and the carrier are illustrated.

1.3.3 Sänger II / Horus (or Cargus)

The Sänger II project, which emerged from the Sänger I program in the late 1980s, aimed to develop a European launch vehicle modeled after the Space Shuttle program.

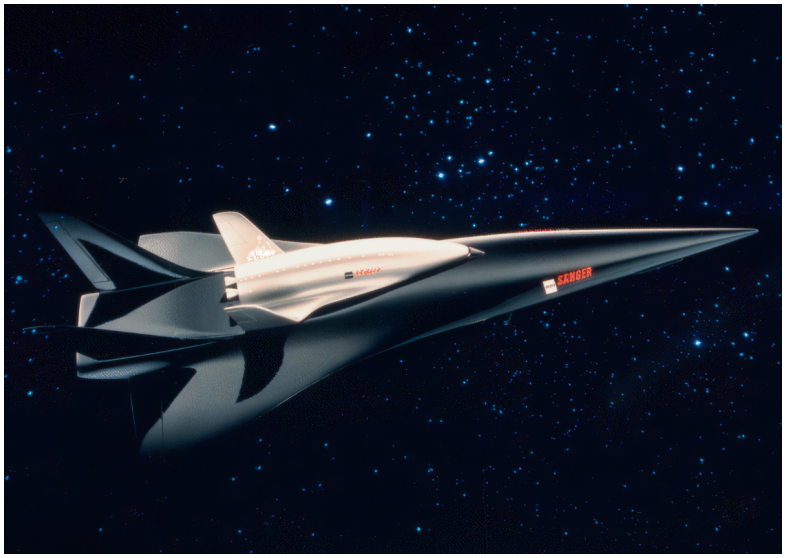

Figure 1.9: Sanger II / Horus (or Cargus).

Originally, Sänger's concept was proposed in the 40s as an innovative high-speed and high-range military aircraft design, due to the incoming war [16]. A few decades later, the study project drew the attention of the German Aerospace Center (DLR), who formally adopted it as a reference concept for a West German hypersonic programme. Sänger II was viewed as being a potential passenger airliner, which would have been both larger and faster than the Anglo-French Concorde. This version was intended to transport 230 passengers over a distance of more than 10,000 km (such as from Frankfurt to Tokyo) at a cruising speed of Mach 4.4 at an altitude of 24.5 km [17].
Another key potential use for Sänger II was as a first stage of a two-stage launch platform for an envisioned spacecraft. Two types of spacecraft were designed as possible second stage, depending on the mission: Horus, a hypersonic manned orbital upper stage, and Cargus, an uncrewed cargo module, both carrying payload into LEO orbit. The first stage vehicle would take off from a runway using 5 turbo-ramjet engines, each providing a dry thrust of 300 kN, reaching an altitude of 30 km and a speed of Mach 7. At this point, the second stage would detach and use its rocket engine to achieve orbital velocity, while the first stage returned to the runway. The spacecraft was designed to carry either a payload of 3300 kg plus crew (Horus) or up to 15000 kg for a LEO orbit (Cargus) [18]. Despite the interest was prominent at the beginning, in 1995, the project was interrupted primarily due to concerns of development costs and limited gains in price and performance compared to the existing space launch systems such as the Ariane 5 rocket. Design lifetime was 300-500 flights for Sänger II first stage, 100-120 orbital flights for the second stage Horus [19]. Figure 1.9 shows a reproduction of the vehicle.

1.3.4 White Knight I / SpaceShipOne

Designed to carry and launch SpaceShipOne, a manned sub-orbital spacecraft, to an altitude of 49kft, the White Knight mothership was a remarkable vehicle, characterized by high thrust-to-weight ratio and enormous speed brakes, allowing the astronauts to train realistically at withstanding flight manouvers and suborbital conditions before departure [20]. White Knight first successful flight occurred in August 2002, but further development proceeded over the next few months. Its propulsion was given by two turbojets with afterburner, the J-85-GE-5 engines, providing a dry thrust of 15.6 kN each. White Knight has also supported other types of missions, such as reconnaissance, surveillance, atmospheric research, data relay, telecommunications, imaging and booster launch for micro-satellites [20].
SpaceShipOne was a spaceplane designed to fulfill a specific need: carrying three people, one pilot and two civilians, in a sea-level pressurized cabin up to an altitude of approximately 100 km following a suborbital path. With SpaceShipOne, private enterprise crossed the threshold into human spaceflight, previously the domain of government programs. The design team aimed for a simple, robust, and reliable vehicle design that could make affordable space travel and tourism possible [21]. The spacecraft was drop-released once reached the separation altitude, and briefly glided unpowered. The rocket engine was ignited a few seconds later, it was then raised into a 65 degrees climb, which was further steepened in the final part of the rising trajectory. Pilot and passengers arced through space, then glided safely back to Earth. Landing occurred horizontally on a standard runway. The record altitude of 112 km was achieved in October 2004, SpaceShipOne last flight before retirement [22]. The aircraft is depicted in Figure 1.10.

Figure 1.10: WK I / SpaceShipOne.

Figure 1.11: WK II / SpaceShipTwo.

1.3.5 White Knight II / SpaceShipTwo

White Knight II and SpaceShipTwo represented the technological evolution of White Knight I and SpaceShipOne. The White Knight II carrier aircraft was flown by two pilots and had a similar size to a Boeing 737 with an estimated take-off weight of 65,000

kg. It was rolled out in July 2008 and performed a successful maiden flight on December 2008. The propulsion system was characterized by four Pratt & Whitney PW308A turbofan jet engines, while a state-of-the-art avionics was installed onboard [23]. SpaceShipTwo was designed avoiding complexity, with a minimum number of moving parts but with multiple levels of redundancy in all the key systems in order to provide an extremely safe and robust system at all stages of flight. A typical mission involved an ascent phase where White Knight II reached 50,000ft (16km) right before the spaceship was dropped and its single hybrid rocket motor (using solid fuel and liquid oxydizer) was fired to launch the craft into space for a suborbital flight, producing a thrust of approximately 270 kN [24]. The apogee was designed to be approximately 110 km in the lower thermosphere, 10 km higher than the Karman line but the maximum height reached was 89.9 km [25]. The cabin was sized in order to accommodate two pilots and six passengers. Moreover, the spacecraft was equipped with distinctive feathering wings. The wings were folded up in space, providing a feather or shuttlecock effect with extremely high drag for re-entry. This mechanism allowed deceleration to occur at a significantly higher altitude than in previous space flight re-entries. SpaceShipOne last flight before retirement was in June 2024. The aircraft is depicted in Figure 1.11.

1.3.6 G III / GoLauncher I

GOLauncher I, developed by Generation Orbit, was a sub-orbital launcher using a Gulfstream G-III business jet as a carrier aircraft. It first flew in 2021 and it supported scientific research, including microgravity and hypersonic testing [26]. This single-stage rocket could carry payloads ranging from 13 to 90 kg and reach an altitude of 300 km, providing up to seven minutes of microgravity. For hypersonic research, its trajectory could be adjusted for sustained captive-carry or free-flight testing. The rocket uses a hybrid engine with a paraffin motor and liquid oxygen (LOX) as an oxidizer, developed by Space Propulsion Group (SPG) [27]. The carrier aircraft flew to a specified location for the mission. At about 13 km of altitude, the rocket was dropped by the Gulfstream G-III and then ignited a few instants later. It performed its last flight in January 2023. In Figure 1.12, both the carrier and the rocket are visible.

1.3.7 IAR III / HAAS II

IAR-III Excelsior was developed by ARCA, a Romanian space systems company with an interesting innovative air-launch system in 2010. It was a carrier aircraft consisting of a supersonic jet that could carry a large rocket as a payload. The jet had two main purposes: to be used as a carrier to drop the rocket at the target altitude or to carry space tourists up to a sub-orbital view [28]. The IAR-III was designed to take off and land on the water, thus no landing gears were conceived. However, also a ground-launch version was produced, in case IAR-III was employed as first stage of a space launcher and not

Figure 1.12: G III / GoLauncher I.

Figure 1.13: IAR III / HAAS II.

for space tourism. It was powered by an Executor engine, that is a LOX/RP-1 rocket engine generating 240 kN of thrust. The HAAS 2 rocket was comprised of another engine developed by ARCA, called the Venator, which was a LOX/RP-1 engine too, as for the carrier, producing 25 kN of thrust [29]. The rocket had remarkable carrying capabilities, being manufactured to bring up to 400 kg into a LEO orbit. It was intended to be released by the carrier aircraft from an altitude of around 16 km [30]. The overall vehicle was never completed, but several successful tests were performed from 2010 and 2013, such as the evaluation of the safety systems, consisting of a drop of the IAR III cabin to verify structural integrity and parachute opening, and the engine performance assessment [31]. In Figure 1.13, IAR III and Haas II are reported.

1.3.8 BlackStar SR3 / XOV

Little information is known about the American programme Blackstar. Aviation Week & Space Technology magazine described Blackstar as a two-stage-to-orbit system in 2006. The first stage, referred to as the SR-3, was a delta-winged supersonic jet similar to the North American B-70 Valkyrie and based on Boeing patents from the 1980s. The SR-3 would carry a smaller airframe, called the XOV (eXperimental Orbital Vehicle), between its two engine banks. At around 100,000 feet, the SR-3 would release the rocket-powered XOV, which, using aerospike engines like those on the Lockheed Martin X-33, could achieve both suborbital and orbital flight. Depending on payload and mission, the XOV could reach an orbit of 480 km. It would then reenter the atmosphere and glide back for a horizontal landing on a conventional runway [32].
The primary use of a military spaceplane such as Blackstar would be to conduct high-altitude or orbital reconnaissance, allowing surprise overflights of foreign locations with very low risk of the spyplane being successfully engaged by existing air-defense systems. Secondly, it could also be used to place small satellites in orbit and to retrieve them. It is unclear if the Blackstar program became fully operational, although it may have been so since the mid-1990s.

Chapter 2

Statistical analysis of HTHL TSTO vehicles

Two-stage-to-orbit hypersonic vehicles designed and developed through the last decades of history do not present a standard configuration to refer to, since several concepts, even by restricting the field to horizontal take off and landing only, have been proposed and investigated.
Technical data, whenever available, of 11 TSTO HTHL hypersonic vehicles have been gathered and organized in a table, by dividing it in major areas: general specifications, weight budget data, geometry data, propulsion data and conceptual design figures. Unfortunately, especially for those projects which were never brought to life, the available data were generally scarce and unreliable. Nevertheless, some important figures could be derived from the ones available, in order to establish some design trends. The aims of this chapter are mainly two:

- showing and commenting on some design trends through plotted figures;
- proposing a possible procedure to design a TSTO HTHL vehicle in the first instance.

It is paramount to stress that is not a recommended procedure for sizing, due to the scarce number of samples and their heterogeneity. A detailed sizing methodology will be discussed in the following chapters, thus the one presented here can be treated as a raw method to delve into the main dependencies and behaviours as far as the essential design quantities are concerned. Moreover, not all the figures show all the collected case studies: data completely deviating from the dominant trend for a specific figure have been removed, resulting in a variable number of samples per each graph. At any rate, a legend is always displayed to realize which designs are plotted and which not. Finally, structural efficiencies ϵ_i and payload ratios λ_i are defined in subsection 4.4.1.

2.1 Main figures from statistical analysis

In Figure 2.1, a relation between the altitude reached by the TSTO vehicle h and the overall payload ratio λ_{tot} is reported. Though the samples are quite randomly distributed, a decreasing trend can be found, as expected. In fact, the higher λ_{tot}, the heavier the payload to inject, in percentage with respect to fuel and structural masses. If they are constant, it means the take off mass increases on one hand, whilst the attainable target orbit altitude decreases on the other.
In Figure 2.2, it is illustrated how the overall payload ratio λ_{tot} and the first stage payload ratio λ_1 are correlated. In this case, only air-breathing engines configurations are taken into account. The general trend is increasing, meaning that if λ_1 rises, so does λ_{tot}. A possible explanation can be the following: if λ_1 increases, the overall mass of second stage increases as well. The need of a heavier second stage is justified by heavier payload to put into orbit. Therefore, even though λ_2 could decrease by increasing λ_1, what matters is their product, that is λ_{tot}. The combined effect results in λ_{tot} increasing with a reducing local slope as λ_1 grows up. In any case, this is just an indicative behaviour.

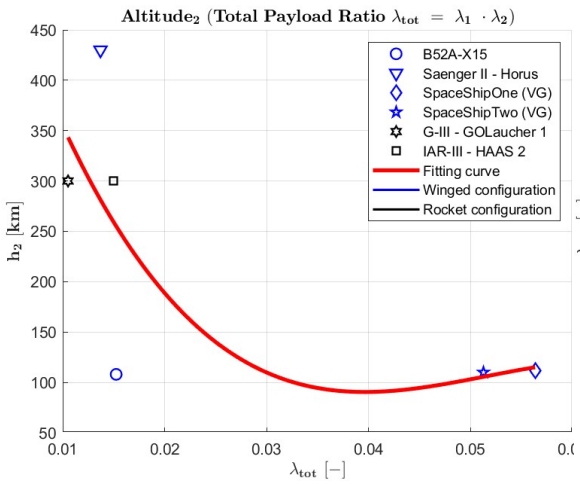

Figure 2.1: h as a function of λ_{tot}.

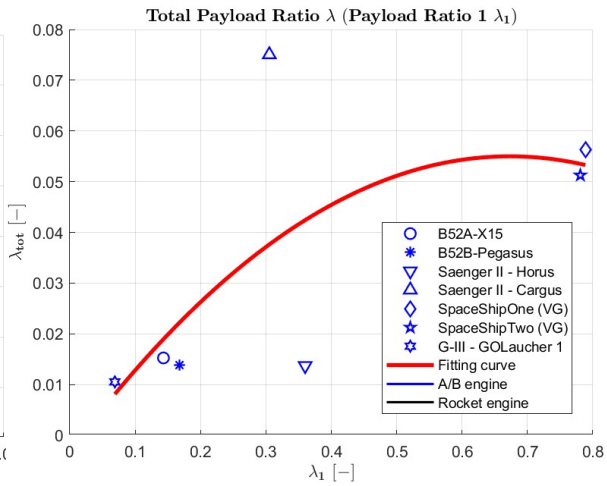

Figure 2.2: λ_{tot} as a function of λ_1.

Another interesting chart is reported in Figure 2.3. It shows the relation occurring between the maximum take off mass $MTOM$ and the payload mass m_{pay} for both stages. Obviously, the order of magnitude is one time higher in the first stage case, even if the profiles seem to be approximately self-similar in either stage. The trend reported is naturally increasing. As a matter of fact, for both stages, a rise in payload has to be followed by a rise in the maximum take off mass, also to accommodate more fuel and more structure to fulfill the same mission requirements.
Figure 2.4 illustrates an important tendency. Both the structural efficiency related to the first stage ϵ_1 and the one related to the second one ϵ_2 seem to be independent on the stage dry mass m_s. In other words, if air-breathing engine vehicles and rocket powered vehicles are considered separately, on the basis of their colour, they seem to

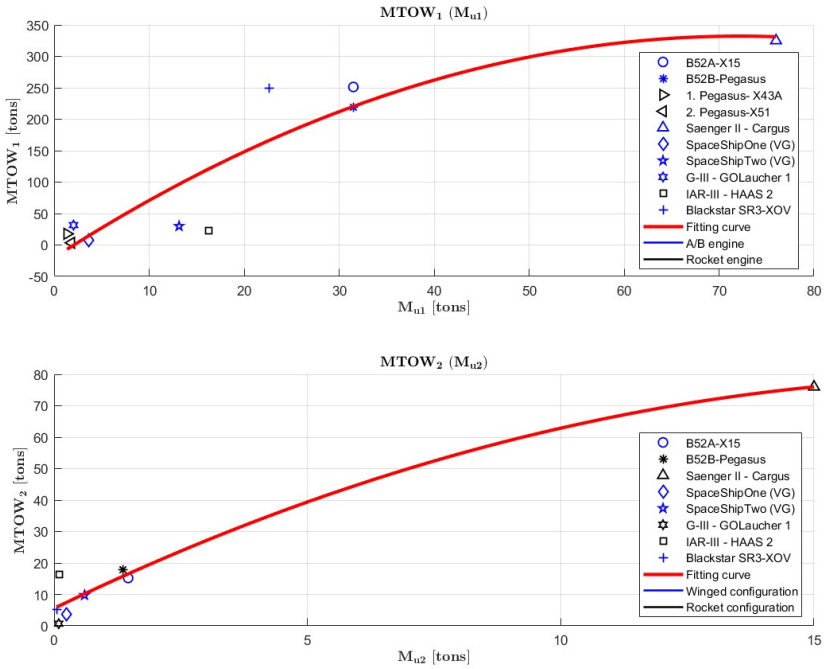

Figure 2.3: $MTOM$ for stage 1 and 2 as a function of their respective payload masses m_{pay}.

show an approximately constant trend over m_s. It is clear that typical values of ϵ_1 for air-breathing configurations fall in the range $0.4 - 0.6$ for the first stage, while in the range $0.25 - 0.5$ for the second. On the other hand, rocket engine configurations present values around $0.05 - 0.1$, regardless of whether stage 1 or 2 is considered. It means rocket configurations are characterized by structural efficiencies five times lower on average with respect to air-breathing configurations. As consequence of that, while designing a first type configuration, higher ratios $\frac{m_{ppl}}{m_s}$ are required. In fact, rockets typically present lower I_{sp} values (specific impulse) than air-breathing vehicles.

Another figure worth to be mentioned is Figure 2.5. It refers to the two main ratios involved in the conceptual design phase of an aircraft, that is the thrust over weight ratio T/W and the wing loading W/S. The estimation of these magnitudes was quite challenging, especially as regards the correct evaluation of thrust. Nevertheless, even if some values could be not totally accurate, the most interesting results are provided by the first stage chart: there is a clear distinction between rocket engine configurations and air-breathing ones, as regards the thrust requirement. In fact, if rockets can reach values of T/W over the unity, also 3 or 4, while air-breathing first stages are encompassed by typical aircraft values, between 0.25 and 0.5. It means that rocket-powered vehicles can produce higher levels of thrust, even some times greater than their weight.

Finally, two remaining figures should be described: Figure 2.6, expressing the relation between maximum take off weight $MTOM$ and wing planform area S_{pln}, and Figure 2.7,

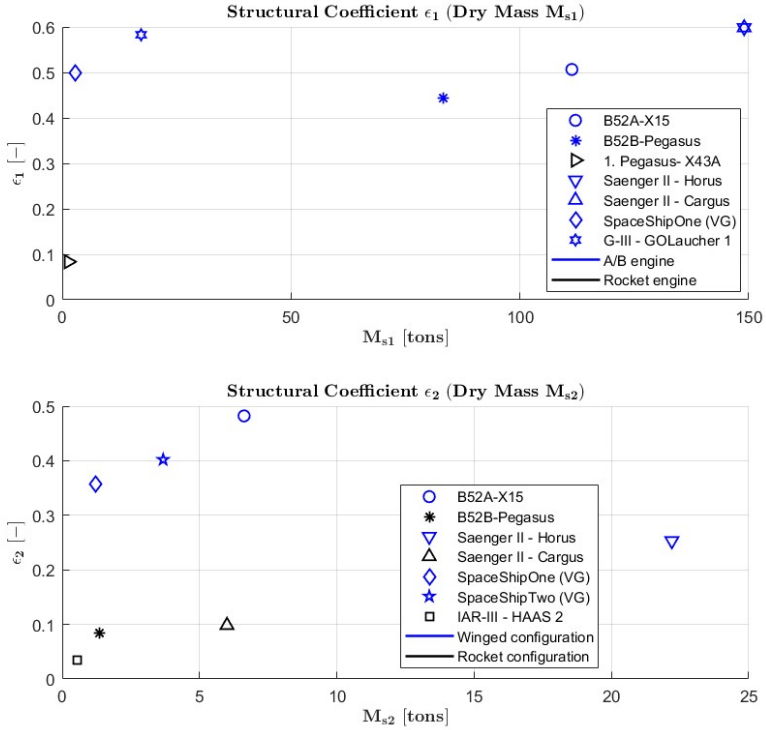

Figure 2.4: Structural eff. ϵ_i for both stages as function of their respective dry masses m_s.

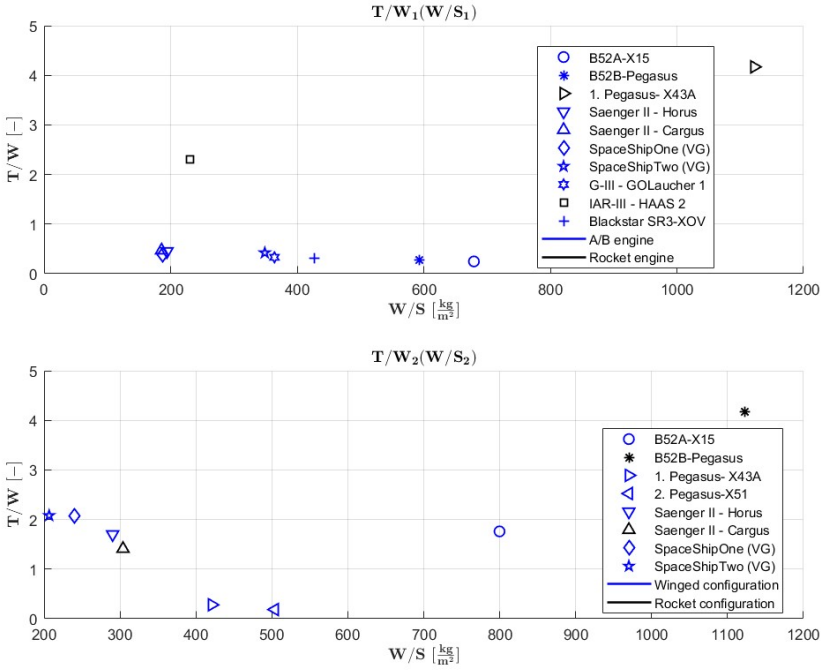

Figure 2.5: T/W ratio for both stages as a function of W/S.

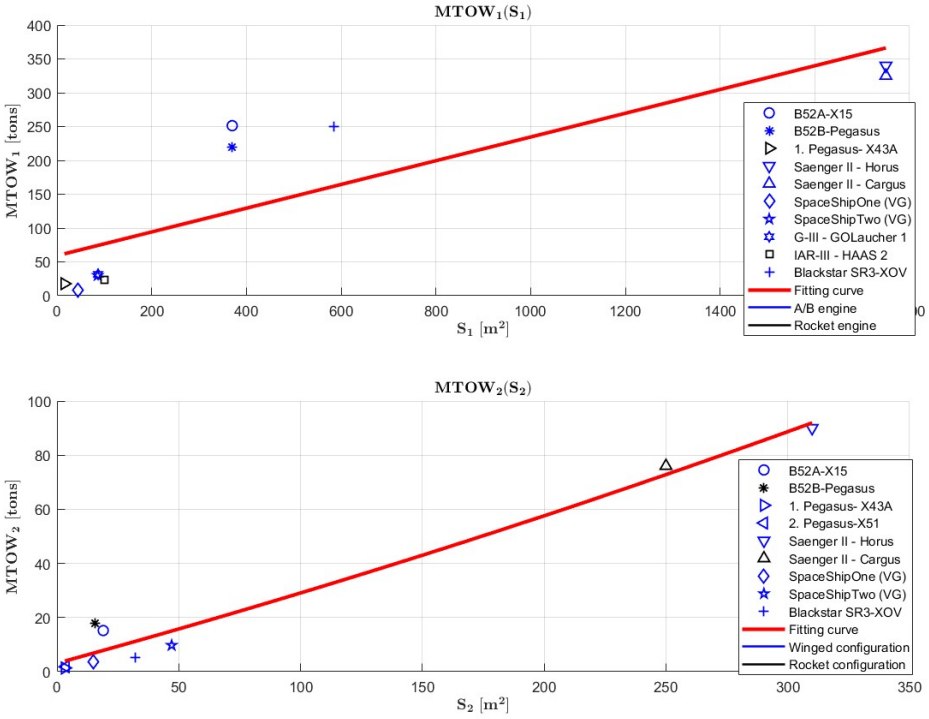

Figure 2.6: $MTOM$ for stage 1 and 2 as a function of their respective wing planforms S_{pln}.

showing how thrust required T is affected by the maximum take off weight $MTOM$. Each figure is divided into two subplots, representing the behaviours of the two stages separately. Here the the trend is increasing and that is easily understandable. As a matter of fact:

- if the $MTOM$ grows up, also a higher wing area S_{pln} is required to increase the lift generated in equilibrium conditions;
- if the $MTOM$ grows up, also higher levels of thrust are requested to reach the target altitude. The heavier the vehicle, the more power is needed to fulfill the mission requirements.

Other relations could be derived from the data extrapolated, but these seemed the most relevant to carry some preliminary studies and investigate on the main inter-dependencies.

2.2 Potential design sequence

The following procedure could be used to determine very fast the sizing of a TSTO HTHL vehicle. Naturally, it is based only on statistical analysis, thus it could result in quite

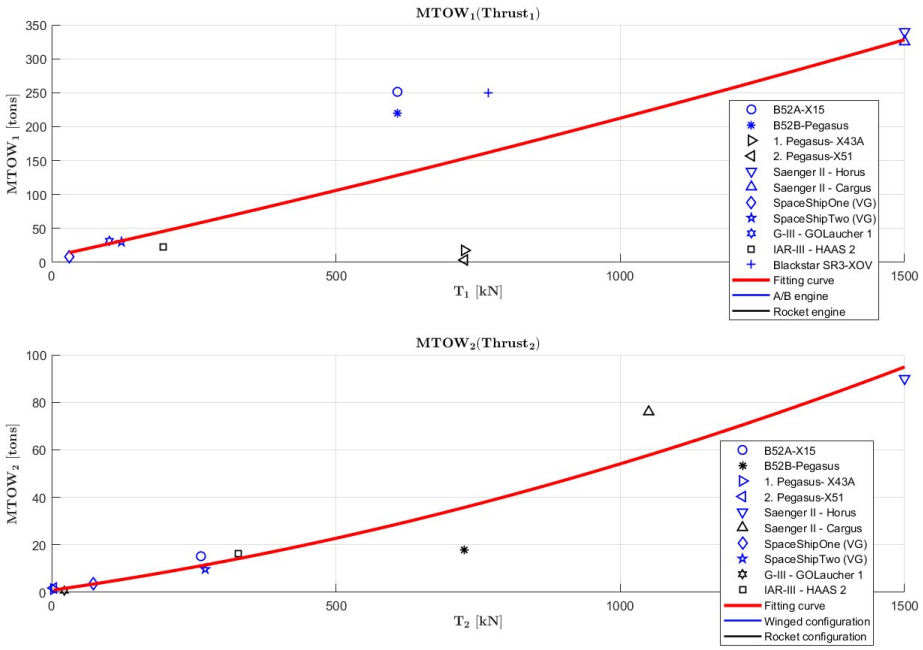

Figure 2.7: $MTOM$ for stage 1 and 2 as a function of their respective thrusts T.

considerable errors. However, a conceptual sizing in broad terms may be performed, being aware of all the limitations.

2.2.1 Steps to follow

Step	Ref. chart	Input	Output
1	2.1	h	λ_{tot}
2	2.2	λ_{tot}	λ_1, λ_2
3	2.3.2	$m_{pay,2}$	$MTOM_2 \approx M_{u,1}$
4	2.3.1	$m_{pay,1}$	$MTOM_1$
5	2.6.1	$MTOM_1$	$S_{pln,1}$
6	2.6.2	$MTOM_2$	$S_{pln,2}$
7	2.7.1	$MTOM_1$	T_1
8	2.7.2	$MTOM_2$	T_2
9	2.4	Engine type	ϵ_1, ϵ_2
10	$m_{s,i} = \frac{\epsilon_i}{\lambda_i} m_{pay,i}$	$\epsilon_i, \lambda_i, m_{pay,i}$	$m_{s,i}$
11	$m_{ppl,i} = m_{s,i}\left(\frac{1}{\epsilon_i} - 1\right)$	$m_{s,i}, \epsilon_i$	$m_{ppl,i}$

Table 2.1: Sequence of steps to follow to reach a first preliminary sizing.

In order to fully understand the simplified procedure, the sequence of steps to take is reported in Table 2.1. Some aspects and hypothesis made require to be clarified, as explained hereafter.

- The only inputs requested at the beginning of the procedure are the three main mission requirements, namely the target altitude h, the mass of payload to inject $m_{pay,2}$ and the type of engine configuration (rocket powered or air-breathing).
- The payload ratio is defined as $\lambda_i = \frac{m_{pay,i}}{m_{ppl,i}+m_{s,i}}$. Since $m_{pay,2}$ is generally very little with respect to $MTOM_2$, an approximation is made:

$$\lambda_{tot} = \frac{m_{pay,2}}{m_{ppl,1} + m_{s,1}} \approx \frac{m_{pay,2}}{m_{ppl,2} + m_{s,2}} \cdot \frac{m_{pay,1}}{m_{ppl,1} + m_{s,1}} = \lambda_1 \cdot \lambda_2 \tag{2.1}$$

  As consequence of that, $m_{pay,1}$, which should include $m_{pay,2}$ as well, is considered equal to $m_{ppl,2} + m_{s,2}$. This simplification enables to compute λ_{tot} by simply multiplying λ_1 by λ_2. Nevertheless, from step 3 on, $m_{pay,1}$ is assumed to be equal to $MTOM_2$, as it is correctly.

- The expressions in step 10 and 11 come from manipulation of λ and ϵ definitions. In fact:

$$\frac{\epsilon_i}{\lambda_i} = \frac{\frac{m_{s,i}}{m_{s,i}+m_{ppl,i}}}{\frac{m_{pay,i}}{m_{s,i}+m_{ppl,i}}} = \frac{m_{s,i}}{m_{pay,i}} \implies m_{s,i} = \frac{\epsilon_i}{\lambda_i} m_{pay,i} \tag{2.2}$$

$$\epsilon_i = \frac{M_{s,i}}{M_{s,i} + M_{ppl,i}} = \frac{1}{1 + \frac{M_{ppl,i}}{M_{s,i}}} \implies M_{ppl,i} = M_{s,i}\left(\frac{1}{\epsilon_i} - 1\right) \tag{2.3}$$

- At the end of the procedure, the ratios T/W and W/S obtained should be checked by looking at the diagram in Figure 2.5 for consistency.

2.2.2 Application to an example

The procedure illustrated, totally relying on the only statistical analysis, may be employed to a specific case. Let's suppose the mission requirements are the following:

- the target altitude has to be 300 km $\rightarrow h = 200\ km$;
- the payload mass to carry is equal to 200 kg $\rightarrow m_{pay,2} = 500\ kg$;
- an air-breathing configuration is chosen for the first stage, a rocket one for the second.

Under these hypothesis, the resulting mass breakdown for both stages is illustrated in Figure 2.8 and Figure 2.9. To be thorough, the bar charts are the outcome of $\lambda_1 = 0.1445, \lambda_2 = 0.1322, \epsilon_1 = 0.5$ and $\epsilon_2 = 0.075$. Moreover, the following thrust and wing planform area values are obtained: $T_1 = 299.25\ kN, T_2 = 221.50kN, S_{pln,1} = 128.36\ m^2$ and $S_{pln,2} = 34.06\ m^2$.
Two main checks can be performed in order to verify to a certain instance the truthfulness of this approach, though really simplified: computing the mass breakdown in reverse and assessing the feasibility of T/W and W/S ratios. As regards the former:

- Stage 1 $\rightarrow MTOM_1^* = 9.40 + 32.53 + 32.53 = 74.46\ tons \rightarrow Err_{rel} = +11.5\%$;
- Stage 2 $\rightarrow MTOM_2^* = 0.5 + 0.29 + 3.49 = 4.28\ tons \rightarrow Err_{rel} = -54.5\%$;

It is clear how the procedure could be just an approximate tool to estimate order of magnitudes. As far as the latter is concerned, in the plane $(W/S\ (kg/m^2), T/W\ [-])$ the two points found are respectively $(512.548, 0.46)$ and $(276.13, 2.4)$, which are perfectly reasonable and fit in the typical trends of their category.

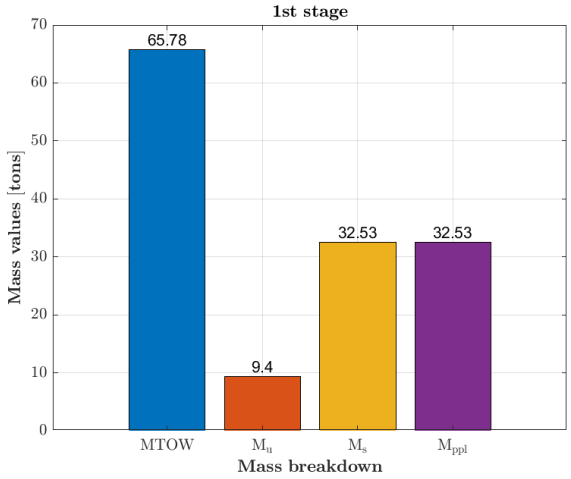

Figure 2.8: Mass breakdown for stage 1.

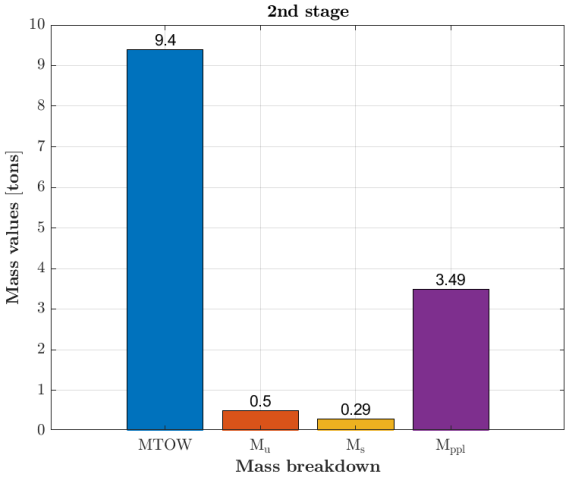

Figure 2.9: Mass breakdown for stage 2.

Chapter 3

Sizing methodology

In this third chapter, the explanation of the entire methodology adopted for the conceptual design of hypersonic TSTO HTHL vehicles will be illustrated. As a starting point, it must be stressed that it derives from the Hypersonic Convergence sizing approach for transonic to hypersonic vehicle applications first developed at formerly McDonnell Aircraft Company between 1970 and 1990. The main purpose of this unit, therefore, is to expand it, updating it with new relations and mixing it with the so-called Multiple Matching Chart approach, developed by the Aerospace Engineering Department of Politecnico di Torino, in order to make it fit with both SSTO and TSTO vehicle configurations.
It does not claim to be the more advantageous procedure to follow for preliminary sizing, but it contains lots of interesting and relevant aspects to converge to a quite reliable solution. The implementation of the methodology will be presented in chapter 4 instead, where a case study analysis will occur.

3.1 Inputs

The methodology requires different types of inputs in order to start the convergence process to a preliminary sizing of the vehicle. Some of these inputs are appointed as independent design variables, since they are set by the user prior to anything else. Others are called dependent, due to the fact they derive from an immediate utilization of the inputs provided but they are still considered as inputs for the methodology itself.

1. Independent design variables:

    - Mission variables. They typically include phase time t_{ph} (i.e. in cruise), m_{pay}, the payload density ρ_{pay}, separation altitude h_{sep}, velocity gain required ΔV, maximum dynamic pressure during the phase q_{max} and so on;
    - Configuration type. It refers to the type of vehicle shape, namely blended body, waverider, missile, half-cone, etc;

- Propulsion system data. They encompass the architecture type, that is rocket, air-breathing, combined-cycle, etc, but also other figures like propellant density ρ_{ppl}, fuel density ρ_f, oxidizer density ρ_{ox}, mixture ratio MR;
- Structural and aerodynamic constants.

2. Dependent design variables:

   - The slenderness parameter τ, deeply correlated to the configuration type;
   - Planform area's first guess S_{pln} for the iterating process;
   - Masses' first guesses (m_{OE}, m_{ppl}), according to statistical analysis available through databases;
   - Thrust T and Specific Impulse I_{sp} initial guesses, according to statistical analysis available through databases.

   Independent design variables are those parameters considered as fixed by the designer, hence they are set a priori. Dependent ones represent a first guess to help accelerate the converging process, therefore can change even several times before reaching a design point.

3.2 Analysis

First of all, τ is chosen appropriately according to the diagram reported in Figure 3.1. All the passages coming next will be reiterated by changing τ in a suitable range. Therefore, if the configuration is selected, a reasonable interval of τ is defined. In formula:

$$\tau = \frac{V_{tot}}{S_{pln}^{1.5}} \tag{3.1}$$

meaning that the overall volume's first guess V_{tot} is got as well. By looking at the figure again, if τ is chosen and fixed, also the ratio K_w/τ is determined, so K_w is. In formula:

$$K_w = \frac{S_{wet}}{S_{pln}} \tag{3.2}$$

which enables us to also obtain a first estimation of S_{wet}.

3.2.1 Geometry

Some methods can be used, in combination with statistical analysis at this stage to determine other features beyond V_{tot} and S_{wet}, for instance wingspan, mean aerodynamic chord, etc. Elaborate methods to obtain a detailed geometrical description of both stages are out of the aim of this work. However, for sake of completeness, a very simple

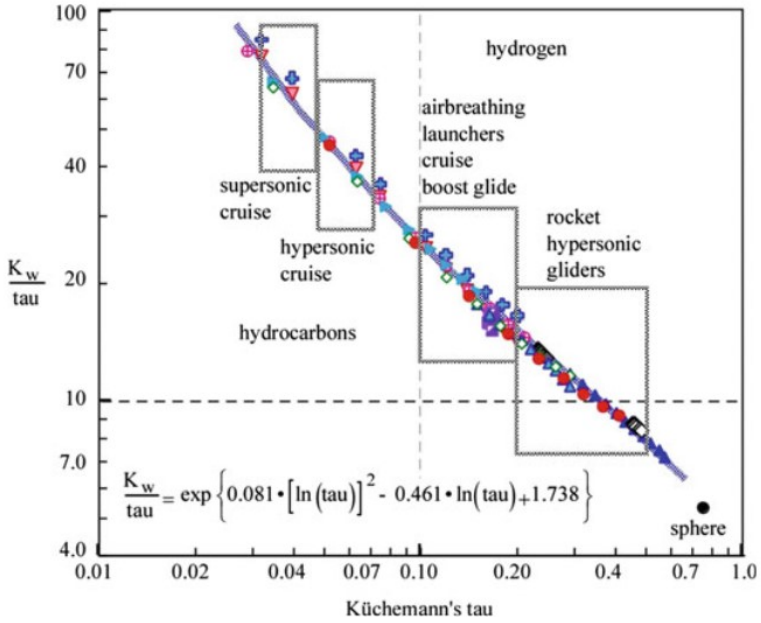

Figure 3.1: Geometric parameters span the complete spectrum of aircraft configurations.

model to achieve some important geometrical parameters given a certain configuration is hereafter illustrated. It is the only one presented because it refers to a typical geometry for hypersonic cruisers and it fits the case study treated in the next chapter.

Hypersonic Cruiser Planform Description Method

This model, illustrated in [33] deals with the planform description of hypersonic cruisers with delta-wing planform given a specific spatular ratio (c/s_Δ). The inputs of the method are:

- $S_{pln} \implies$ the planform surface is a suggested value at the beginning of iterations;
- $(c/s_\Delta) \implies$ the spatular ratio (equal to 0 for triangular configuration);
- $\Lambda_{LE} \implies$ the angle at the leading edge.

The nomenclature used refers to Figure 3.2. Once the previous magnitudes have been established, the following passages lead to L_w (planform length), s_Δ (outer transverse extension), c (inner transverse extension) and b (wingspan).

$$L_w = \sqrt{\frac{S_{pln} \cdot \Lambda_{LE}}{1 + (c/s_\Delta)}} \tag{3.3}$$

$$s_\Delta = \frac{L_w}{tg(\Lambda_{LE})} \tag{3.4}$$

$$c = (c/s_\Delta) \cdot s_\Delta \tag{3.5}$$

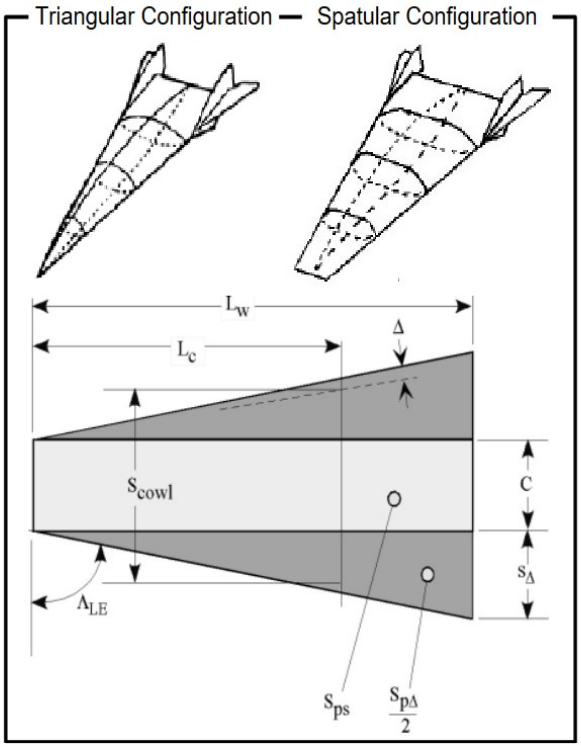

Figure 3.2: Up and side views of a typical hypersonic cruiser.

And finally:

$$b = 2 \cdot s_\Delta + c \tag{3.6}$$

3.2.2 Aerodynamics

The computation of aerodynamic coefficients is crucial in order to permit the iteration of the methodology for convergence. Several models appeared through the decades and some of them lead to more accurate results than others due to an increasing complexity. Since the methodology illustrated applies to a 2-stage vehicle, it is necessary to consider an aerodynamic characterization able to describe all the possible flight regimes (subsonic, supersonic, hypersonic). For this purpose, the Curran Model is presented hereafter, in order to obtain lift and drag coefficients in whatever condition: C_L, C_D, C_{D0} (drag coefficient at null lift) and $(L/D)_{max}$ (maximum efficiency). Naturally, due to its simplicity, it yields results which may be somehow inaccurate, though it is useful for conceptual design stage calculations. Before delving into details, it seems necessary to stress the range of applicability of the model:

- it works for subsonic, supersonic and hypersonic regimes;
- the empirical coefficients were obtained for a CAV, therefore it can be applied to the second stage with no problems emerging. In the test case, it will be applied to first stage as well;

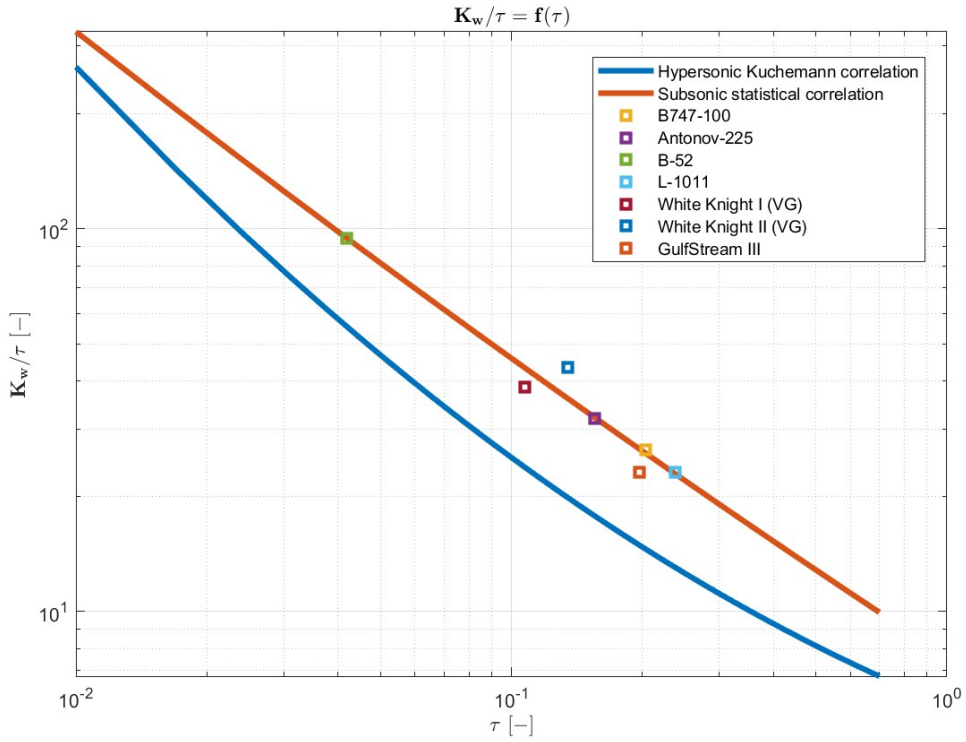

Figure 3.3: New correlation for subsonic carriers.

- the validity is subjected to the relation linking K_w/τ and τ.

The last bullet suggests that the aircraft configuration chosen as first stage affects the validity of the model, and ultimately its sizing. For this reason, further studies should be carried out to extend the applicability of the relation plotted in Figure 3.1 to a subsonic regime. In fact, the carrier could be either a CAV itself, like Sänger II s concept (no issues in this case) or a subsonic aircraft, like B52 (in this case, the point $(\tau, K_w/\tau)$ is defined provided that the curve is extended to subsonic regime as well, with the appropriate trend coming from statistical analysis).

New correlation $\frac{K_w}{\tau} = f(\tau)$ for subsonic carrier

In Figure 3.3, the correlation between the two input parameters of the hypersonic sizing methodology applied to subsonic aircraft is shown. It does not claim to be exhaustive, but it represents a possible way to proceed once the sizing of the first stage occurs: if a CAV is chosen as carrier vehicle, then the blue line is the one to refer to (the same as the one reported in Figure 3.1). On the other hand, if a subsonic carrier is chosen, the red line is the one to refer to. That has been obtained through curve fitting of 7 cases of existing subsonic carrier aircraft. In Table 3.1 the main data to achieve both K_w and τ are reported.

Two observations require to be made:

1. V_{tot} was calculated by assuming a cylindrical fuselage in absence of more precise

A/C	L_f	D_f	S_{pln}	V_{tot}	S_{wet}	τ	K_w	K_w/τ
B747-100	70.67	6.5	510	2344	2647	0.2035	5.19	25.50
Antonov 225	84	8	905	4222	4293	0.1550	4.74	30.59
B-52	48.5	2.8	370	299	1394	0.0419	3.77	89.77
L-1011	54.17	5.77	329	1416	1734	0.2370	5.27	22.21
WK I (VG)	8.5	1.52	44	31	180	0.1076	4.15	38.57
WK II (VG)	23.7	1.70	86	107	505	0.1349	5.87	43.51
GulfStream III	25.3	2.00	87	159	394	0.1964	4.54	23.12

Table 3.1: Table with data to get τ and K_w for subsonic aircraft.

data (the volume computed in excess can partially consider tail and wing volumes):

$$V_{tot} = \pi L_f \frac{D_f^2}{4} \tag{3.7}$$

2. The wetted surface S_{wet} was computed through an approximation of a formula found in [34], where in particular the effects of the engine nacelles and the thickness ratio of the the wing are neglected:

$$S_{wet} = \pi D_f (L_f - 1.3 D_f) + 2(S_{pln} + S_{ht} + S_{vt}) \tag{3.8}$$

   In absence of more accurate details, by referring to suggested values of [35], $S_{ht} = 0.25 S_{pln}$ and $S_{vt} = 0.2 S_{pln}$ were assumed.

3. The two previous consideration do not apply to both White Knight I and II, due to the unconventional airframe configuration chosen by the manufacturer. Appropriate modifications to Equation 3.7 and 3.8 are then used to derive quite reliable technical data.

Thanks to the curve fitting toolbox, a particular function shape was imposed for the new subsonic correlation, equal in the general terms to the Kuchemann correlation K_w/τ but different in the coefficients for consistency. Therefore:

- Kuchemann correlation $\implies K_w/\tau = e^{0.081\cdot(\log\tau)^2 - 0.461\cdot\log\tau + 1.738}$
- Subsonic correlation $\implies K_w/\tau = e^{0.01591\cdot(\log\tau)^2 - 0.7433\cdot\log\tau + 2.03}$

This second expression represents an important achievement of this work, being an expansion of the model already existing in literature valid only for regimes above transonic.

Curran's Model for aerodynamics

It consists of a set of parametric equations that allows a simple estimation of the external aerodynamics of a generic high speed vehicle. This model is widely used and extremely useful in conceptual design, here illustrated for 2 main reasons:

- it demands for a restricted number of inputs;
- it is applicable to all flight regimes, from subsonic to hypersonic.

. The only inputs required are three: the configuration parameters τ and K_w, and the Mach number M of the involved flight segment. Starting from these data, it is possible to estimate all the main parameters used in the convergence algorithm.

- $\left(\frac{L}{D}\right)_{max} \implies$ the maximum efficiency can be calculated through the following equation:

$$\left(\frac{L}{D}\right)_{max} = \frac{a}{M}(M+b)(c - d \cdot F) \tag{3.9}$$

  where the semi-empirical coefficients given were statistically evaluated for a CAV resulting in $a = 3.063, b = 3, c = 1.11238$ and $d = 0.1866$. As far as F is concerned, that is a coefficient correlating τ with K_w, since it is defined as:

$$F = \tau^{0.333} \cdot K_w^{0.75} \tag{3.10}$$

  As consequence of that, by knowing F and M, $(L/D)_{max}$ is found.

- C_{D0} and $C_D \implies$ the coefficient of zero-lift drag can be computed as follows:

$$C_{D0} = \frac{f \cdot e^{gF}}{\sqrt{|M^2 - 1|}} \tag{3.11}$$

  where $f = 0.0577$ and $g = 0.4076$. To estimate the coefficient of total drag, considering induced drag too, the approach of Vinh is a viable option, which introduces the correction factor ψ, specialized for each segment of flight:

$$\begin{cases} C_D = C_{D0}(1+\psi), & \psi = 0.075, \quad \text{Acceleration phase} \\ C_D = C_{D0}(1+\psi), & \psi = 0.750, \quad \text{Minimum fuel flow cruise} \\ C_D = C_{D0}(1+\psi), & \psi = 1.000, \quad \text{Maximum efficiency glide} \end{cases} \tag{3.12}$$

- $C_{L,Emax}$ and $C_L \implies$ in order to compute the coefficient of lift at maximum efficiency, the definition is recalled:

$$E_{max} = \left(\frac{L}{D}\right)_{max} = \frac{C_{L,Emax}}{C_{D,Emax}} \implies C_{L,Emax} = \left(\frac{L}{D}\right)_{max} \cdot C_{D,Emax} \tag{3.13}$$

  Finally, the coefficient of lift for each phase of flight can be estimated as a fraction of $C_{L,Emax}$ as follows:

$$\begin{cases} C_L = i \cdot C_{L,Emax}, & i = 0.10, \quad \text{Acceleration phase} \\ C_L = i \cdot C_{L,Emax}, & i = 0.82, \quad \text{Minimum fuel flow cruise} \\ C_L = i \cdot C_{L,Emax}, & i = 1.00, \quad \text{Maximum efficiency glide} \end{cases} \tag{3.14}$$

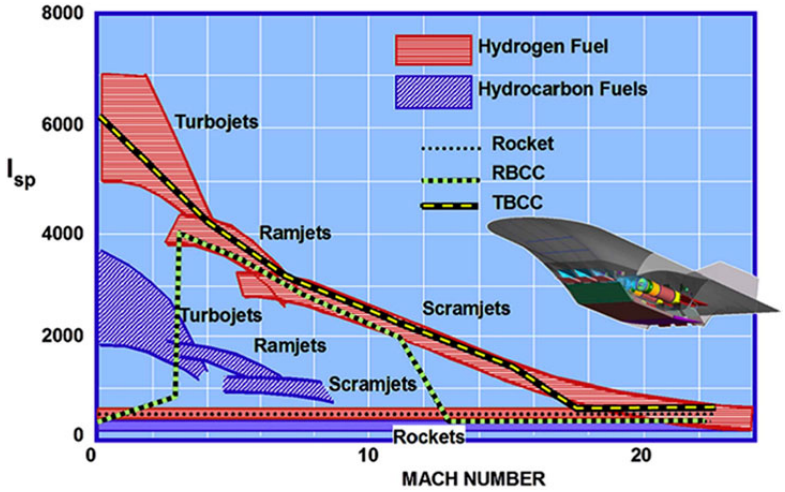

Figure 3.4: Propulsion performance for different engines.

As a final remark, in this model, for a fixed configuration, the aerodynamic coefficients depend only on Mach number M, while the dependence on the angle of attack α is not considered. Naturally, the knowledge of variation of α with time belongs to a later stage of design and this represents one element of decrease in accuracy.

3.2.3 Propulsion strategies

Apart from rocket engine, none of the main aeronautical powerplant architectures is suitable, alone, to reach the space, even a LEO orbit. The employment of two stages instead of one improves the overall capabilities of the vehicle, but it is clear that the entire range of Mach from incompressible subsonic to hypersonic must be covered. Each engine has its Mach range in which it performs better: $0 < M < 2$ for turbojets, $1 < M < 6$ for ramjets, $5 < M < 15$ for scramjets [36], as it is shown in Figure 3.4. Consequently, at least one stage of the vehicle for orbital access must use diverse types of engines sequentially, transitioning from one to another at an appropriate Mach number. Alternatively, combined-cycle propulsion systems can be employed, but they won't be discussed here, since the methodology do not take them into account in the actual version.

Turbojet

Turbojets represent the most common propulsion strategy used in civil aviation. They offer the highest specific impulse due to the large amount of air moved. Despite they provide higher levels of thrust, turbojets have mainly evolved into turbofans, which offer a higher efficiency. However, the principle of working is basically the same. A turbojet engine is characterized by three bigger parts: the inlet, the gas turbine engine, consisting of a compressor, a combustion chamber and a turbine, and the exhaust nozzle. Air is

conveyed into the engine through the inlet; its divergent shape induces the air to slow down, causing the pressure to increase. Compression and heating are performed by the compressor. Fuel is then added in the combustion chamber and ignited according to a proper mixture ratio. The exhaust stream gains additional energy due to burning. The overall energy extracted is used for a dual purpose: a small amount is required by the turbine, to drive the compressor, while the rest is employed to produce thrust, a process which is affected by the geometry of the exhaust nozzle. As the exhaust gas passes through the nozzle, it is accelerated to high speed due to the expansion. The thrust produced can be increased by the pilot provided that an afterburner is incorporated. Military supersonic aircraft are usually powered by low bypass ratio turbofans with afterburners. These systems can be used to take-off and propel the vehicle to low supersonic speeds. On the other hand, unducted configurations like turboprops or propfans are not viable for hypersonic vehicles due to high levels of dynamic pressures they face over the flight [37].
The formula for specific thrust (the thrust F is made non-dimensional through the product of mass flow $\dot{m}$ by free stream speed of sound a_0) applied to a turbojet can be written as follows,

$$\frac{F}{\dot{m}a_0} = M_0 \left[\left\{ \left(\frac{\theta_0}{\theta_0 - 1} \right) \left(\frac{\theta_T}{\theta_0 \tau_c} - 1 \right) (\tau_c - 1) + \frac{\theta_T}{\theta_0 \tau_c} \right\}^{\frac{1}{2}} - 1 \right] \tag{3.15}$$

where the terms appearing are defined respectively:

- $\theta_0 \rightarrow$ is the incremental term for stagnation quantities, equal to $\left(1 + \frac{\gamma-1}{2} M^2\right)$;
- $\theta_T \rightarrow$ is the turbine inlet temperature ratio, equal to $\frac{T_4^0}{T_0}$;
- $\tau_c \rightarrow$ is the compressor temperature ratio, equal to $\frac{T_3^0}{T_2^0}$.

To get the specific impulse $I_{sp,TJ}$, it is sufficient to remember the definition:

$$I_{sp,TJ} = \frac{F}{\dot{m}_f \cdot g_0} \implies I_{sp,TJ} = \frac{F}{\dot{m}a_0} \cdot \frac{a_0}{f g_0} \tag{3.16}$$

where f represents the ratio $\frac{\dot{m}_f}{\dot{m}}$ ($\dot{m}$ refers to the inlet air mass flow). In Figure 3.5 a schematic view of the engine is portrayed.

Ramjet

A ramjet exploits the high speed of the aircraft to compress the air at the inlet of the engine, thus neither a compressor nor a turbine are required, greatly reducing the complexity compared to a conventional turbojet. However, due to the absence of a compressor, they cannot produce thrust at low Mach numbers, resulting in the necessity of either a propulsive mode transition or an accelerating carrier. They also present a

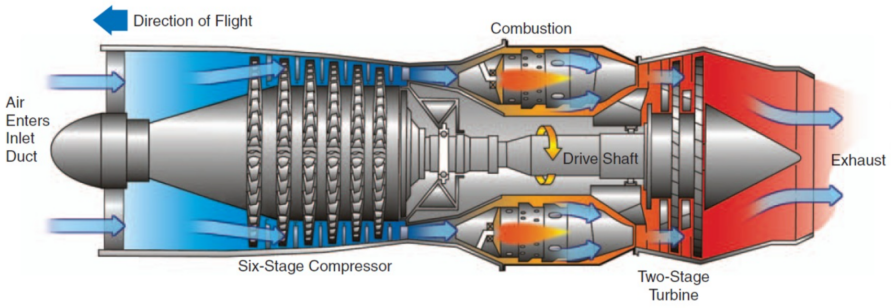

Figure 3.5: Turbojet engine.

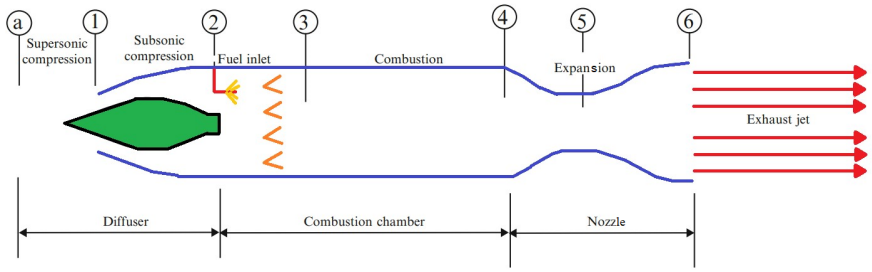

Figure 3.6: Ramjet engine.

functioning upper limit, around Mach 5.5. The principle of working is briefly described: the air is slowed going through the inlet, and the high dynamic pressure due to the kinetics is converted into higher static pressure, higher than freestream pressure. While the free stream velocity may be either subsonic or supersonic, the flow exiting the inlet of a ramjet is always subsonic. In other words, the combustion process in a ramjet is always subsonic. In the burner, a small amount of fuel is combined with the air and ignited, while flame holders are installed to enhance and localize the combustion process. Leaving the burner, the hot exhaust gases pass through a nozzle, which is shaped to accelerate the flow. A typical configuration is represented by a convergent-divergent nozzle. Since very little fuel mass flow is introduced in the burner, freestream mass flow and exit mass flow are approximately the same [38]. The specific thrust can be calculated through the following expression,

$$\frac{F}{\dot{m}a_0} = M_0\left(\sqrt{\tau_b} - 1\right) \tag{3.17}$$

where τ_b is defined as the combustion chamber temperature ratio, that is $\frac{T_4^0}{T_3^0}$. The specific impulse $I_{sp,RJ}$ is computed in the same way as the turbojet, starting from a different expression of the specific thrust as just illustrated.

$$I_{sp,RJ} = \frac{F}{\dot{m}a_0} \cdot \frac{a_0}{fg_0} \tag{3.18}$$

In Figure 3.6 a schematic representation of the engine is reported.

Scramjet

Scramjet stands for supersonic combustion ramjet. The working principle is the same as a ramjet, but the combustion occurs at supersonic speeds, which enables the engine to operate above the Mach limit of normal ramjets previously indicated. In fact, the high-speed airflow through the combustor allows for supersonic combustion, where the fuel is rapidly mixed and burned with compressed air. Scramjet engines are still under development, since potentially can lead aircraft to reach flight speeds in the order of Mach 10 and more. As for ramjets, they have a limited operational range at lower speeds, since they are not equipped with compressors and turbines. They are primarily intended for hypersonic flight applications where sustained high-speed operation is needed. Designing a scramjet engine is a complex task that requires expertise in several interconnected fields, such as aerodynamics, propulsion systems, materials science and computational modelling. As a matter of fact, supersonic combustion in scramjets introduces multiple technical challenges and issues that need to be addressed in order the engine operation to be successful. Key issues associated with supersonic combustion in scramjets include mainly inlet design, fuel-air mixing, flame stabilization, heat transfer, combustion efficiency, ignition and dynamic stability [39]. Naturally, a part of the same issues can be found in ramjet engines design process as well. The expression that can be derived through mathematical steps and physical considerations yielding the specific thrust is the following,

$$\frac{F}{\dot{m}a_0} = M_0 \left\{ \sqrt{\eta_{\mathrm{KEO}}(1+f)} \left[1 + \frac{\eta_b f \, h_{pr}}{c_p T_0 \theta_0} \right] - 1 \right\} \tag{3.19}$$

where the terms appearing are defined respectively as follows:

- $\eta_{KEO} \rightarrow$ is the total kinetic energy efficiency, falling into the range $0.65 < \eta_{KEO} < 0.75$;
- $\eta_b \rightarrow$ is the combustion chamber pressure drop ratio, that is $\frac{p_4^0}{p_3^0}$;
- $h_{pr} \rightarrow$ is the lower heating value of the fuel.

As regards the specific impulse, the same considerations done before apply here as well:

$$I_{sp,SJ} = \frac{F}{\dot{m}a_0} \cdot \frac{a_0}{f g_0} \tag{3.20}$$

In Figure 3.7 a schematic representation of the engine is illustrated.

Rocket

The rocket carries both fuel and oxidizer on board. This feature leads to two important consequences: it does not need atmospheric oxygen to generate combustion, thus

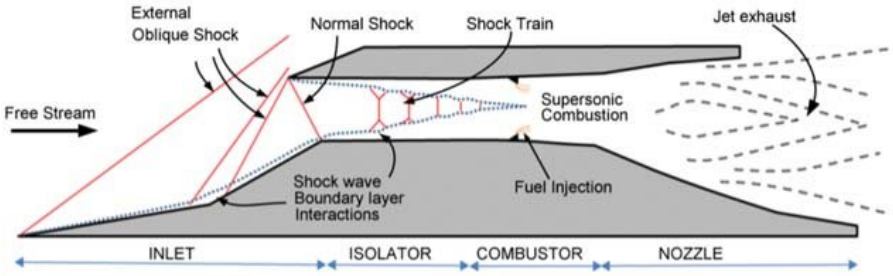

Figure 3.7: Scramjet engine.

its functioning is extended outside the atmosphere as well; it does not need an inlet, since both the oxidizer and the fuel are carried in dedicated tanks. Either solid or liquid propellant can be employed: the latter family is more reliable and permits a cryogenic storage, although a right insulation has to be guaranteed. They produce a constant amount of specific impulse during burning time, but their thrust depends on altitude because the exhaust nozzle is optimised to one expansion ratio. To overcome the issue, adaptable nozzles could be utilised, but the additional weight introduced as well as the increasing complexity are not worth the investment [37].
In the rocket case, the computation of the specific impulse requires some deeper considerations. As a matter of fact, it can be obtained through the following expression:

$$I_{sp,RK} = \frac{c^* C_F}{g_0} \tag{3.21}$$

where c^* and C_F are respectively the characteristic velocity and the coefficient of thrust of the rocket. As regards c^*, it is computed through:

$$c^* = \frac{\sqrt{RT_c}}{\Gamma} \tag{3.22}$$

where R is the universal gases constant, T_c is the combustion chamber temperature and Γ is the mass flow function, dependent only on γ.
On the other hand, C_F is defined as follows:

$$C_F = \frac{F}{p_c A_t} = \frac{\dot{m}_e w_e + A_e(p_e - p_0)}{p_c A_t} \tag{3.23}$$

By rearranging appropriately and through some mathematical steps, it is possible to obtain the final formulation:

$$C_F = \Gamma \sqrt{\frac{2\gamma}{\gamma - 1}\left[1 - \left(\frac{p_e}{p_c}\right)^{\frac{\gamma-1}{\gamma}}\right]} + \varepsilon\left(\frac{p_e}{p_c} - \frac{p_0}{p_c}\right) \tag{3.24}$$

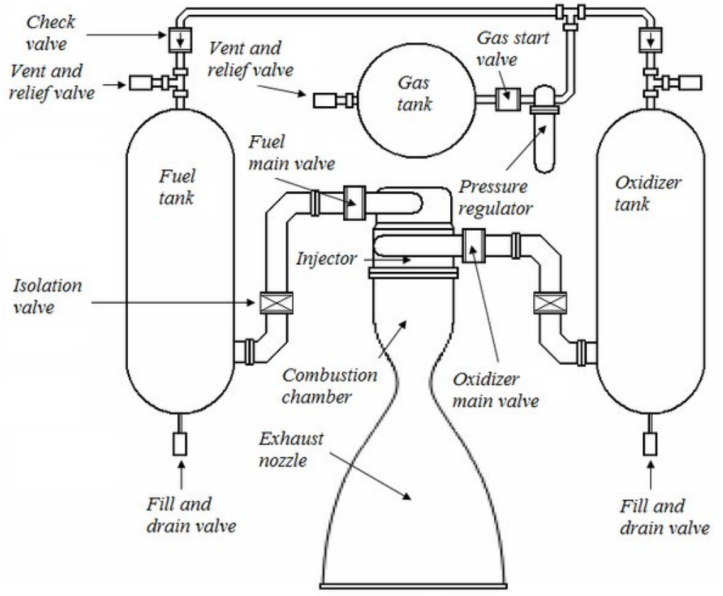

Figure 3.8: Example of liquid rocket engine with pressurized gas propellant feed system.

where it results clear how C_F is a function of Γ, γ,the exit section pressure p_e, the chamber pressure p_c, the free stream pressure p_0 and the expansion ratio ε, defined as $\frac{A_e}{A_t}$ (ratio between the exit section area and the throat section area). In Figure 3.8 a possible liquid rocket engine architecture is reported.

3.2.4 Trajectory and estimation of mass ratio m_r

In order to achieve a feasible conceptual design for a TSTO vehicle, the predicted trajectory must be an input, since it represents the core of the mission requirements. The main reason this is required is because the estimation of the total fuel mass and thus the overall mass ratio m_r are crucial in mass budget determination. Therefore, a model capable of assessing fuel consumption per each phase of flight is necessary. Despite lots of models are available, this paragraph will focus on Breguet's approach, since it has been implemented in ASTRID-H, the software developed by Politecnico di Torino for conceptual design of hypersonic vehicles.

Computation of fuel mass m_{ppl} per each segment

The presence of two stages leads to a complication in the formulation of the mass budget for the first stage. In fact, the release of payload has to be treated independently with respect to fuel consumption. For this reason, the well-known formula

$$\left(\frac{m_{ppl}}{m_{TO}}\right)_1 = 1 - \left(\frac{m_{LAN}}{m_{TO}}\right)_1 = 1 - \prod_{i=1}^{N_s}\left(\frac{m_{f,i}}{m_{f,i-1}}\right) \tag{3.25}$$

is not applicable anymore, since it would bring to wrong results due to the depletion of second stage. Therefore, the effect of payload plays a crucial role in the computation and a new formulation can be obtained:

$$\left(\frac{m_{ppl}}{m_{TO}}\right)_1 = 1 - \left[\prod_{i=1}^{N_{s,bs}} \left(\frac{m_{f,i}}{m_{f,i-1}}\right)\right] \cdot \left[\prod_{j=N_{s,bs}}^{N_s-1} \left(\frac{m'_{f,j+1} + m_{pay}}{m'_{f,j} + m_{pay}}\right)\right] \tag{3.26}$$

where:

- $N_{s,bs}$ is the number of segments before separation occurs (the last segment shows separation at its end);
- $m_{f,i}$ is the mass of first plus second stage at the end of segment i;
- N_s represents the total number of segments for stage 1, including the ones after separation;
- $m'_{f,j}$ is the mass of only first stage at the end of segment j;
- m_{pay} is the overall mass of second stage, namely the payload of stage 1.

As far as the second stage is concerned, Equation 3.25) is still valid, provided that in the first term the denominator m_{TO} is replaced with $m_{G,2}$, that is the initial gross mass of second stage at separation. In fact, referring to take off mass as regards the second stage would not make any sense. To achieve the mass ratio m_r, we use its definition:

$$(m_r)_n = \frac{1}{1 - \left(\frac{m_{ppl}}{m_i}\right)_n} \tag{3.27}$$

where $i = TO,\ n = 1$ for the first stage, whilst $i = G_2,\ n = 2$ for the second. Figure 3.9 illustrates a hypothetical trajectory of both stages: obviously, before separation, stage 2 is carried by stage 1, therefore its mass is constant.

Application of Breguet's formula to each segment

It is evident that m_r for each stage can be computed if the mass fractions per each segment of flight are estimated. The formula used to get them is here presented [40]:

$$\frac{m_{f,i}}{m_{f,i-1}} = e^{\left(\frac{-R}{V \cdot I_{sp} \cdot \left(\frac{L}{D}\right)}\right)} \tag{3.28}$$

which can be written alternatively as

$$\frac{m_{f,i}}{m_{f,i-1}} = e^{\left(\frac{-Rg \cdot SFC}{V \cdot \left(\frac{L}{D}\right)}\right)} \tag{3.29}$$

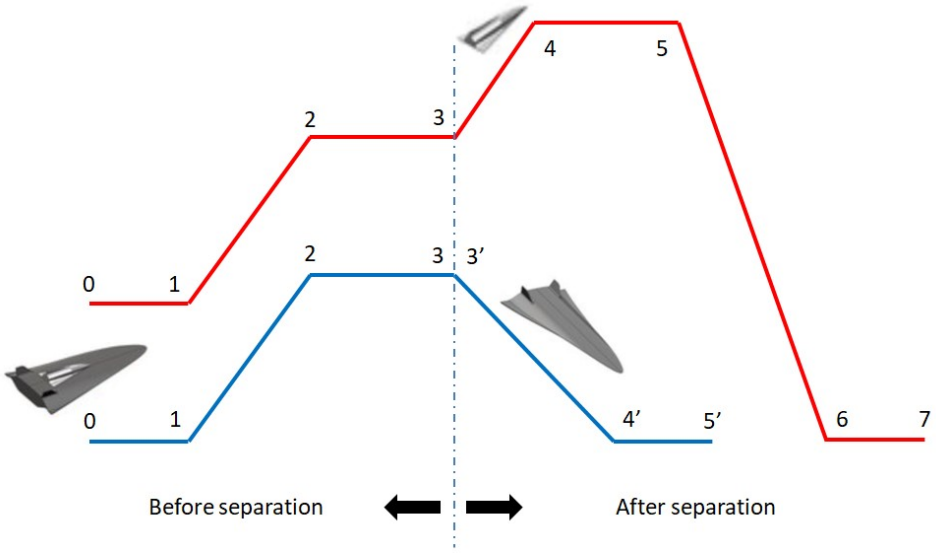

Figure 3.9: Example of trajectory for both stages. The apex ' refers to the mass of stage 1 after the depletion of stage 2.

where SFC is the specific fuel consumption of the engine mode of segment i, measured in $[kg/s/N]$, R is the range in $[m]$ covered by the stage considered in segment i, while V and (L/D) are respectively the reference speed of the phase $[m/s]$ and the aerodynamic efficiency of the phase [41]. It is worth noticing that the expression derived by Breguet lays its basis on some assumptions:

- it is obtained for cruise flight;
- SFC and L/D are constant in each segment considered.

If the second hypothesis can be accepted more easily, the first seems to restrict the validity of the formula only to cruise flight, excluding climb and descent phases. Nevertheless, a new derivation of Breguet's formula which is valid for both descent and ascent will be illustrated in Chapter 4.
For higher path angles, that can affect the trajectory of the rocket-propelled second stage, the employment of the Rocket equation seems more adapt:

$$\frac{m_{f,i}}{m_{f,i-1}} = e^{\frac{-\Delta V}{gI_{sp}}} \tag{3.30}$$

where $i-1$ and i represent respectively the initial and final instant of rocket-propelled phase, while ΔV takes into account also drag and gravity losses, that can be estimated on the basis of the predicted trajectory, and not only the increment of speed required to reach the target altitude in ideal conditions.

New formulation for mass ratio of first stage

As previously stated, the computation of fuel mass for the second stage does not represent a big deal, since it is not affected by a mass discontinuity as in the first stage instead. On the other hand, due to the utilization of the mass ratio m_r in the convergence procedure, it is crucial to get a reliable and consistent value for the first stage design, which can be based on take off mass and treated as there is not any separation. By referring to the hypothetical flight path in Figure 3.9 (blue line), each phase mass ratio contribution can be computed by using the Breguet's formula, but after separation, the fractions become based on a different mass value, the current one minus the second stage. In other words, if the mass ratio is computed by simply multiplying the single contributions over the trajectory, an overestimation of fuel mass is obtained as result of the design process, because the algorithm considers a higher mass value (due to the apparently not deployed second stage) also through the descent and landing path.
To tackle the issue, the Equation 3.26 seemed appropriate, but has a big problem: though it is formally correct, it is not applicable to determine the real mass ratio required, because the evolution of mass would be requested in advance, which is actually unknown until the end of convergence process. Therefore, an alternative way must be pursued, explained hereafter. From now on through the paragraph the following nomenclature is applied:

- $m_r \implies$ wrong mass ratio, computed through the application of Breguet's formula to each phase and multiplication of all the contributes;
- $m_r^* \implies$ correct mass ratio, adjusted through a coefficient to derive, in order to relate it to m_r, which is the output of Breguet's application, and to provide right results in terms of fuel mass considering the variable effect of second stage.

Referring to the hypothetical flight path in Figure 3.10, the mass ratio m_r would be calculated as follows:

$$m_r = \frac{m_a}{m_b} \cdot \frac{m_b}{m_c} \cdot \frac{m_c}{m_d} \cdot \frac{m_d}{m_e} \cdot \frac{m_e}{m_f} = \frac{m_a}{m_f} \tag{3.31}$$

The idea is to determine, as a function of known quantities before the mass breakdown is available, the real mass ratio m_r^* so as to:

$$m_r^* = k \cdot m_r \implies m_r^* = k \cdot \frac{m_a}{m_f} \tag{3.32}$$

The actual mass of propellant required can be obtained as follows (along the red line):

$$m_{ppl} = (m_a - m_d) + [(m_d - m_{pay}) - m_{f'}] = m_a - m_{pay} - m_{f'} \tag{3.33}$$

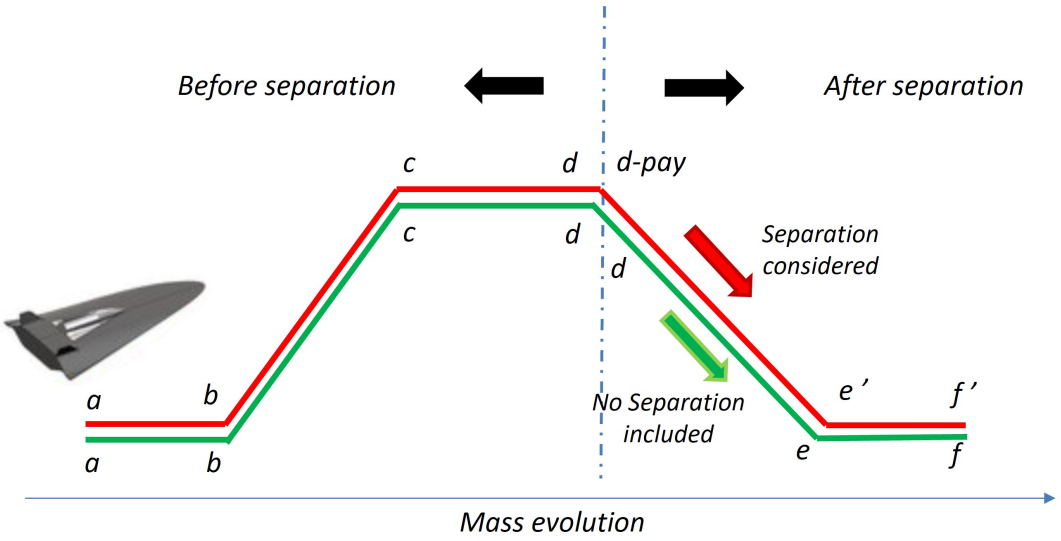

Figure 3.10: Generic mission profile for stage 1, where letters indicate the correspondent value of mass at the specific point along the path. The green line refers to the classical approach, through Breguet without any correction, whilst the red one takes into account stage 2 separation.

Thus, the actual mass ratio is given by:

$$m_r^* = \frac{m_a}{m_a - (m_a - m_{pay} - m_{f'})} = \frac{m_a}{m_{pay} + m_{f'}} \tag{3.34}$$

If Equation 3.31 and 3.34 are compared, it is possible to get:

$$m_r^* = \frac{m_a}{m_f} \cdot \frac{m_f}{m_{pay} + m_{f'}} \implies m_r^* = m_r \cdot \frac{m_f}{m_{pay} + m_{f'}} \tag{3.35}$$

Therefore, the expression of k is given by:

$$k = \frac{m_f}{m_{pay} + m_{f'}} \tag{3.36}$$

Through some mathematical manipulation, the aim is expressing k as a function of known quantities. Let's introduce here $m_{r,bef}$ and $m_{r,aft}$, respectively the mass ratio computed up to the separation event (before) and the mass ratio required for the post-separation phases (after). Clearly, $m_{r,bef} \cdot m_{r,aft} = m_r$. Consequently:

$$k = \frac{\frac{m_f}{m_d}}{\frac{m_{pay}+m_{f'}}{m_d}} = \frac{1}{m_{r,aft}} \cdot \frac{1}{\frac{m_{pay}+m_{f'}}{m_d}} \tag{3.37}$$

The second factor can be obtained remembering that, for definition:

$$m_{r,aft} = \frac{m_d - m_{pay}}{m_{f'}} = \frac{m_d}{m_f} \tag{3.38}$$

Therefore:

$$\frac{m_d - (m_{pay} + m_{f'}) + m_{f'}}{m_{f'}} = m_{r,aft} \implies \frac{m_{pay} + m_{f'}}{m_d} = 1 + \frac{m_{f'}}{m_d}(1 - m_{r,aft}) \tag{3.39}$$

By combining Equation 3.39 with 3.37 and 3.32, the following expression is determined:

$$m_r^* = \frac{m_r}{m_{r,aft}} \cdot \frac{1}{1 + \frac{m_{f'}}{m_d}(1 - m_{r,aft})} \tag{3.40}$$

The ratio $m_{f'}/m_d$ can be managed appropriately (for $m_{f'}/m_f$, the Equation 3.38 is used):

$$\frac{m_{f'}}{m_d} = \frac{m_{f'}/m_f}{m_d/m_f} = \frac{1 - \frac{m_{pay}}{m_d}}{m_{r,aft}} \tag{3.41}$$

After the substitution, it is obtained:

$$m_r^* = \frac{m_r}{m_{r,aft}} \cdot \frac{1}{1 + \frac{1 - \frac{m_{pay}}{m_d}}{m_{r,aft}}(1 - m_{r,aft})} \tag{3.42}$$

If the equation is rearranged more suitably, it is determined:

$$m_r^* = m_r \cdot \left[\frac{1}{\frac{m_{pay}}{m_d}(m_{r,aft} - 1) + 1} \right] \tag{3.43}$$

Finally, if we multiply both m_{pay} and m_d by m_a, the conclusive formulation is achieved:

$$m_r^* = m_r \cdot \left[\frac{1}{\frac{m_{pay}}{m_a} \cdot m_{r,bef} \cdot (m_{r,aft} - 1) + 1} \right] \tag{3.44}$$

Equation 3.44 provides the adjusted value of mass ratio to put inside the successive iterating process, so as to obtain the actual amount of propellant mass required by the first stage, considering the effect of stage separation. The great advantage of this formulation lays its basis on the fact the 4 data required are already available from the trajectory only and from statistical correlations. In fact, $m_r, m_{r,aft}$ and $m_{r,bef}$ are a result of the trajectory chosen as input, whilst the ratio m_{pay}/m_a is nothing else than the ratio between payload mass and maximum take off mass for the first stage, which can be estimated quite confidently on the basis of a statistical analysis. Refined laws, depending also on the number of samples, could be feasible, but for the test case treated in this work, the following law has been derived as consequence of the statistical analysis carried out in chapter 2, after linearization of the upper curve shown in Figure 2.3:

$$m_a = 4.041 \cdot m_{pay} + 29.875 \quad [tons] \tag{3.45}$$

Since m_{pay} is given as a mission input, a good approximation of the ratio m_{pay}/m_a can be determined and used inside Equation 3.44. From now on, the equations will show simply m_r, meaning the corrected value m_r^* every time the first stage is treated.

3.2.5 Convergence between $m_{OE,w}$ and $m_{OE,v}$

The operative empty weight of the stage considered, either the first or the second, can be computed through an iterative process, involving two different expressions, until convergence between them is reached. The expressions describe respectively the weight budget and the volume budget of the stage and they are reported hereafter, made explicit in the variable m_{OE}. They follow the formulation provided by Coleman/Czysz [33].

$$m_{OE,w} = \frac{I_{str} K_w S_{pln} + C_{sys} + m_{cprv} + \frac{(T/W)\cdot m_r}{E_{TW}}(m_{pay} + m_{crew})}{\frac{1}{1+\mu_A} - f_{sys} - \frac{(T/W)\cdot m_r}{E_{TW}}} \tag{3.46}$$

$$m_{OE,v} = \frac{\tau S_{pln}^{1.5} \cdot (1 - k_{vv} - k_{vs}) - V_{fix} - V_{pay} - V_{crew}}{\frac{1}{I_P} + k_{ve} \cdot (T/W) \cdot m_r} - m_{pay} - m_{crew} \tag{3.47}$$

All the variables appearing are collected and explained, also in terms of suitable range to fall within, in Table 3.2.

It is very crucial to remember that this iteration process involves three variables, organized on the basis of a hierarchical choice. As a matter of fact, the inner iteration is performed on S_{pln}, when all the other parameters appearing in the 2 equations have been determined. During the first inner iteration, since S_{pln} is just a guess, Equation 3.46 and 3.47 will surely give different results. The process of S_{pln} update is repeated until both Equation 3.46 and 3.47 lead to the same value, within a certain tolerance. Once this condition is achieved, a possible design point is identified and stored as a row into a matrix, consisting of the resulting S, m_{OEW}, m_{ppl}, m_{TO}, W/S, V, T/W and τ.

Each row of the matrix provides a potential design point reiterating exactly the explained process over τ, which represents the middle-loop iteration. In fact, the user is asked at the beginning the configuration he desires to choose for the design of the stage. Depending on the configuration defined and the sampling frequency inside the corresponding τ range, the number of τ iterations and their values are fixed. In this way, once τ is fixed during a specific iteration, also K_w and m_r are frozen.

A certain number of matrixes like the one described are produced for a specific stage, depending on the number of T/W values that are given as input by the user. In fact, the user is asked to type an interval of T/W values in which the vehicle category falls and to define how many samples to pick inside the range. This type of iteration is at a higher level with respect to τ, resulting during a fixed step of this outer loop in a frozen T/W value for the equations.

As far as all the other coefficients are concerned, they are either chosen to be the aver-

age inside their typical range or computed by using combinations of trajectory and input data. As consequence of that, at the end of the iterative design process of a stage, a stack of matrixes of potential design points is available. To decide among all the found points, Matching Chart Analysis, or Multiple Matching Chart Analysis (MMCs) if needed, is carried out.

3.2.6 Multiple Matching Chart Analysis

In 1980s, NASA introduced a simple way of representing propulsion plant requirements matching with vehicle configuration within the so-called Matching Chart (MC). It consists of a graphical representation of all the high-level propulsion and aerodynamic requirements of the aircraft on a 2D chart, expressed through mathematical equations relating T/W to W/S for each mission segment. In other words, this chart allows the identification of a feasible design space and the definition of a design point describing the optimal vehicle configuration in terms of maximum thrust, maximum take-off mass (MTOM), and wing surface [42].
Thus, the objective of this part of the methodology is to identify the optimal design point in terms of $T/W = f(W/S)$. Obviously this is achieved by representing all the necessary constraints related to the different segments of mission that the vehicle, either the second stage or the carrier, is expected to go through. In case typical subsonic aircraft are considered, only one chart is necessary, because they are conceived to operate in just one design condition. On the other side, SSTO vehicles, high-speed transportation aircraft and TSTO vehicles may involve several power plant design conditions, due to different flight regimes, from subsonic to hypersonic, and in certain cases also stage separation events. This leads to significant differences in terms of mission profile and propulsion plant with respect to conventional aircraft, making the application of a pure MC analysis pointless and unreliable. To cover the wide spectrum of flight regimes and operative environments, a MC analysis per each flight mode is obtained, since it seems clear that a single MC is no more sufficient to represent the whole set of requirements. Examples of issues emerging from the employment of a single MC can be:

- the comparison between subsonic and hypersonic cruises requirements is not meaningful anymore, because in reality, the two cruise legs are performed by different engines or even by the same engine but working in different modes of operations;
- the normalization of T/W based on a specific altitude, typically sea level, is without any sense, because thrust requirements change not only with altitude but also with power plant and design conditions. Thus, different reference altitudes thresholds shall be identified per each flight phase.

As consequence of that, an overestimation of the T/W requirement is encountered unless a Multiple MCs (MMCs) approach is pursued. A MMCs analysis is a high-level

Par.	Name	Expression	Range	Origin
I_{str}	Structural index	$10\frac{I_P}{ICI}$	-	I_P and ICI computation
K_w	-	$\frac{S_{wet}}{S_{pln}}$	-	Kuchemann's chart
S_{pln}	Planform area	-	-	Iterative update
C_{sys}	Constant system mass	$C_{un} + f_{mnd} \cdot N_{cr}$	$1900 < C_{un} < 2100\ kg$ $1050 < f_{mnd} < 1450\ \frac{kg}{pers}$	Statistics
m_{cprv}	Crew provision mass	$f_{pcrv} \cdot N_{cr}$	$450 < f_{cprv} < 500\ \frac{kg}{pers}$	Statistics
(T/W)	Thrust-Weight ratio	-	-	Multiple Chart Analysis
m_r	Mass ratio	-	-	Trajectory
E_{TW}	Effective take-off weight	-	$4 < E_{TW} < 25\ \frac{kg\ thrust}{kg\ weight}$	Statistics
m_{pay}	Payload mass	-	-	Input
m_{crew}	Crew mass	$m_p \cdot N_{cr}$	-	Crew features
μ_A	Inert weight margin	$m_{max,i} - m_{act,i}$	Very little ($\approx$ negligible)	Statistics
f_{sys}	Variable system mass	-	$0.14 < f_{sys} < 0.24\ \frac{kg}{kg}$	Statistics
τ	Slenderness parameter	$\frac{V_{tot}}{S_{pln}^{1.5}}$	-	Input from configuration
k_{vv}	Void volume coeff.	-	$0.1 < k_{vv} < 0.2\ \frac{m^3}{m^3}$	Statistics
k_{vs}	Variable system volume	-	$0.02 < k_{vs} < 0.04\ \frac{m^3}{m^3}$	Statistics
V_{fix}	Constant system volume	$V_{un} + f_{crew} \cdot N_{cr}$	$5 < V_{un} < 7\ m^3$ $11 < f_{crew} < 12\ \frac{m^3}{pers}$	Statistics
V_{pay}	Payload volume	$\frac{m_{pay}}{\rho_{pay}}$	$48 < \rho_{pay} < 130\ \frac{kg}{m^3}$	Input
V_{crew}	Crew volume	$(k_{cprv}+k_{crw}) \cdot N_{cr}$	$5 < k_{cprv} < 6\ \frac{m^3}{pers}$ $0.9 < k_{crw} < 2\ \frac{m^3}{pers}$	Statistics
I_P	Propulsion index	$\frac{\rho_{ppl}}{m_r - 1}$	-	Input+trajectory
k_{ve}	Engine volume coeff.	-	$0.25 < k_{ve} < 0.75\ \frac{m^3}{tons\ thr}$	Statistics

Table 3.2: List of parameters appearing in the mass equations.

requirements and performance assessment, carried out for each speed regimes separately. Naturally, a synthesis among the charts is necessary to guarantee the fulfillment of some physical and geometrical constraints. Indeed, even if the MMC brings the designers to define different scales to draw T/W requirements for the various flight regimes, this is not applicable for the W/S requirements, since the wing surface cannot change during flight. Therefore, iterations shall be carried out to identify a unique value of wing surface able to generate the required amount of lift in each flight phase [42].
It is crucial to stress the importance of the subsonic flight segment. The subsonic condition, and in particular, the landing requirement, generally drives the selection of the overall design point, being the most demanding requirement. In fact, a certain minimum value of surface shall be guaranteed to land safely, imposing a $W/S \leq (W/S)_{LAN}$ constraint. In reality, local design points for subsonic, supersonic, and hypersonic regimes are probably different in terms of required surface, because smaller wing requirements are asked at high speed regimes. Moreover, the selection of a suitable W/S at high speed is influenced by a lower vehicle mass (the take off mass is not an appropriate choice anymore to refer to), if compared to subsonic regimes, due to previous propellant consumption.
These different aspects contribute to define local design points for each regime (i.e. for each MC), identified by specific values of W/S and T/W. The consistency of the final solution shall be guaranteed, iterating the process up until all selected design points are characterized by the same wing surface (determined within the most critical flight regime) as well as by the reference mass of the considered phase, as qualitatively shown in Figure 3.11. The target value of thrust to be used for the sizing of the propulsion plant will then be the one corresponding to the value of W/S specified by the consistency requirement, which typically does not coincide with the local design point in supersonic and hypersonic regimes. Indeed, in the subsonic case, global and local solutions usually coincide, for its criticality concerning the wing planform area.

This analysis is carried out by relying on a MATLAB code developed by the Aerospace Engineering Department of Politecnico di Torino, which was accurately customized for fitting with the methodology presented. The Multiple Matching Chart function inherits as input all the potential design points stored into the stack of matrixes and overlaps them to the constraint curves graphically in a chart $T/W = f(W/S)$. Then it identifies the point that best approximates the overall design point coming from only the constraint curves themselves, based on two conditions that shall be satisfied:

- $(T/W)^* \geq (T/W)_{MCA}$
- $(W/S)^* \leq (W/S)_{MCA}$

where the magnitude with $*$ refer to the selected design point coming from all the potential ones. Naturally, the denser the sampling frequency of potential design points, the smaller the error between the voted point and the design point coming from the

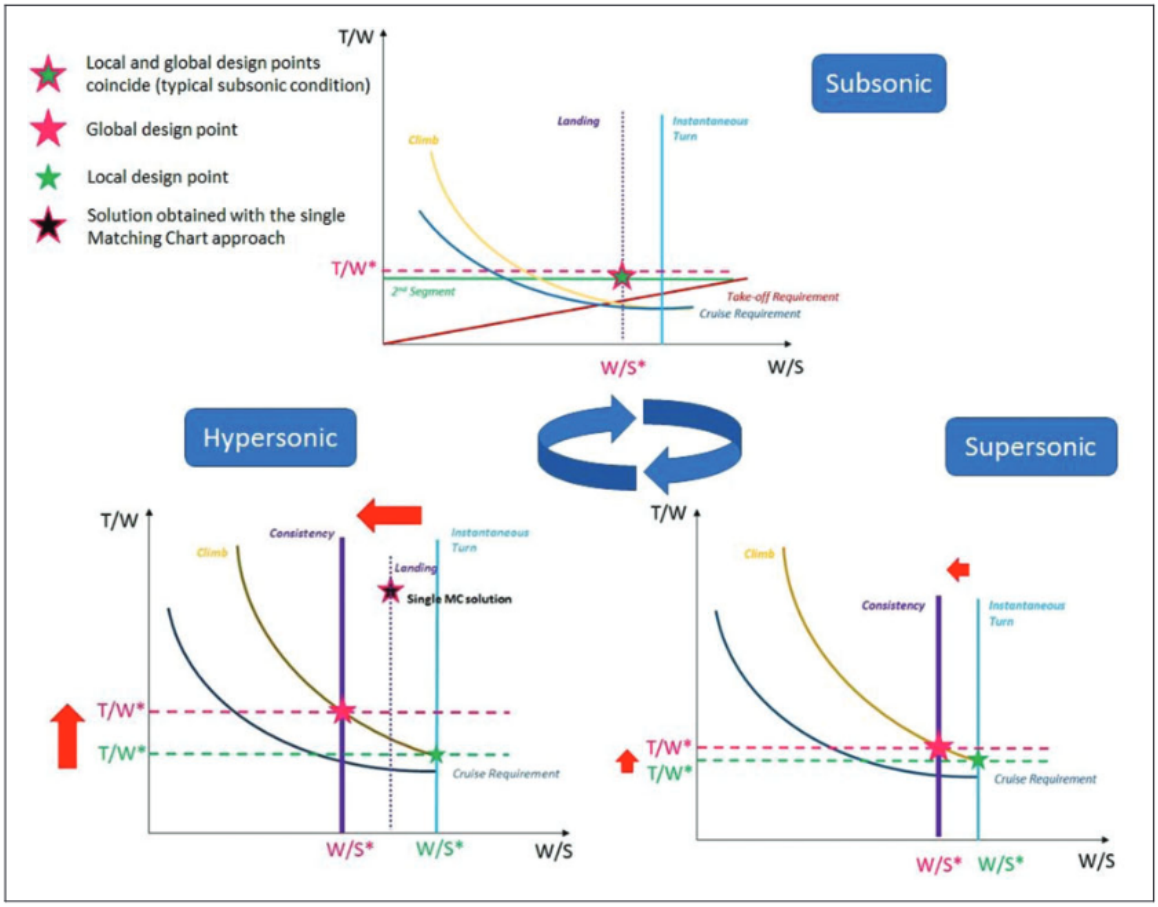

Figure 3.11: Multiple Matching Charts approach for SSTO, TSTO and HST vehicles design.

MMCs analysis. Once the design point has been selected, it is saved and stored into either the second row of a matrix (if the second stage is sized) or the first (if the first stage is sized instead) and the sizing process is terminated.
According to the stage considered, different constraints are due to be applied, as shown in Table 3.3. Depending on the specific mission scenario, different requirements have to be included: here, a HTHL TSTO vehicle typical mission is considered.
Every time W appears into an expressions defining requirements, it has to be intended in kg, not in N, unless explicitly stated. On the other hand, T/W is always dimensionless.

Carrier (1st stage)	CAV/SC (2nd stage)
Take-off distance	Target altitude achievement
Climb gradient with OEI	Climb rate (hypersonic)
Climb rate (subsonic, supersonic, hypersonic)	Cruise (hypersonic)
Cruise (subsonic, supersonic, hypersonic)	Landing distance
Instantaneous Turn	-
Sustained Turn	-
Landing distance	-

Table 3.3: Main constraints involving T/W and W/S for a TSTO vehicle.

Take off distance requirement

The constraint to impose involving the dynamics of the carrier including the second stage at take off is as follows [40]:

$$\left(\frac{T}{W}\right)_{TO} \geq \frac{1}{\rho_{sl}\sigma C_{L,max} \cdot TOP}\frac{W_{TO}}{S} \tag{3.48}$$

The relation is linear and depends on:

- the altitude of the airport, since $\sigma = \rho/\rho_{sl}$;
- the maximum coefficient of lift at take off $C_{L,max}$;
- the Take-Off Parameter TOP. According to Roskam, page 98, for FAR 25 certified aircraft, the take off field length s_{TOFL} is directly proportional to TOP. By converting from imperial to IS units:

$$s_{TOFL}[m] = 2.3413 \left[\frac{m^3}{kg}\right] \cdot TOP \left[\frac{kg}{m^2}\right] \tag{3.49}$$

The value of TOP can be achieved by setting a limitation in the s_{TOFL} and putting it in Equation 3.48. The linearity in Equation 3.48 is justified by considering that:

- using a large wing causes the aircraft to decrease the take off speed due to higher lift, thus a smaller engine may be enough;
- using a small wing causes the aircraft to increase the take off speed due to lower lift, thus more thrust is required.

Climb gradient with OEI at 2nd segment requirement

The second segment is the portion of flight path during take-off starting from gear-up altitude (after the 35 ft obstacle) and ending at 400 ft minimum. Climb gradient G is defined as the ratio between vertical and horizontal components of speed. It can be related to the path angle γ through $G = tg\gamma$ ($\approx sin\gamma$ if γ is reasonably small). FAR 25 requests the following for the so-called 2nd segment climb gradient after takeoff, with one engine inoperative:

- 2.4 % gradient G for aircraft with 2 engines;
- 2.7 % gradient G for aircraft with 3 engines;
- 3 % gradient G for aircraft with 4 engines.

Accordingly to calculations provided by [43], the requirement is formulated as follows:

$$\left(\frac{T}{W}\right)_{OEI} \geq \frac{N_{eng}}{N_{eng}-1}\left(\frac{1}{E}+G\right)\frac{1}{\sigma} \tag{3.50}$$

where N_{eng} is the number of engines ad E represents the aerodynamic efficiency in the second segment of climb. This requirement is not affected by W/S, thus in the chart is shown as a horizontal line.

Climb rate requirement

The climbing phase can be encountered through the all three flight regimes, namely subsonic, supersonic and hypersonic. Despite they certainly present different numerical values, the formulation of the climb requirement is formally the same. The MMCs approach establishes three different requirements for climb rate, one per each phase since the coefficients change. By assuming null acceleration, the dynamic balance equation along the longitudinal axis of the aircraft is (W in Newton here):

$$T - D - W sin\gamma = 0 \tag{3.51}$$

Rearranging Equation 3.51 and multiplying each side by V_∞ it yields:

$$V_\infty \cdot \frac{T-D}{W} = V_\infty sin\gamma = ROC \tag{3.52}$$

Finally, if drag is made explicit under the assumption of parabolic lift-drag polar and remembering trigonometry, namely $cos^2\gamma = 1 - sin^2\gamma$ the following expression is obtained:

$$\left(\frac{T}{W}\right)_{cl} \geq \frac{ROC}{V_\infty} + \frac{q_\infty C_{D0}}{gW/S} + \frac{1 - (\frac{ROC}{V_\infty})^2}{q_\infty e\pi AR/g} \cdot \frac{W}{S} \tag{3.53}$$

It is clear that this constraint depends on the rate of climb ROC (alternatively the climb gradient $G = tg\gamma \approx ROC/V_\infty$), the velocity, aerodynamics, aspect ratio AR and dynamic pressure. The entire expression has to be corrected by a factor taking into account the altitude, namely σ. If σ is not included, the thrust requirement is underestimated, since Equation 3.53 is valid at a certain altitude, changing with time. For instance, in case a subsonic climb is considered, the correction to do is:

$$\left(\frac{T}{W}\right)_{cl,TO} = \left(\frac{T}{W}\right)_{cl} \cdot \frac{W_{cl}}{W_{TO}} \cdot \frac{T_{TO}}{T_{cl}} \tag{3.54}$$

Therefore, in a single chart, the ratio T/W has to be referred to the initial condition of flight, namely the take off for a subsonic climb. Not considering the mass ratio due to propellant consumption results in a conservative approach, but the inclusion of $\frac{T_{TO}}{T_{cl}}$ is mandatory. In the troposphere, $\frac{T_{TO}}{T_{cl}} = (\frac{1}{\sigma})^k$, with $k = 0.823$. Actually, the correction should consider also the effects of velocity and throttle, but here are neglected. Outside the troposphere, the exponent will be different but there's still a decrease of thrust with altitude [44].
Despite the requirement expressed in Equation 3.53 is formally correct, for practical uses and for consistency of implementation on the tool all over the flight regimes, the requirement is defined as follows:

$$\left(\frac{T}{W}\right)_{cl,i} \geq \left(\frac{q_\infty C_D}{gW/S} + G_i\right) \cdot \frac{1}{\sigma^* \phi} \tag{3.55}$$

where ϕ indicates the throttle, σ^* refers to the density ratio normalized to the reference altitude for the phase (i.e. equal to σ only for subsonic segment) and i shows the specific phase considered. Indeed, the climb gradient G_i can be different depending on $i =$ subsonic, supersonic or hypersonic. Only for subsonic flight, $C_D \approx C_{D0}$.

Cruise requirement

Cruise is a typical phase encountered by an aircraft during its mission profile, thus an equivalent reasoning is valid as for the climb rate requirement: different charts have to be considered, according to the flight regimes involved. It means that a new requirement is demanded for cruise every time a switch from a flight regime to another occurs and at stage separation, since the vehicle changes. Cruise conditions are simply described by

the following couple of equations (W is in Newton here):

$$L = W \tag{3.56}$$

$$T = D \tag{3.57}$$

By dividing appropriately, it yields $T/W = D/L$. If we explicit the drag under the assumption of parabolic polar and the lift, that is $L = QSC_L$, the requirement is formulated as follows:

$$\left(\frac{T}{W}\right)_{cr} \geq \frac{q_\infty C_{D0}}{gW/S} + \frac{g}{q_\infty e\pi AR}\frac{W}{S} \tag{3.58}$$

This is formally similar to the climb rate requirement, where now $G = 0$. As for climbing, the actually implemented formulation of the requirement appears as follows:

$$\left(\frac{T}{W}\right)_{cr,i} \geq \left(\frac{q_\infty C_D}{gW/S}\right) \cdot \frac{1}{\sigma^* \phi} \tag{3.59}$$

where the same considerations about σ^* and i apply.

Landing requirement

Landing conditions require the introduction of the stall velocity V_s, as the minimum speed the aircraft can achieve provided $C_{L,max}$ is attained (flap extracted condition). Actually, during the approaching phase, the velocity is V_A (approaching velocity) prescribed to be equal to $1.3V_s$ according to the normative FAR 25. In formula:

$$\left(\frac{W}{S}\right)_{LD} \leq \frac{1}{2}\sigma\rho_0 V_A^2 C_{L,max} \tag{3.60}$$

Landing defines an upper limitation for the value of wing loading. In fact, higher values of $\frac{W}{S}$ would cause the aircraft to be too heavy to maintain the landing path at given $C_{L,max}$ and V_A. Moreover, the landing distance at ground (not including the safety factor of 0.6 to add also the approaching phase from an height of 50 fts) s_{LFL} can be computed through the following expression (the units are m and m/s)[35]:

$$s_{LFL} = 0.3455 V_A^2 \tag{3.61}$$

It means that a constraint in either V_s or s_{LFL} defines V_A. $C_{L,max}$ is given by the aerodynamic characterization instead. The Equation 3.60 is referred to the weight at landing. To be useful for plotting reasons, it is crucial to trace back to the equivalent wing loading at the beginning of flight, which is take off is the vehicle is a carrier, alternatively the mass at separation for a reusable second stage vehicle with horizontal

landing:

$$\left(\frac{W}{S}\right)_{LAN,in} = \left(\frac{W}{S}\right)_{LAN} \cdot \frac{W_{in}}{W_{LAN}} \tag{3.62}$$

Target altitude achievement

The main purpose of the mission is enabling the second stage to reach the target altitude, which can be either orbital or suborbital. In any case, a certain ΔV has to be achieved. The final expression relating T/W and W/S associated to target altitude requirement at the end of this paragraph derives from [36]. Here the main steps are reported.

- The rocket equation is applicable, but drag losses and gravity losses have to be taken into account, on the basis of the altitude reached. It means considering $\Delta V = \Delta V_{orbit} + \Delta V_{loss}$:

$$\Delta V = I_{sp} \cdot g_0 \cdot ln\left(\frac{W_i}{W_f}\right) \tag{3.63}$$

- If Equation 3.63 is rearranged by making I_{sp} explicit and dividing each member by W , it yields:

$$\frac{T}{W} = \frac{W_{ppl}}{W} \cdot \frac{\Delta V}{g_0 t_b} \cdot \frac{1}{ln\left(\frac{W_i}{W_i - W_{ppl}}\right)} \tag{3.64}$$

- At this point, a semi-empirical formulation of the Propulsion Index I_p is introduced, which is a function of the maximum Mach number attainable with the propulsion system chosen [4]:

$$I_p = \frac{\rho_{ppl}}{W_R - 1} = 107.6 \cdot 10^{-0.081M} \tag{3.65}$$

- By remembering the definition of W_R and rearranging Equation 3.65, we get as follows:

$$W_{ppl} = \frac{\rho_{ppl} \cdot W_f}{I_p} \tag{3.66}$$

- A crucial step consists of expressing W_f as a function of S_{pln}. In this way, Equation 3.64 relates directly T/W to W/S. To accomplish that, a formulation of S_{pln} is provided [4]:

$$S_{pln} = \left[\frac{I_p}{I_{str}} \cdot \left(\frac{K_w}{\tau}\right) \cdot \frac{1}{K_v \cdot K_{str}} \cdot \left(1 + \frac{W_{pay}}{W_f}\right)\right]^{1.409} \tag{3.67}$$

- All the parameters I_{str}, K_w, K_v and K_{str} can be obtained either through statistical analysis or by semi-empirical correlations in the variable τ [36]. By isolating W_f and putting it inside Equation 3.66, a new expression of W_{ppl} is obtained:

$$W_{ppl} = \frac{\rho_{ppl} W_{pay} K_w}{(W/S)^{-0.71} \cdot W^{0.71} \cdot A - B} \tag{3.68}$$

where the complete expressions of A and B are:

$$\begin{cases} A = I_{str}\tau K_v K_{str} \\ B = I_p K_w \end{cases} \tag{3.69}$$

- In conclusion, by substituting Equation 3.68 in Equation 3.64, the final target altitude requirement can be formulated as follows:

$$\left(\frac{T}{W}\right)_{ht} \geq \frac{\rho_{ppl} W_{pay} K_w}{(W/S)^{-0.71} \cdot W^{1.71} \cdot A - W \cdot B} \cdot \frac{\Delta V}{g_0 t_b} \cdot \frac{1}{ln\left(\frac{1}{1-\frac{\rho_{ppl} W_{pay} K_w}{(W/S)^{-0.71} \cdot W^{1.71} \cdot A - W \cdot B}}\right)} \tag{3.70}$$

It results clear that in this expression W_i has been replaced by W, but they represent the same thing, that is the initial gross mass of second stage.

Instantaneous turn requirement

The instantaneous turn requirement is a key constraint for assessing military aircraft maneuverability, particularly for fighters. It measures the maximum load factor achievable during a turn, which also relates to structural integrity. For this reason, since also a TSTO or SSTO vehicle could go through high load factor turning maneuvers, this requirement can be applied to this category of aircraft too. The turn rate $\dot{\psi}$ is given by:

$$\dot{\psi} = \frac{g\sqrt{n^2 - 1}}{V} \tag{3.71}$$

where n is the load factor. Intuitively, n equal to 1 is required to sustain the aircraft, while the remaining load can be used to accelerate the vehicle in the horizontal plane on a circular trajectory. As a matter of fact, n is defined as follows:

$$n = \frac{q_\infty C_L}{gW/S} \tag{3.72}$$

The associated requirement is expressed in terms of W/S, not affecting T/W (it appears as a vertical line in the charts):

$$\left(\frac{W}{S}\right)_{ITR} \leq \left(\frac{q_\infty C_{L,\mathrm{MAX}}}{ng}\right)\frac{1}{\sigma} \tag{3.73}$$

The density correction can be usually referred to sea-level conditions, since the most of high-load maneuvers are per- formed at low speed, in subsonic conditions. In other regimes, altitude corrections may apply by replacing σ with σ^* [42].

Sustained turn requirement

Sustained turn is defined as a turn performed at constant altitude and speed. This is, similarly to the case of the instantaneous turn, a typical requirement for fighter aircraft, as well as hypersonic aircraft when maneuvers close to minimum speed during subsonic flight are possible to occur. Since it does not represent a primary importance constraint for the analysis of a TSTO vehicle, just the mathematical expression of the requirement is here reported:

$$\left(\frac{T}{W}\right)_{\text{STR}} \geq \left(\frac{q_\infty C_{D0}}{gW/S}\right)\frac{1}{\sigma} + \left(\frac{W}{S}g\left(\frac{n^2}{q_\infty \pi Ae}\right)\right)\sigma \tag{3.74}$$

Sustained turn maneuver is always associated to subsonic conditions, thus σ is normalized with sea level density [42].

3.3 Outputs

The sizing methodology illustrated so far is repeated two times, in case the user desires to obtain the conceptual design of a HTHL TSTO vehicle. On the contrary, the possibility to design a SSTO vehicle is permitted anyway, but obviously the overall procedure is iterated only once. The output of the sizing methodology consists of 5 main types of results per each stage considered:

- a N_r x N_c matrix, containing $T/W, W/S, m_{tot}, m_{OEW}, m_{ppl}, S_{pln}, V_{tot}, \tau$ and m_{pay}, where N_r is the number of rows (stages, either 1 or 2) and N_c is the number of columns.
- Two bar charts, representing respectively the general mass breakdown and the geometrical design magnitudes.
- A spider diagram indicating the deviation of the methodology obtained results from the reference values available in literature.
- A bar chart assessing the reliability of each of the results achieved, through the representation of relative errors in percentage on the basis of three acceptance regions.
- A series of charts, deriving from the combination of the multiple potential design points inherited by the pure sizing methodology and the graphical plot of the Matching Chart analysis (multiple in case more flight regimes and propulsion modes are involved for the stage considered).

In Figure 3.12, the flow chart of the entire methodology is reported for sake of clarity.

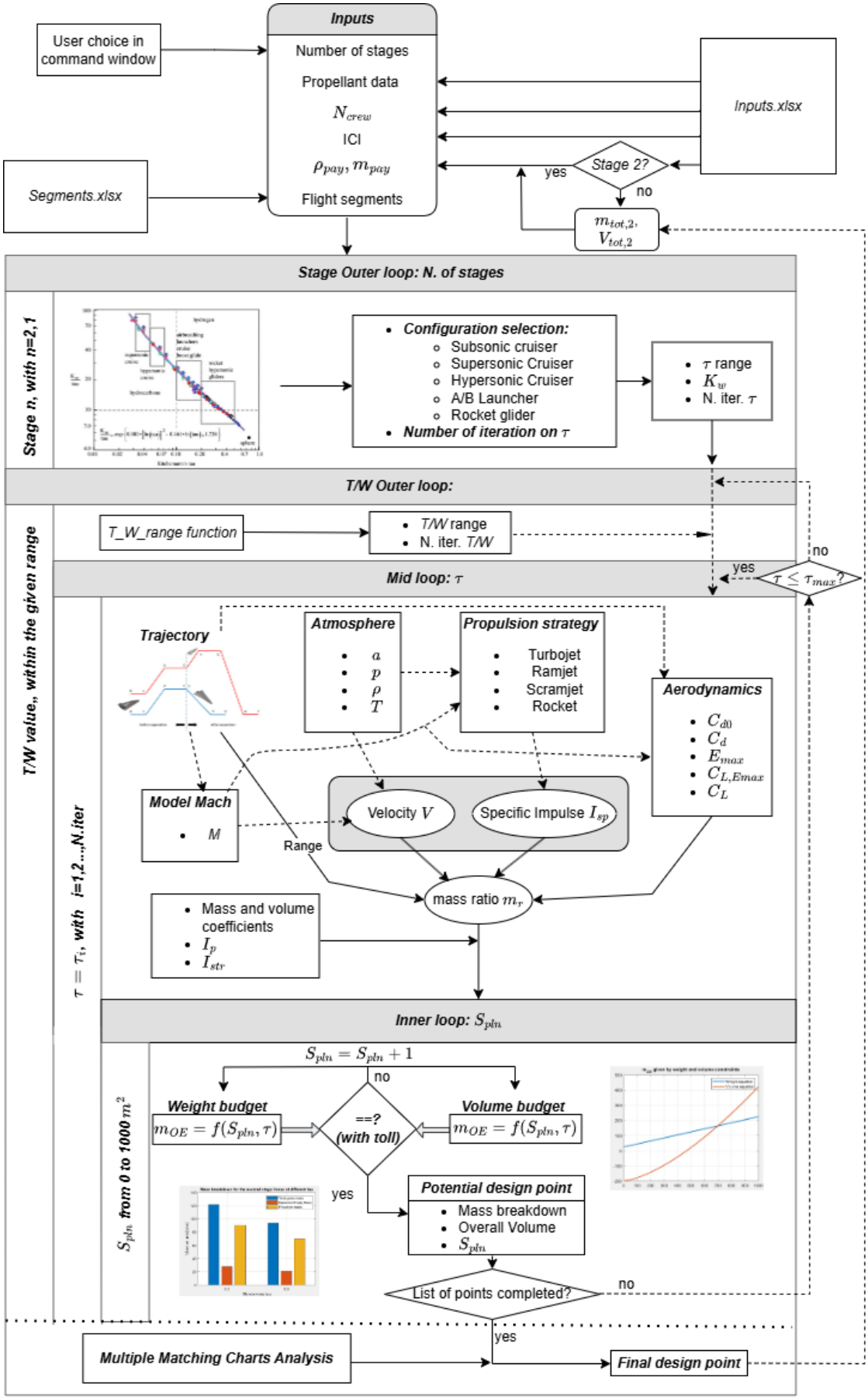

Figure 3.12: Flow chart of the methodology.

.

3.4 Further considerations about the first stage sizing

The presence of more than one stage implies a high-level iteration of the methodology, as if it had to be used to size another single-stage vehicle. The first high-level iteration aims at generating the conceptual sizing of the upper stage (namely the second). Once the upper stage is defined, the sizing of the lower one imposes some additional constraints:

- m_{pay} of the carrier has to be set equal to the m_G of the upper stage;
- The independent design variables of the carrier have to be modified accordingly to the requirements for the first part of the flight;
- The geometry of the upper stage affects the geometry of the carrier as well, for instance clearance from ground and spacing between fuselage and inboard engine (in case of underwing installation) are set as additional limitations in geometry computations.

Provided only two stages are considered, the methodology can be applied a second time for the carrier by paying attention to the modifications illustrated.
The third constraint mainly depends on the interface between first and second stage. As a matter of fact, as a preliminary discernment, the second stage can be classified either internal or external. The former case is conceptually similar to a classical vertical take-off launcher, since the separation involves the detachment of a smaller unit from a unique assembly. The latter case, more frequent on the basis of design examples found in literature as well as real technology demonstrations over the years, refers to a second stage located outside the first one, as they were two different units physically discernible even before separation, kept together by suitable links. This last situation involves both a carrier, typically a mother aircraft, and a cruiser (for high speed technology demonstrations) or a spacecraft (for either suborbital or orbital flight). This is the case that will be taken into account for the following considerations.
In case of more than 2 stages, a re-iteration of the methodology n-times (where n is the number of stages) shall be followed, by considering an update of the previous constraints each time moving from inner to outer stages .

Chapter 4

Test case

The considerations illustrated in the previous chapter are now tested through the implementation of a simplified version of the methodology applied to a specific case study, among the ones described in the statistical analysis part. Sänger II was chosen as reference case study, in particular the configuration involving the second stage Horus, as described hereafter.

4.1 Description of Sänger II concept

The Sänger II is a cutting-edge hypersonic vehicle design developed by Germany as part of its advanced aerospace ambitions in the 80s. Named after Eugen Sänger, a pioneer in rocket technology, Sänger II aimed at representing the advanced generation of high-speed aircraft. Capable of reaching speeds above Mach 5, this vehicle was designed for rapid global travel and potentially space access. Sänger II required a blend of advanced materials, propulsion systems, and aerodynamics to withstand the extreme conditions of hypersonic flight, pushing the boundaries of what was already possible in both military and civilian aerospace technology.

Figure 4.1: Sänger II during ascent.

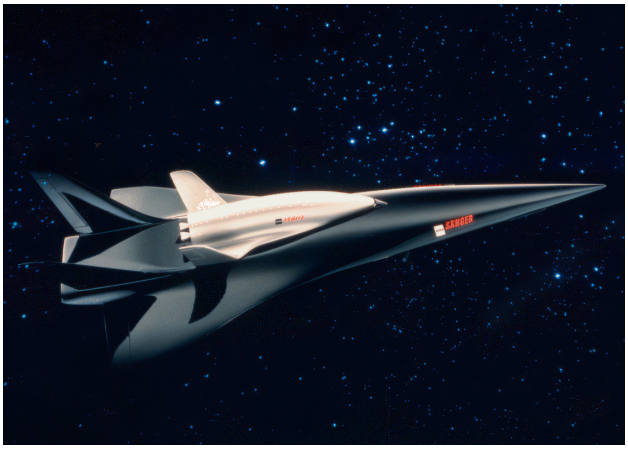

Figure 4.2: Reproduction of Sänger II.

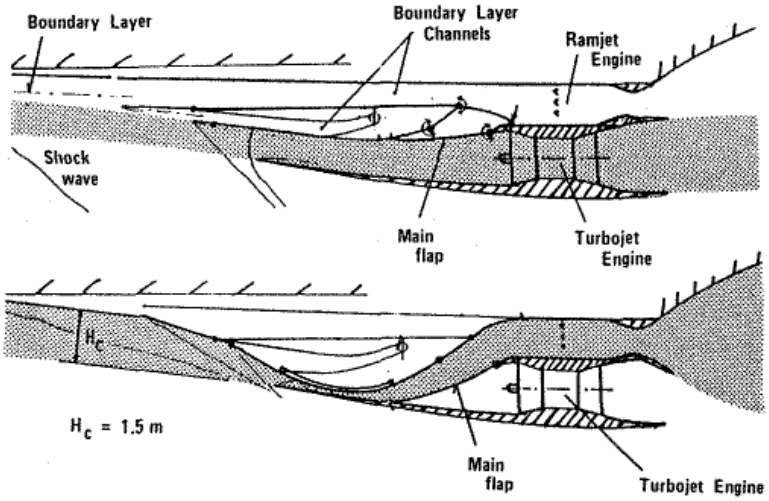

Figure 4.3: Variable air inlet, functioning either as turbojet or ramjet.

.

4.1.1 Technical features

The Sänger II is a HTHL TSTO vehicle, formed by a carrier, called EHTV (European Hypersonic Transport vehicle) and conceived for a dual purpose, that is serving either as the first stage of a launch vehicle with cruise capability or as 230-passenger plane with 10000 km range [18]. The EHTV is powered by 6 turbo-ramjet engines, resulting in a parallel arrangement for both flight regimes, with a variable air inlet. As shown in Figure 4.3, the engine is installed in the bottom part of the wing, since it guarantees an easier access for maintenance and leads the boundary layer through the ramjet duct. Whenever the EHTV is employed as launcher, its payload is represented by the second stage spacecraft. Two different second stage configurations were proposed:

- ***Horus***, a manned winged vehicle with small payload for space station supply missions and crew exchange;
- ***Cargus***, an expendable ballistic upper stage to carry payloads up to 15 *tons* to LEO orbit.

In the following sections, only one configuration will be considered for sizing purposes, namely Horus. In Table 4.1, the most relevant figures and data about Sänger II are gathered. It is paramount to stress the gross mass of the EHTV takes also into account the weight of the second stage that is transported, thus the value is different when the EHTV is simply used as passenger aircraft. As a matter of fact, Horus can be categorized as the first stage payload and the actual gross mass of the first stage only is easily computed by subtracting Horus's mass to the overall gross mass indicated, resulting in $340,000 - 91,000 = 249,000\ kg$. The reason why it was decided to include Horus mass into the first stage breakdown lies into the attempt of generalizing the sizing procedure

and the necessity of using the overall second stage's mass as input payload mass for the lower stage in the iterated process of sizing.

Characteristic	Stage 1 (EHTV)	Stage 2 (Horus)
Gross Mass	340,000 kg	91,000 kg
Empty Mass	149,000 kg	22,200 kg
Propellant Mass	100,000 kg (LH2)	65,500 kg
Payload Mass	91,000 kg (Horus)	3,300 kg
Thrust	1,500 kN (sl)	1,500 kN (vac)
Burn time	6,565 s	298 s
Isp	3,600 s (sl)	490 s (vac)
Diameter	14.00 m (45.00 ft)	5.50 m (18.00 ft)
Span	41.40 m (135.80 ft)	15.60 m (51.10 ft)
Length	84.50 m (277.20 ft)	27.60 m (90.50 ft)
Propellants	Air/LH2	LOX/LH2
N. Engines	6	1
Engine	Co-axial turboramjet	ATCRE (rocket)

Table 4.1: Technical Data of Sänger II - configuration EHTV+Horus.

4.2 Implementation of the methodology

4.2.1 Structure of the code for the tool

The MATLAB code implemented by Tommaso Molinari for a SSTO vehicle [45] has been reviewed and expanded with two main purposes in mind: generalization to a TSTO vehicle design procedure and modularity through functions, in order to make the code user-friendly. This subsection's objective is to illustrate and describe how the newest version of the code is organized.

Reading functions

Inputs are not given through the MATLAB main script: two different *Excel* files are required to be filled appropriately before running the code. For this reason, reading functions result necessary to import the data provided by the user to the workspace.

- ***read_inputs***: as the name suggests, its aim is to read and load input data from the *Excel* file *inputs.xlsx* to the workspace in MATLAB. Inputs are organized into two separated columns, starting from the upper stage, namely the second for a TSTO.

- ***read_segments***: the entire mission trajectory, which has to be an input, can be divided into several parts, each classified according to three criteria, namely the flight speed regime (subsonic, supersonic or hypersonic), the mission segment

(take off, climb, cruise, rocket ascent, glide or propelled descent) and the propulsion strategy employed (turbojet, ramjet, scramjet or rocket engine). The function reads each line of the *Excel* file *segments.xlsx*, corresponding to a precise segment of mission, and saves the information in the workspace. In this case, sheet 1 is used for the upper stage (the first to be processed into the design procedure) while sheet 2 refers to the lower one. Finally, *segments.xlsx* is an interactive worksheet since the list of segments can be chosen through a drop-down menu; once the choice is made, the not necessary boxes for that segment appear in red, meaning that they do not have to be filled with data, because the processing algorithm does not use them.

Performance functions

The core functions of the code are the ones computing performance or helping achieve it. In order to do that, aerodynamics, propulsion and trajectory represent crucial aspects to deal with. Though they seemed to work quite well in the computation of preliminary design results, these functions can be modified to estimate data more accurately.

- ***aerodynamics***: the values of τ, M and the type of flight segment are given as inputs. As explained in the previous chapter, the Curran Model is implemented for simplicity, where the outputs include $C_{D0}, C_D, E_{max}, C_{L,Emax}$ and C_L. The trajectory is divided into short segments where linearization gives quite reliable aerodynamic results.

- ***prop_ strategy***: propulsion strategy for a specific segment of flight is defined by this function. The inputs are represented by free stream atmospheric conditions, namely a, T_0 and p, free stream Mach number M and the type of propulsion required. This version of the code enables to choose among 4 types of engine: turbojet, ramjet, scramjet and rocket. The output is the specific impulse I_{sp}.

- ***mass_ ratio***: this is undoubtedly the paramount part of the entire algorithm, because it computes the mass ratio required in a specific part of a flight segment and then it integrates all the contributions over the whole trajectory. It receives as inputs τ, the specific phase, the type of engine as illustrated in *prop_ strategy* and a list of data requested for performance calculation, like flight path angle, initial and final altitude, time of segment and rocket features if the phase is rocket-propelled. These data are the ones inserted by the user in *segments.xlsx*. On the basis of the phase, different models are used: for cruise, climb and propelled descent Breguet's equation is employed, glide and take off are characterized by fixed values of mass ratios whilst rocket ascent mass ratio is determined through Tsiolkovsky's equation.

- ***mr_ correction_ 1stage***: the role of this function is to provide a correctly adjusted value of mass ratio for stage 1 sizing, avoiding the issue illustrated in section 3.2.4,

concerning the mass discontinuity due to second stage release. Naturally, it is applied only for the lower stage sizing.

- ***expEarthAtmosphere***: it enables to compute a, ρ, p and T (respectively sound speed, air density, pressure and temperature) at a specified altitude. The validity of the function is bounded to altitudes inferior to 100 km. It reveals to be particularly useful for the aerodynamic coefficients determination along the trajectory as well as for the propulsion strategy.

- ***mca_ stage1***: this function is essential in the last part of the first stage sizing procedure. In fact, it implements the Multiple Matching Charts Analysis for stage 1, which is required to go through 3 different flight regimes and see a propulsion operative mode change during its flight from turbojet to ramjet. Thus, it sends as output three different charts, combining the thrust and wing loading requirement curves with the net of potential design points inherited from the methodology.

- ***mca_ stage2***: this function is essential in the last part of the second stage sizing procedure. In fact, it implements the MMCs Analysis for stage 2, which is required to go only through one flight regime, namely hypersonic, and does not see a propulsion operative mode change during its flight, being simply rocket-powered. Thus, it sends as output one single chart, combining the thrust and wing loading requirement curves with the net of potential design points inherited from the methodology. The MMCs analysis, in this case, is actually a traditional Matching Chart analysis, because it doesn't requires changes in either flight regime or propulsion mode. Obviously, the reference mass is the mass at the instant of separation.

Customized models functions

Some functions have been developed considering the specific test case, that is Sanger II. For this reason, either the functions illustrated hereafter apply only to the specific case and not in general or can be customized differently to reach a varied degree of approximation in the calculations. Therefore, by modifying them suitably, other cases can be investigated.

- ***model_ Mach***: by referring to the ascent mission profile reported in [18], this function replicates through polynomial interpolation the relation $M(h)$ for the first stage from take off to second stage separation.

- ***Model_ Mach_ descent***: since no information is provided about the descent mission profile of first stage, a raw approximation has been made, that is a linear decrease of Mach number with altitude, up to landing. Moreover, both the ascent and the descent phases of second stage do not require knowledge of $M(h)$, due to different reasons: the former is based upon the rocket equation whilst the latter

is characterized by glide, that is a non-propelled phase, not important for sizing concerns.

- ***Model_ V_ losses***: this function was introduced to compute the ΔV losses during rocket ascent of second stage. The three main sources of loss are given by drag, gravity and not adapted nozzle. No precise models are considered here, but only approximations based on experience.

Plotting functions

To plot the most relevant results, two main functions were created to manage the outcomes of the sizing procedure more effectively.

- ***plot_ design_ mass***: by taking the results of the converged procedure in terms of mass budget (m_{OE}, m_{ppl} and m_{tot}), it plots the figures as bar charts for different values of τ. The payload mass is not depicted since it is a constant, provided as input by the user in *inputs.xlsx*. It works properly both for a SSTO and for a TSTO.

- ***plot_ area_ and_ volume***: the outcome is analogous to *plot_ design_ mass*, but the figures are different. In fact, here, both wing planform S_{pln} and overall volume budget V_{tot} are shown for several values of τ. Also in this case, it works properly both for a SSTO and for a TSTO.

- ***spider_ plot***: the aim of this function is to plot the final design results through a spider-like representation, by comparing the outcome of the methodology with the reference values available in literature or in data sheet. In this way, depending on the magnitude of the overlapping region and its contour precision, a visual estimation of the accuracy of results is provided.

- ***err_ rel_ plot***: the visual outcome of this function is a bar chart, illustrating, for each design variable obtained at the end of the sizing methodology, to what extent the found values deviate from the reference ones in terms of relative errors in percentage. Three different bands are highlighted, on the basis of the error's entity: acceptable, if the error is less than 25%, critical, if the error ranges from 25% to 50% and unacceptable, if the error exceeds 50%.

Other functions

For a complete description of the algorithm, other functions require to be presented, which have been implemented in order to make the functioning of the code more fluent and do not fit in a specific classification. okay

- ***Area_ wing_ Sanger2***: the purpose of this function, which does not directly affect the sizing algorithm, is to plot and compute the area of the wing planform of Sänger

II's first stage. Since a reliable value of wing area is not available in literature, the code replicates the shape from a drawing in scale and uses numerical integration to find the reference S_{pln}.

- ***call_mass_and_volume_coeff***: it is not an active function, it is simply used as a repository of most of the mass and volume coefficients appearing in Table 3.2. The function recalls the numerical values to the main code. Average values are considered as default.

- ***Tau_iteration***: this is a high-level function, since it manages the number of iterations on the slenderness parameter τ. The entire sizing methodology aims at reaching convergence given a certain value of τ, which is fixed. By choosing the number of iterations on τ, the code enables the user to obtain different converged configurations in order to determine the best. In other words, it represents the outer iteration loop. The user is also asked to choose the desired configuration for the stage considered (subsonic cruise vehicle, supersonic cruise vehicle, hypersonic cruise vehicle, air-breathing launcher or rocket glider), in order to iterate within a suitable range of τ, according to the classification in Figure 3.1.

- ***T_W_range***: this is a high-level function, since it manages the number of T/W sample values the user desires to obtain, within a typical range for the vehicle configuration chosen. Together with the number of τ iterations, it defines the overall number of potential design points resulting from the methodology, before the MCCs Analysis is carried out.

Main program

The set of functions previously described is used appropriately to generate the convergence process into the ***main***. The crucial steps are summarized in order as follows:

1. The user is asked the number of stages he desires to divide the hypersonic HTOL vehicle into. Only single or dual stage are permitted choices in this version of the program.

2. The input data written in *inputs.xlsx* are read and loaded in the workspace.

3. The most external loop is stage-based. It means that the process of convergence for different τ values is repeated for a specific stage, by starting from the upper. Then, in case of TSTO, the entire process is performed again for the lower stage.

4. *Tau_iteration* is called and the user opts for the desired configuration and the number of iteration on τ for the stage considered.

5. For the upper stage, both m_{pay} and ρ_{pay} are inputs, whilst for the lower stage they become constraints, since the payload mass of the first stage is the entire second

stage mass and its density can be easily computed by dividing mass of second stage by total volume. Propellant data, number of crew people and ICI are inputs anyway instead.

6. *read_segments* is called to load all the inputs required for *mass_ratio*, both for first and for second stage. In other words, the trajectory data are imported.

7. *T_W_range* is called to ask the user for a reasonable range of T/W values in which to perform the research of the design point and the sampling frequency of data to pick within it. Reasonable values could derive from statistical analysis for a specific category of vehicle or from tabled data.

8. The total mass ratio is computed for each value of the set of τ established, for the stage considered. *mr_correction_1stage* is called for the first stage sizing, so as to adjust the mass ratio according to the initial take off mass, regardless of the separation event discontinuity.

9. Mass and volume coefficients are recalled through *call_mass_and_volume_coeff*.

10. Other data are computed, namely $I_p, I_{str}, C_{sys}, m_{cprv}, m_{crew}, E_{TW}, V_{fix}, V_{pay}$ and V_{crew}. All these values are defined and set as constants after the previous calculations.

11. The expressions of masses m_{OE} reported in Equation 3.46 and 3.47 are written under the form of functions, with main variables τ and S_{pln}. Through an inner loop based on S_{pln} convergence between the two expression is found (or not found), then the process is reiterated via an outer loop on τ and again, through an even outer loop, on T/W. A tolerance of 500 kg is used, while a range of $0-1000\ m^2$ is applied for wing planform convergence. As a matter of fact, higher values of S_{pln} become strongly inconvenient. A message at the end of each iteration on τ is shown on the screen to inform on the status of convergence within the range set.

12. As soon as the entire iterating logic stops, the stack of matrixes containing all the potential design points identified (each row of a matrix is for a specific *tau* value, while each matrix is for a specific T/W value), the appropriate Multiple Matching Charts Analysis function is called, with the aim of voting the best candidate among all the points.

13. The selected design point is stored, so that all the main design figures associated to it are collected, divided into mass budget, volume overall budget, wing planform required and effective τ achieved. If two stages are set by the user, the entire procedure from point 3 is repeated for the lower stage, which is the first one.

14. The results are finally displayed in the form of both bar charts (for the mass breakdown, the geometric characterization and the % relative errors) and spider dia-

grams, through the plotting functions previously described. The curves resulting from MMCs Analysis are shown as well.

At this point, the architecture of the program should be clear, since it is the implemented version of the methodology illustrated through the flow chart in Figure 3.12 . Therefore, in the next sections, the application of the methodology to Sänger II as test case will be presented, together with the simplifying assumptions which the process is based on.

4.2.2 Assumptions

The sizing methodology applied to Sänger II relies on several assumptions, here gathered. It's paramount to stress the limitations, thus the degree of approximation employed in different parts of the code, in order to highlight potential improvements that can be operated in future works. However, each assumption relies on physical or statistical reasoning, thus nothing is left to chance or randomly defined and works quite well for an early conceptual design phase.

Number of stages

Since the thesis focusses on TSTO vehicles, the code is programmed to give the user the chance to choose between a single and a dual stage vehicle. Having more than 2 stages is not possible, though a further expansion may be viable in improved versions.

Mixture ratio MR

The mixture ratio is defined as the ratio $\frac{\dot{m_{oxy}}}{\dot{m_{fuel}}}$. According to the type of stage, two different values have been selected:

- Upper Stage Horus $\rightarrow$ since it is rocket-propelled with LOX/LH2, a $MR = 6$ is chosen, as a trade-off between a higher specific impulse for lower propellant mass and lower tank volumes.
- Lower Stage EHTV $\rightarrow$ since it is powered by turboramjet engines working with Air/LH2, the MR is highly affected by altitude and engine regime, thus greatly variable. However an average value of 39.4 was computed. To achieve this result, $\dot{m_{air}}$ and $\dot{m_{LH2}}$ are separately estimated.
  - $\dot{m_{air}} = \rho \cdot A_{in} \cdot V \rightarrow$ by computing the arithmetical average of air densities in the middle altitude of each of the five segments during ascent [18], a reference $\rho = 0.218\ kg/m^3$ is obtained, corresponding to a reference altitude of 14250 m. From $M(h)$ profile, M results in 1.77 and the speed of sound $a = 295.07\ m/s$. As consequence of that, $V = 522.27\ m/s$. In the end, the inlet area A_{in} is estimated to be 13.5 m^2 large, by looking at the drawings provided.

– $\dot{m_{LH2}} = SFC \cdot T \rightarrow$ The average value of SFC is obtained through fuel consumption chart in [18], resulting in 26 $g/s/kN$, while the reference thrust T is chosen at take off, being the only data available, equal to 1500 kN.

At this point the reference values of $\dot{m_{air}}$ and $\dot{m_{LH2}}$ can be evaluated, respectively equal to 1537 kg/s and 39 kg/s, yielding $MR = 39.4$.

Industrial capability index ICI

ICI is a measure of the practicality of the vehicle under consideration, in terms of the industrial materials/fabrication/propulsion capability available, thus it represents the relative measure of technological maturity in several areas, like aerodynamics, propulsion, manufacturing and integration [4]. It is defined as:

$$ICI = 10 \cdot \frac{I_p}{I_{str}} \tag{4.1}$$

By referring to the calculations in Tjonneland [46], a maximum ICI of 37.7 m^{-1} is used for both stages, meaning that this kind of vehicle requires the highest technological maturity.

Number of iterations on τ

Potentially, no limitations in the number of iterations on τ are set. However, this version of the code requires the same number for either stage, in case a TSTO vehicle is chosen.

Subsonic carrier configuration

In the event that a configuration of subsonic cruiser is selected for the first stage, since Kuchemann's correlation is no longer valid, the code implements the logarithm-exponential law given by the subsonic correction provided in chapter 3. However, it is not the case of Sänger II, thus it was not applied in the design process.

Thrust over Weight ratio

T/W represents one of the loop variables affecting the convergence process. The MMCs Analysis is conducted to identify the optimal design point among the ones obtained at the end of the methodology iterative procedure. Since the major aim of the chapter is to prove a consistency between an already existing concept and the methodology, a range of T/W for each stage has been provided as input, including

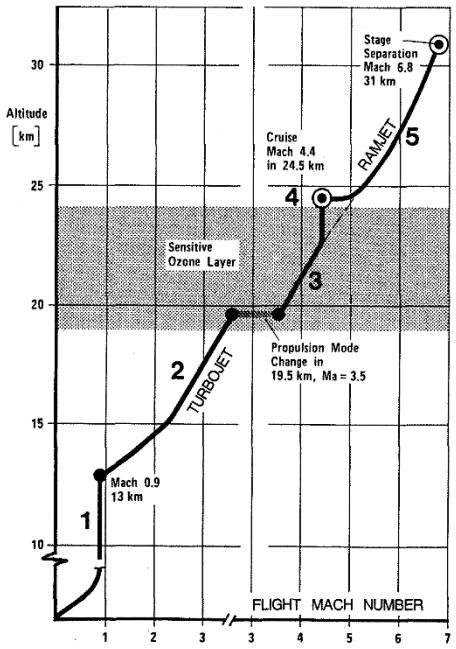

Figure 4.4: Ascending flight profile of Sänger II, before separation of second stage.

the reference value achieved from the official manual of the program [18]. These reference values are reported in Table 4.2:

Stage	Thrust $[kN]$	Gross Weight $[ton]$	T/W $[-]$
1.EHTV	1500 (sl)	340	0.45
2.Horus	1500 (vac)	91	1.7

Table 4.2: T/W for both stages.

Mission flight segments

According to the flight profile provided by [18] and reported in Figure 4.4, it was quite intuitive to derive the sequence of flight segments as regards the ascent phase of the EHTV before separation of second stage. Nevertheless, some data were estimated on the basis of reasonable assumptions, for instance the flight path angle during climbs, mainly based on aeronautical experience or quantitative translation of vague information available on reports or documents online about Sanger II. The same reasoning applies to the descent profile and to the entire flight path of second stage.

In Table 4.3 and Table 4.4 the history of flight per each stage is reported. Some boxes contain a dash, meaning that the related parameter is not necessary for computational purposes in the mass ratio estimation of the phase. It is noteworthy to stress the most important assumptions:

- In *type* column, TJ stands for turbojet propulsion mode, RJ for ramjet mode.

- For the hypersonic cruise phase of stage 1 a time of 900 s has been chosen respectively to consider a reasonable time to reach the geographical point to start the final phase of ascent and the initial phase of descent after second stage release.
- Standard values of 12° and −3° have been established as flight path angles γ during climb and descent respectively.
- To model the first stage descent fuel consumption, a linear decrease of M with altitude has been decided for simplicity: in particular, EHTV decelerates from $M = 6.8$ to $M = 3.5$ up to an altitude of 19.5 km, corresponding to the engine switching mode altitude from ramjet to turbojet. Then, always linearly, M drops from 3.5 to 0.1 at landing.
- As regards the ascent phase of second stage, $h_{end,b}$ and M_{fin}, respectively the altitude at which the rocket propellant ceases to push the spacecraft and the Mach number reached at that point, have been adjusted in order to provide a $I_{sp} = 490$ s, as indicated into the manual. It means that, even though $h_{end,b}$ and M_{fin} could be individually wrong, their combination is what matters in determining the specific impulse used in the mass ratio function.

Phase	**Type**	γ	$\mathbf{h_{in}}$	$\mathbf{h_{fin}}$	$\mathbf{t_{phase}}$	$\mathbf{V_{in}}$	$\mathbf{h_{end,b}}$	$\mathbf{M_{fin}}$	$\mathbf{M_{in}}$
1.Take-off	TJ	-	-	-	-	-	-	-	-
2.Subsonic climb	TJ	12°	0 km	13 km	-	-	-	-	-
3.Supersonic climb	TJ	12°	13 km	19.5 km	-	-	-	-	-
4.Supersonic climb	RJ	12°	19.5 km	24.5 km	-	-	-	-	-
5.Hypersonic cruise	RJ	-	24.5 km	24.5 km	900 s	-	-	-	-
6.Hypersonic climb	RJ	12°	24.5 km	31 km	-	-	-	-	-
8.Propelled descent	RJ	−3°	31 km	19.5 km	-	-	-	3.5	6.8
9.Propelled descent	TJ	−3°	19.5 km	0 km	-	-	-	0.1	3.5

Table 4.3: Segments of flight for first stage EHTV.

Equations used for the mass ratio

On the basis of the phase of flight considered, a specific formula is used in order to compute its contribution to the overall mass ratio of the stage. The distinction here illustrated refers to whichever stage.

Phase	Type	γ	h_{in}	h_{fin}	t_{phase}	V_{in}	$h_{end,b}$	M_{fin}	M_{in}
1.Rocket climb+orbit	Rocket	-	31 km	400 km	-	2057 $\frac{m}{s}$	40 km	30	6.8
2.Glide descent	No-propelled	-	-	-	-	-	-	-	-

Table 4.4: Segments of flight for second stage Horus.

- Take-off: a statistical value from Raymer [43] of 1.02 is applied, no matter the configuration selected.
- Climb phases: Breguet's equation adjusted through the effective aerodynamic efficiency is employed. A detailed explanation about the meaning of effective aerodynamic efficiency is provided in the next paragraph.
- Propelled descent phases: Breguet's equation adjusted through an effective aerodynamic efficiency is employed as well.
- Cruise phases: classical Breguet's equation, represented by Equation 3.28, is applied.
- Glide descent phase: a constant value equal to 1 is set, due to the fact no fuel is consumed during this type of flight segment.
- Rocket ascent phases: Tsiolkolvsky's equation is employed starting from knowledge of the velocity budget, namely Equation 3.30.

As far as the computation of mass ratio of the first stage is concerned, two important aspects have to be clarified:

- as stated and described in chapter 3, the mass ratio which is used within the iterative process is an adjustment of the simple mass ratio obtained through multiplication of each segment's contribution, considering the separation event;
- the adjusted value of mass ratio is then multiplied by itself, before entering the sizing loop, since the hypothesis of a back and forth typical scenario without refilling the tanks was considered. This apparent overestimation of fuel demand is actually justified, because it finds also reason in Sänger II other use, that is serving as high-speed transportation aircraft over a 10000 km range [18].

The following two paragraphs contain more details as regards the definition of the effective aerodynamic efficiency and the modelisation of the ΔV required to second stage Horus to reach the target orbit.

The effective aerodynamic efficiency E_{eff}

The introduction of the effective aerodynamic efficiency results necessary in order to be able to use Breguet's equation not only for horizontal level flight, but also for climb and descent phases. Its derivation is here presented.
Provided that the flight path angle γ contains its sign (positive for climb and negative for descent), both phases are described by the same set of two equations for longitudinal and vertical balance:

$$\begin{cases} T = D + W sin\gamma \\ L = W cos\gamma \end{cases} \tag{4.2}$$

By using this set of equations, the aim is to derive an alternative form of Breguet's equation, valid for climb and descent. By referring to [40] the range expression is given by:

$$R = \int_{W_f}^{W_i} \frac{V}{T \cdot SFC}\, dW = \int_{W_f}^{W_i} \frac{V}{SFC} \frac{W}{T} \frac{dW}{W} \tag{4.3}$$

If we simplify W and combine the thrust equation with the definition of efficiency, it is obtained as follows:

$$R = \int_{W_f}^{W_i} \frac{V}{SFC} \frac{1}{D + W sin\gamma} dW = \int_{W_f}^{W_i} \frac{V}{SFC} \frac{1}{\frac{W cos\gamma}{E} + W sin\gamma} dW \tag{4.4}$$

If γ, V, E and SFC are assumed to be constant (reasonable in case the integration is operated on a highly discretized segment), the new formulation of Breguet'equation is the following:

$$R = \frac{V}{SFC} \cdot \frac{1}{\frac{cos\gamma}{E} + sin\gamma} \cdot log\left(\frac{W_i}{W_f}\right) \tag{4.5}$$

where the term

$$\frac{1}{\frac{cos\gamma}{E} + sin\gamma} \triangleq E_{eff}. \tag{4.6}$$

is the effective aerodynamic efficiency. Some interesting considerations can be done on E_{eff}, also referring to Figure 4.5 and Figure 4.6.

- when $\gamma \to 0°$, $E_{eff} \to E$, thus the formulation is consistent with horizontal flight, being a generalization of classical Breguet's formula;
- when $\gamma > 0°$, E_{eff} is minor than the real efficiency: this can be interpreted as a measurement of the decrease of range in terms of reduced efficiency of an equivalent cruise segment. In other words, it is reasonable to witness a decrease in E_{eff}, since climb phases require more fuel and the weight component adds to drag as resistant force.
- when $\gamma < 0°$ the situation gets more complex. Since $sin\gamma$ is now negative, for

each value of E, γ^* exists, where E_{eff} becomes negative, losing physical meaning. In fact, a negative efficiency would cause the mass to increase along the segment, instead of decreasing. Physical meaning is maintained as long as:

$$\frac{cos\gamma}{E} + sin\gamma > 0 \implies E < -cotg(\gamma) \tag{4.7}$$

As a matter of fact, if $E = 5, E = 7$ and $E = 9$ are considered, the corresponding γ^* result respectively in $-11.31°, -8.13°$ and $-6.34°$, where the peaks with inversion of sign are shown in Figure 4.6. Therefore, for $\gamma^* < \gamma < 0°$, E_{eff} is greater than E, justified by the fact that less fuel needs to be consumed during propelled descent, since the weight component adds to thrust. In other words, higher values of effective efficiency mean an increase of range with respect to an equivalent cruise segment. On the other hand, if $\gamma < \gamma^*$, from a physical point of view, the aircraft does not need propellant anymore to descend: the propelled descent turns into a glide maneuver, thus a mass ratio equal to 1 is applied.

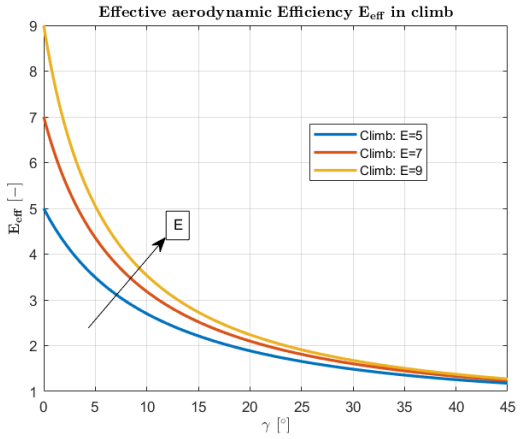

Figure 4.5: $E_{eff} = f(\gamma)$ for climb.

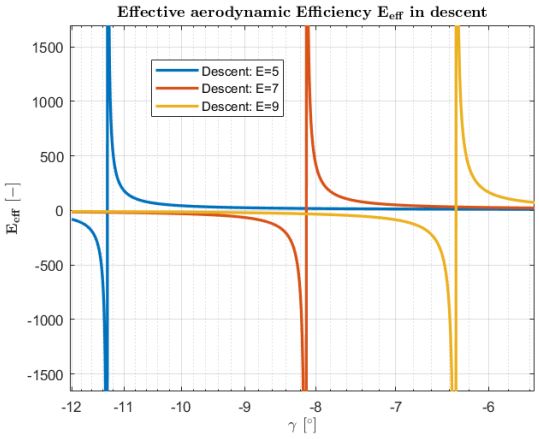

Figure 4.6: $E_{eff} = f(\gamma)$ for descent.

ΔV computation for Horus

The overall ΔV computed for the second stage Horus to reach the target orbit of 300 km is given by:

$$\Delta V = \Delta V_{orb} - \Delta V_{Earth} + \Delta V_{loss} \tag{4.8}$$

Each of the three contributions was calculated on the basis of some assumptions.

- ΔV_{orb} : it represents the major term and it is computed by considering a 2-burn Hohmann transfer maneuver plus an additional change in velocity to match the velocity at release with the circular velocity at that altitude. By summing up the three impulsive burns, a ΔV_{orb} of 5.99 km/s is achieved.

- ΔV_{Earth} : the Earth rotation along its axis provides a little advantage in case take off is performed towards East. For simplicity, take off at the equator latitude is established as well as a perfect alignment with East direction. In this condition, the beneficial effect of Earth rotation is maximum, resulting in 464 m/s gained at take off.

- ΔV_{loss} : the main sources of losses are given by atmospheric drag, not-adapted nozzle and gravity. After some considerations, based on some documents provided by [47] it was possible to estimate roughly a value of 1 km/s. Though classical vertical take-off launchers examples normally take into account around 2 km/s of losses, it is crucial to remind that here gravity losses are considerably reduced since $sin\gamma$ is lower with respect to a quasi vertical ascent. Moreover, the ascent segment begins at 31 km, at stage separation, therefore the contribution to ΔV_{loss} given by atmospheric drag is lower as well, since the lower the altitude, the denser the atmosphere.

To sum up, a final velocity budget of about $\Delta V = 6.53$ km/s is required to Horus to reach the target orbit at 400 km.

Mass and volume coefficients

The great majority of mass and volume coefficients illustrated in tab. 3.2 was defined to be the average value within the correspondent range indicated. In absence of more specific tips, that seemed the most reasonable choice.

Margin factors MF

By running the code the first time with the data referred to Sanger II, it was immediate to realize that the slope of the line describing $m_{OE,w} = f(S_{pln})$ (Equation 3.46) was too high. In fact, Sanger II's second stage is characterized by a I_{str} which is out of the normally tolerated range, according to literature references. For this reason and to take into account potential displacements of the mass and volume coefficients from their average values, a margin factor MF was introduced. The slope of Equation 3.46 is then modified by multiplying it by MF. The slope is now written as follows:

$$\frac{MF \cdot I_{str} \cdot K_w}{\frac{1}{1+\mu_A} - f_{sys} - \frac{(T/W)\cdot m_r}{E_{TW}}} = \frac{MF \cdot I_{str} \cdot K_w}{X - K^{-1}} \tag{4.9}$$

where

$$\frac{1}{1+\mu_A} - f_{sys} \triangleq X \tag{4.10}$$

$$\frac{(T/W)\cdot m_r}{E_{TW}} \triangleq K^{-1} \tag{4.11}$$

To determine a reasonable range for MF, it was decided to relate the nominal value of the slope without corrections to the minimum and the maximum possible, considering the typical constraints of the terms appearing. In particular:

- Minimum value $\implies I_{str} = 17\ kg/m^2, X = 0.71, K = 7.7$;
- Maximum value $\implies I_{str} = 23\ kg/m^2, X = 0.63, K = 4.8$;
- Nominal value $\implies I_{str} = 33\ kg/m^2, X = 0.67, K = 6.25$;

By dividing the maximum and minimum values by the nominal one, the following range for MF was achieved:

$$0.452 < MF < 0.842 \tag{4.12}$$

which contributes to reduce the slope as predicted. By opting for a lower limit value, for instance $MF = 0.46$ for both stages, reasonable results are determined. Obviously, this approach does not claim to be chosen as a way to proceed meticulously and it is quite raw. Nevertheless, to adjust the values for this particular test case it revealed to be useful and seemed an acceptable price to pay to overcome the long list of approximations leading to inevitable mistakes.
The introduction of MF describes, within the permissible range, all the possible sets of variables affecting the slop of $m_{OE,w} = f(S_{pln})$, but it quite clear that this is related to the known term as well. In fact, being the denominator of the known term the same, it has to be corrected through another margin factor, MF_2, which is correlated to MF only through X and K, not I_{str}. As reported hereafter the known term becomes:

$$\frac{C_{sys} + m_{cprv} + \frac{(T/W)\cdot m_r}{E_{TW}}(m_{pay} + m_{crew})}{\frac{1}{1+\mu_A} - f_{sys} - \frac{(T/W)\cdot m_r}{E_{TW}}} = \frac{...}{MF_2 \cdot (X - K^{-1})} \tag{4.13}$$

By replacing boundary conditions into the linearized relation $MF_2 = f(MF)$, it was possible to get the following:

$$MF_2 = 1.496 - 0.7828 \cdot MF \tag{4.14}$$

Finally, a third margin factor was introduced to consider the possible adjustments concerning the volume budget equation slope. By recalling Equation 3.47 ($m_{OE,v} = f(S_{pln})$, the updated formulation of the slope (coefficient multiplying $S_{pln}^{1.5}$) is:

$$\frac{\tau \cdot (1 - k_{vv} - k_{vs}) \cdot S_{pln}^{1.5}}{\frac{1}{I_P} + k_{ve} \cdot (T/W) \cdot m_r} = \frac{...MF_3 \cdot (1 - k_{vv} - k_{vs})}{...} \tag{4.15}$$

The value of MF_3 was computed considering the typical constraints of the term in brackets appearing. In particular:

- Minimum value $\implies k_{vv} = 0.2,\ k_{vs} = 0.04$;

- Maximum value $\implies$ $k_{vv} = 0.1,\ k_{vs} = 0.02$;
- Nominal value ($MF_3 = 1$) $\implies$ $k_{vv} = 0.15,\ k_{vs} = 0.03$;

By dividing the maximum and minimum values by the nominal one, the following range for MF_3 was achieved:

$$0.927 < MF_3 < 1.073 \tag{4.16}$$

The idea is to minimize both the void and variable system specific volume employed, in order to avoid additional volume in excess, thus the maximum value $MF_3 = 1.073$ is chosen.

Wing areas computation

Since no official data are available online, the values of wing area for both first and second stage were determined through a visual analysis based on a scaled up view drawing of Sänger II [18]. Two different approaches have been employed:

- Stage 2 Horus $\implies$ the semi-wing has been modelized as the summation of three polygons, namely three trapezoids;
- Stage 1 EHTV $\implies$ due to the higher complexity, the shape was re-created in MATLAB and the area was computed through numerical integration.

Figure 4.7 and Figure 4.8 give a portray of the wing planforms schematized.

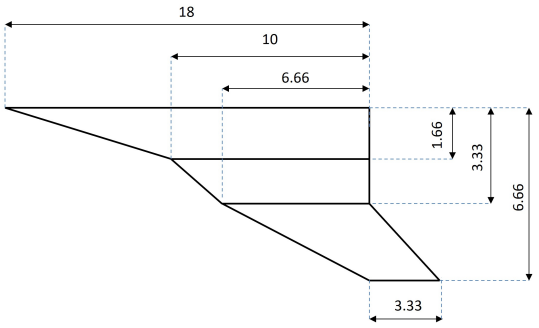

Figure 4.7: Horus semi-wing area.

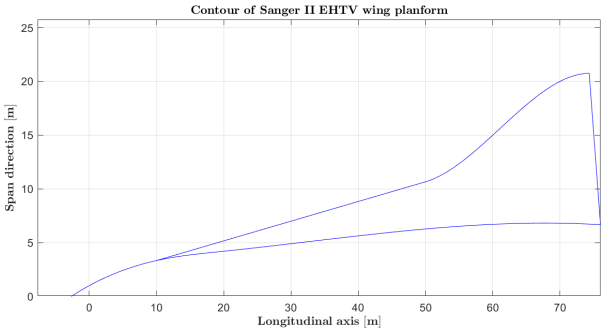

Figure 4.8: EHTV semi-wing area.

Through computations, the values of 107 m^2 and 880 m^2 have been obtained as a reference for successive checks during the sizing process. The actual number coming from numerical integration for the EHTV area is 648.4 m^2, but it takes into account only the area confined by the blue line. As consequence of that, the value has been increased, since the reference planform normally considers also a part of the fuselage plant projection, not included here.

Determination of m_{pay} for the first stage

It is paramount to remind that the result coming from the sizing of the second stage, consisting of the already presented procedure, that is the selection of the design point as the optimal one on the basis of the position it covers in the $T/W - W/S$ chart, is used as input for the first stage sizing. In particular, payload mass and density for the first stage are computed as follows:

- $m_{pay,1} = m_{G,2}$;
- $\rho_{pay,1} = \frac{m_{G,2}}{V_{tot,2}}$;

The other input data are provided through the input file as for the second stage.

Multiple Matching Chart Analysis

The first stage, based on its mission profile, has to go through 3 different flight regimes, thus 3 different charts will be presented. Moreover, the transition occurring to the propulsive mode at a certain altitude is taken into account in the curves.
On the other hand, the second stage does not have to fly in other flight regimes than hypersonic. In addition to that, no propulsive mode transitions are defined, thus a normal Matching Chart Analysis with only one chart is carried out. Obviously, the reference conditions are the ones characterizing the separation altitude.
Every number inserted as input in the functions computing MCA derives from either reasonable assumptions or available data.

4.3 Results

4.3.1 Matching Chart Analysis

From the beginning to the end of the sizing procedure, a total of 5 charts are displayed by the tool, referring to the multiple matching chart analysis applied to the second (upper) stage before and to the first (lower) stage later. This number must not be taken as a general reference, since it depends on the case study only.

Upper stage

The Matching Chart for the upper stage is reported in Figure 4.9. It is clear that 4 main requirements have been considered as sizing for the stage:

- the hypersonic cruise, occurring for a few seconds after release from the lower stage;
- the hypersonic climb, occurring for a few seconds after cruise;

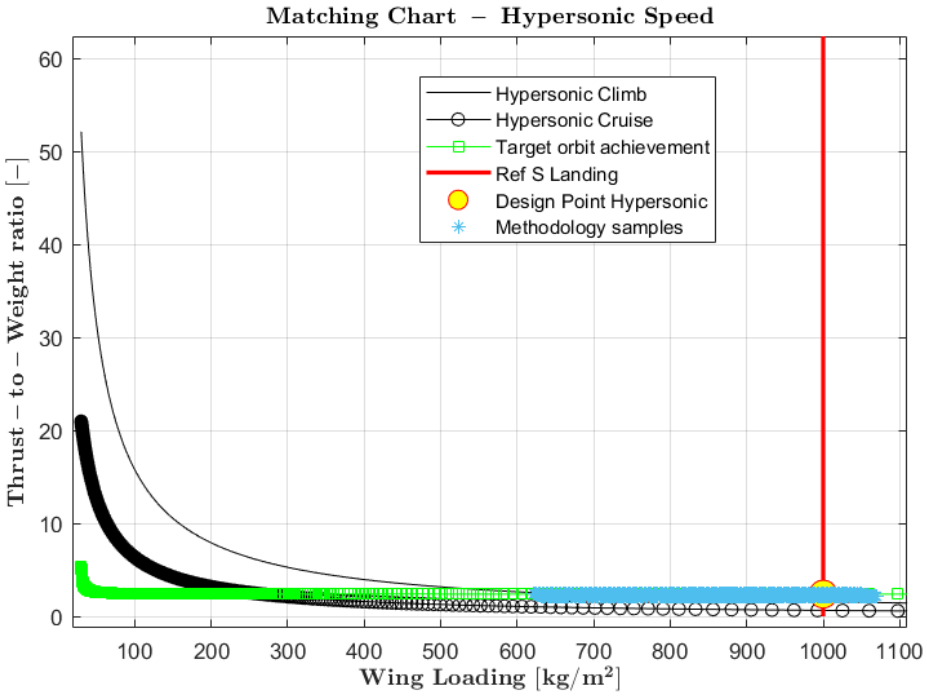

Figure 4.9: Matching Chart results for the second stage.

- the target orbit achievement requirement, consisting of the main part of the flight propelled phase and the most demanding condition to fulfill in terms of thrust;
- the minimum wing surface to guarantee at landing after gliding.

The point in yellow reveals the best condition of T/W and W/S to size second stage, while the net of blue points is the result of the methodology as potential design points. Among the blue points, the final design point is identified (Table 4.6)

$(T/W)_2$ $[-]$	$(W/S)_2$ $[kg/m^2]$
2.45	999.67

Table 4.5: T/W and W/S for the upper stage.

Lower stage

As far as the first stage is concerned, the operative scenario is definitely more complex. In fact, the ascent profile may be divided into three main parts:

- a subsonic segment, where turbojet mode is the only propulsion plant working;
- a supersonic segment, encompassed by both an initial turbojet-powered and a successive ramjet-powered climb. The two different requests for thrust are displayed in the same graph;

- a hypersonic segment, where only ramjet mode is used to reach the separation altitude.

The chart in Figure 4.10 is the overall requirement representation which should result if no reference altitude and phase transitions were taken into account. In other words, it is the outcome of a classical Matching Chart Analysis, as if there were no changes in both the propulsive mode and in the flight speed regime. As announced in chapter 3, the resulting thrust demand would be completely overestimated; indeed, a T/W of 121.1 would be asked for the feasibility of the mission, but that is clearly a wrong approach to follow.
On the other hand, the charts in Figure 4.11, Figure 4.12 and Figure 4.13 each represent the three flight segments reported. The consistency among them is provided by adjustment of the wing planform area requirement at landing, as explained in chapter 3.
The subsonic condition reveals to be the most demanding in terms of thrust required as expected. As consequence of that, the net of potential design points coming from the methodology iteration process is overlapped to the subsonic diagram and the overall design point is chosen to be the closest possible to the yellow point, still in compliance with thrust and wing loading constraints.
Both supersonic and hypersonic charts define two design points, as expected: the one in yellow and the one in green. The former refers to a fulfillment of the only requirements affecting the specific phase considered, as it were isolated from the rest; the latter derives from the consistency constraint with the subsonic and landing phase, thus it is the one to consider for sizing purposes. To sum up:

Phase	$(T/W)_1$ $[-]$	$(W/S)_1$ $[kg/m^2]$
Subsonic	0.610	401.20
Supersonic	0.598	382.32
Hypersonic	0.476	372.88
Final choice	0.611	401.14

Table 4.6: T/W and W/S for the upper stage.

4.3.2 Mass breakdown

The major result of the methodology is the mass breakdown of both stages. This version of the code computes the overall mass of the stage by splitting it into only 3 contributions: payload mass, propellant mass and operative empty mass. Further refinements could be performed, by improving the code, though a quite good estimation of the main magnitudes is already possible.
The bar chart in Figure 4.14, illustrating the mass breakdown for either stage, is self-explanatory. The only aspect to focus on is the fact that the total gross mass of stage 2 is equivalent to the payload mass of stage 1, as described in the methodology stage loop

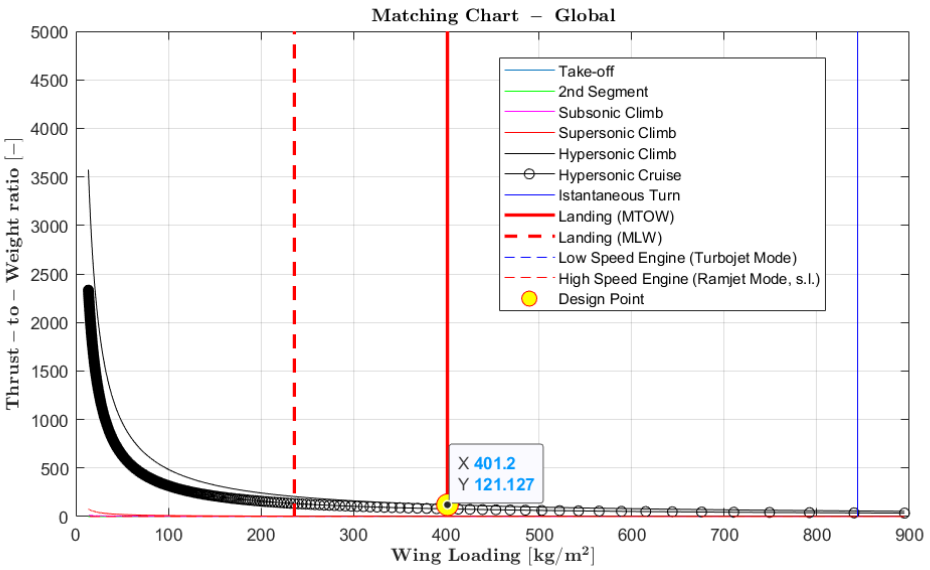

Figure 4.10: Matching Chart results for the first stage (global, with no corrections).

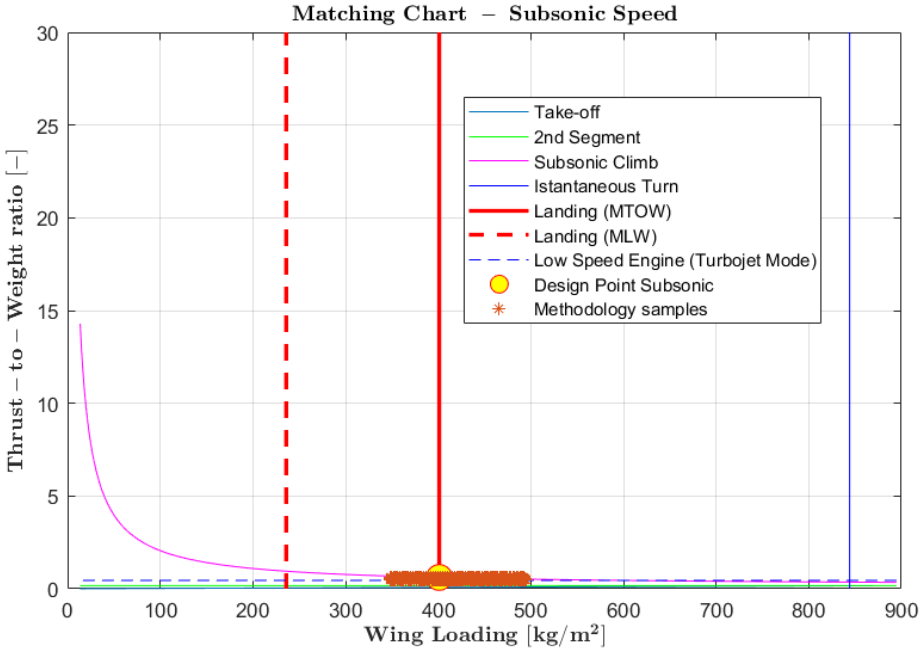

Figure 4.11: Matching Chart results for the first stage (subsonic flight).

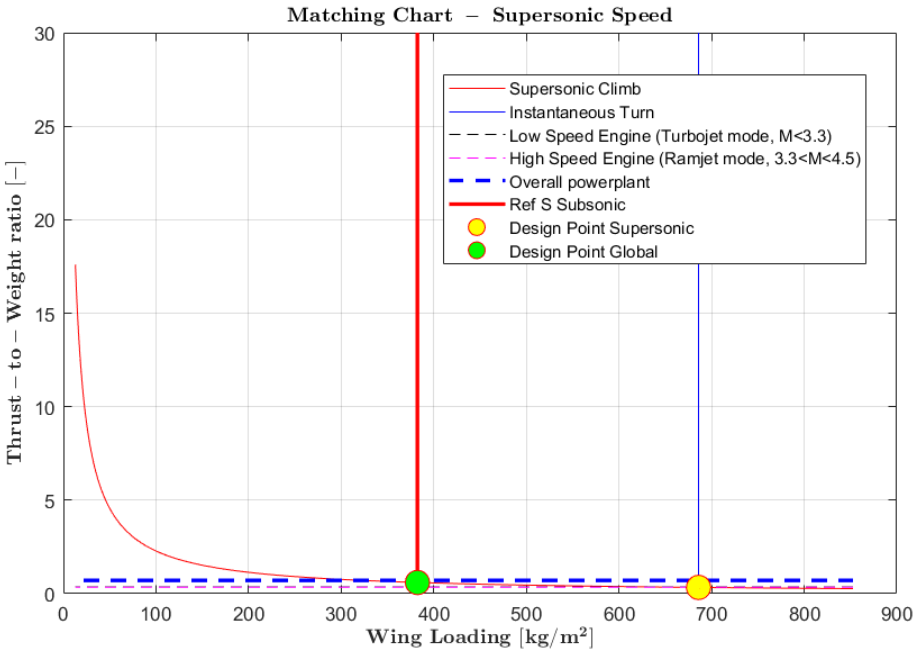

Figure 4.12: Matching Chart results for the first stage (supersonic flight).

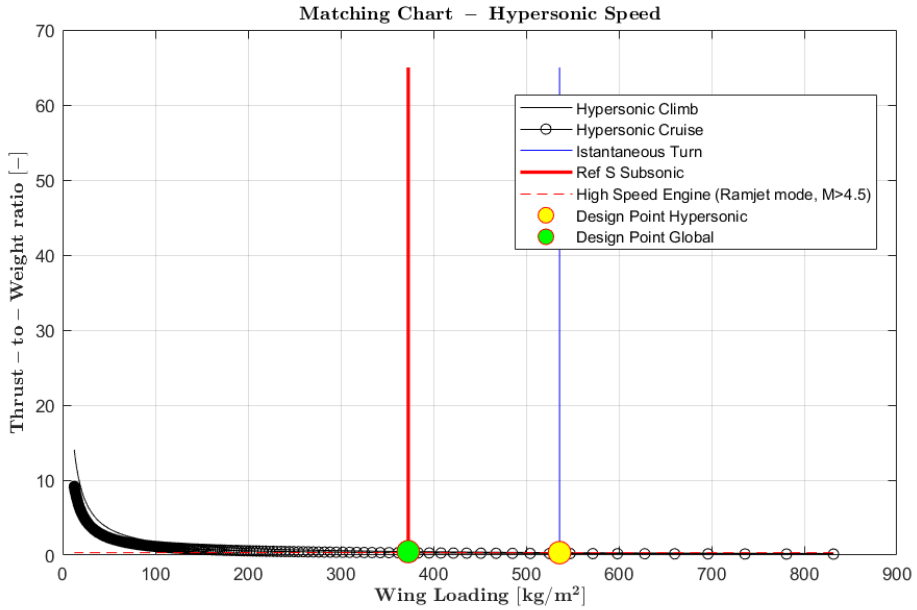

Figure 4.13: Matching Chart results for the first stage (hypersonic flight).

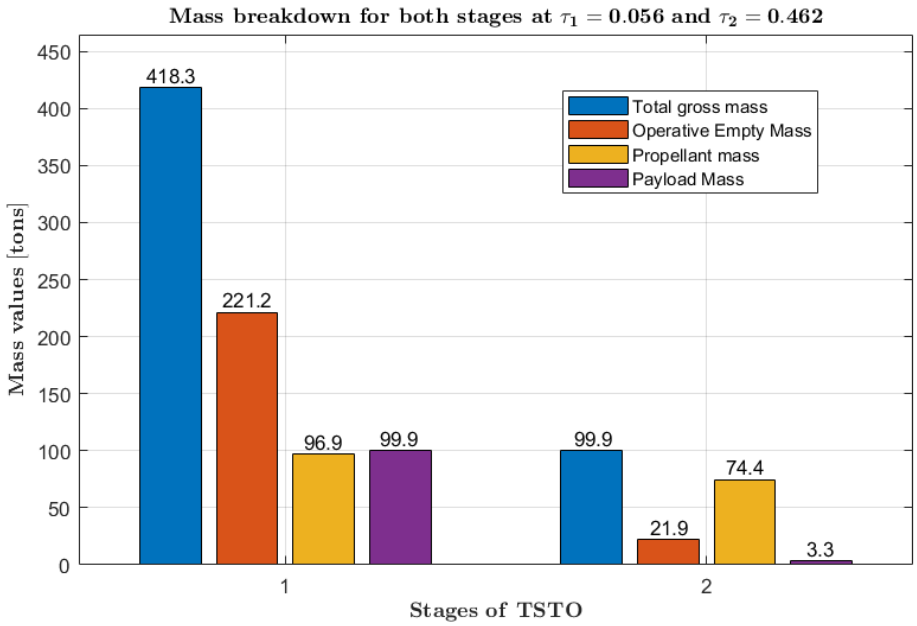

Figure 4.14: Mass breakdown for both stages.

functioning.
Finally, in the title, the values of τ for which convergence has been reached for both stages are reported.

4.3.3 Geometric characterization

Another remarkable outcome of the process is the geometric characterization. With this expression, both the wing planform area and the overall volume required are meant. Also in this case, further improvements could be made, in order to achieve more detailed information concerning the volume breakdown itself, but it is not the scope of this work. The bar chart in Figure 4.15, illustrating the wing planform area S_{pln} and volume V_{tot} for either stage, is self-explanatory. Reasonably, passing from stage 2 to stage 1, both the magnitudes show an increase of about one order of magnitude.
Finally, also in this case, in the title, the values of τ for which convergence has been reached for both stages are reported (the same as before).

4.3.4 Post-processing: comments and accuracy of the methodology

In order to have a better understanding of the results obtained and to assess the feasibility as well as the accuracy degree of the methodology employed, a comparative investigation is carried out. This is done through visual diagrams, aiming at giving both a qualitative and a quantitative evaluation of the deviation occurring between the results of the

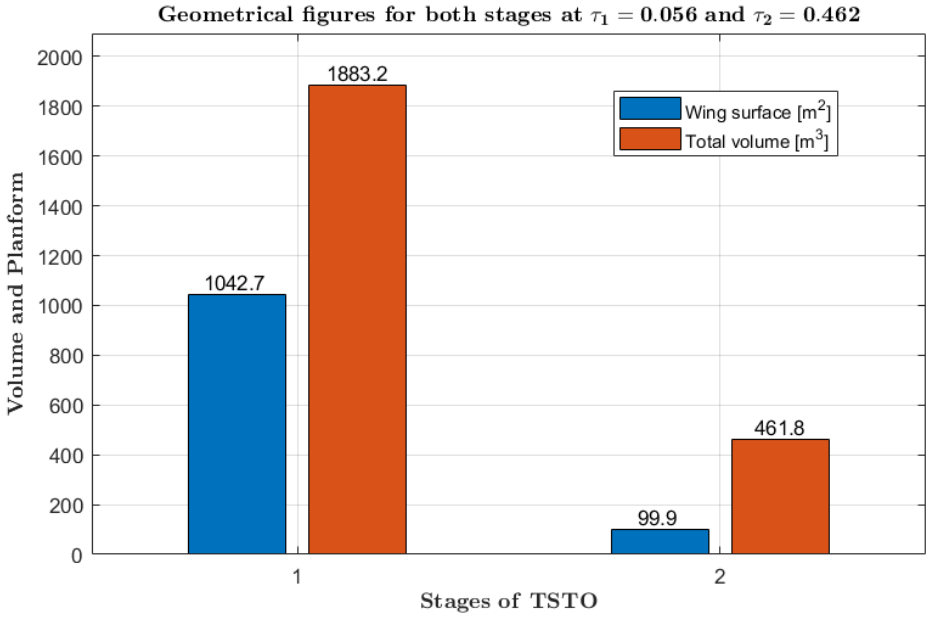

Figure 4.15: Wing area S_{pln} and volume V_{tot} for both stages.

methodology and the reference values available in the manual of Sänger II. Despite this approach is undoubtedly a powerful and appropriate instrument for critical comments about the entire methodology, it has to be stated that Sänger II does not present a large range of technical documents easily available. The so-called reference values come from manuals which typically tend to give approximate numbers to each magnitude involved, thus the comparison is affected by uncertainty also because the values to refer to are often approximated. Moreover, Sänger II never flew, remaining a design concept: this contributed to higher margins of errors.

Spider plots

Spider plots are a very effective way to compare results through the overlapping of design areas. Figure 4.17 and Figure 4.18 illustrate this comparison for both lower and upper stage respectively. The following considerations arise:

- The preliminary sizing of the second stage is affected by less errors than the first stage. This was predictable, since stage 2 is sized at the first cycle of iterations, whilst stage 1 is sized later: obviously, the results of stage 2, already affected by errors, are used as inputs for stage 1, propagating and amplifying the deviation from reference values.

- The results obtained from the methodology tend to overestimate the actual values, especially as regards the T/W ratio. This could be either a typical behavior of the methodology or an underestimation of thrust levels in the manual.

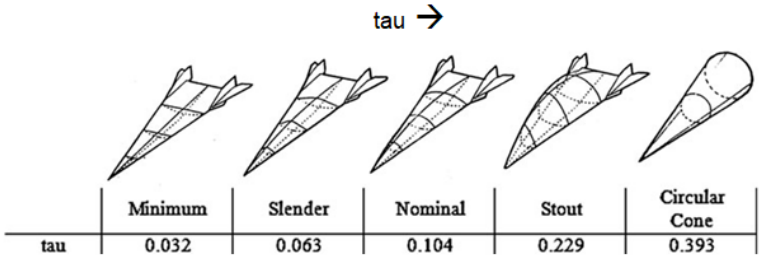

Figure 4.16: Vehicle shape evolution with τ.

- The values of τ_1 and τ_2 seem to exert a huge impact in the deviation attitude from the reference, but it is important to remember that, depending on the vehicle configuration chosen for the stage considered, τ can assume whichever value within a certain range (Figure 3.1). In particular:

  1. Stage 1: $\tau_1 = 0.056 \implies$ it belongs to the hypersonic cruiser category;
  2. Stage 2: $\tau_2 = 0.462 \implies$ it belongs to the rocket hypersonic glider category.

  Since τ is deeply correlated to the external shape of the vehicle, it is possible to conclude that the stage 1 EHTV is asked to be sized through a slender configuration, not only compliant with carrier but also high speed transportation purposes, while stage 2 requires a more conical (or blunted cone) configuration, reasonably true since for *Horus* also a non-propelled gliding phase is expected.

Relative errors plot

To have a quantitative measurement of the deviation between official data reported in manuals and the results of the methodology, the bar chart in Figure 4.19 was generated. It shows the relative error in percentage for each major design magnitude with respect to the reference values. Three different bands are defined, to assess the entity of deviation, namely the severity of error:

- acceptable error band, with $Err_{\%} \leq 25\%$;
- critical error band, with $Err_{\%} > 25\%$ and $Err_{\%} \leq 50\%$;
- not acceptable error band, with $Err_{\%} > 50\%$;

For sake of clarity, the relative error $Err_{\%}$ in percentage is calculated as follows, per each design variable x and each stage:

$$Err_{\%} = \frac{x_{des} - x_{ref}}{x_{ref}} \cdot 100 \tag{4.17}$$

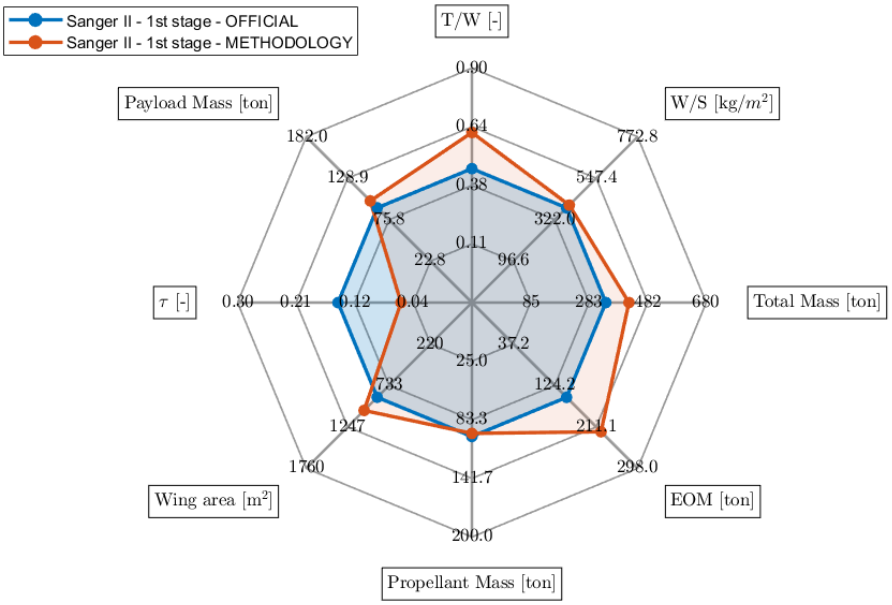

Figure 4.17: Spider plot for stage 1.

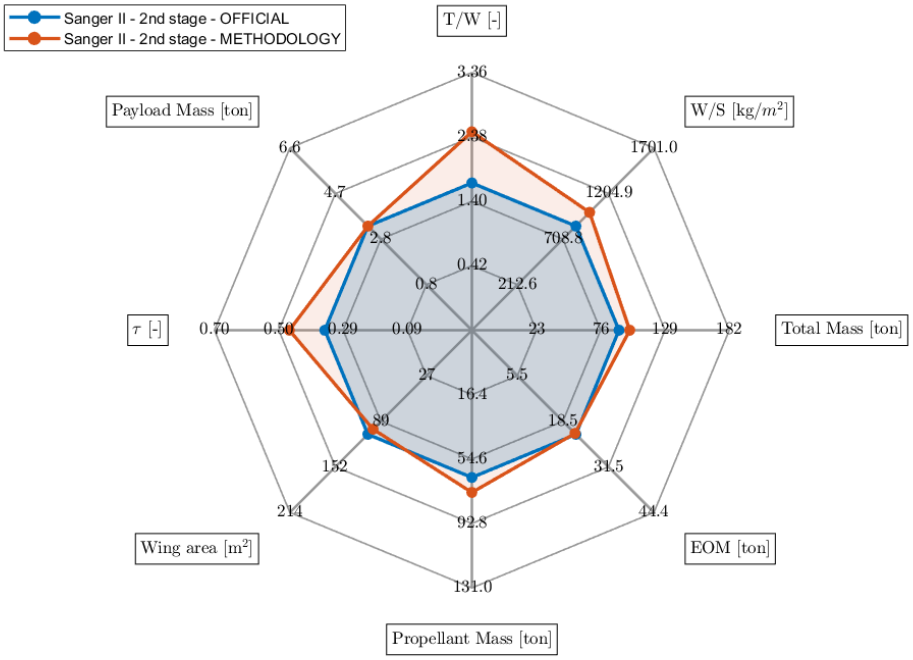

Figure 4.18: Spider plot for stage 2.

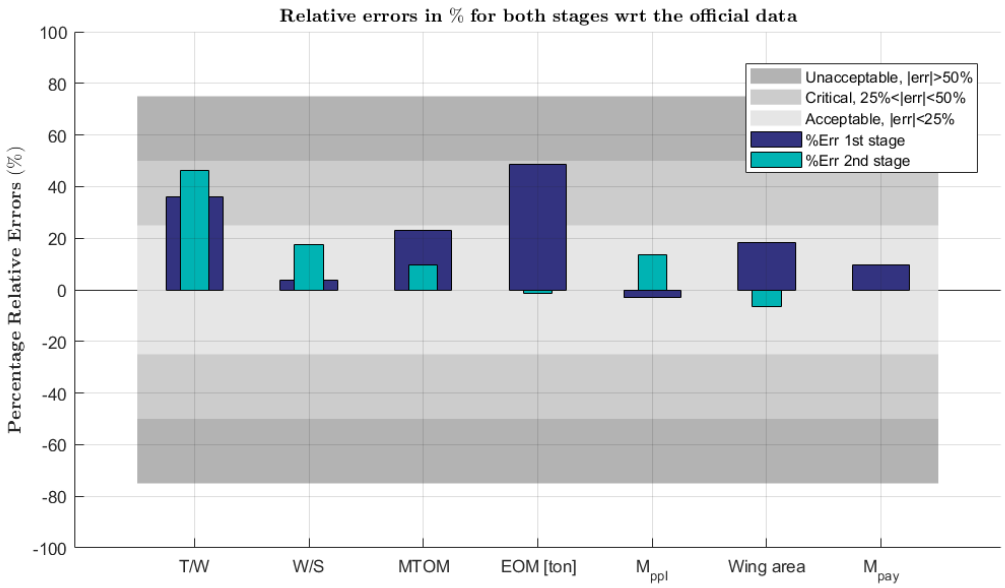

Figure 4.19: Relative errors in percentage for both stages.

Among the investigated variables, both τ and V_{tot} do not appear, since no reference value was found in literature to refer to for comparison. The following considerations arise:

- All the variables considered show deviations not exceeding the critical error band. In particular, if T/W is left apart, seen the already explained potential motivations of its overestimation, only the operative empty mass of stage 1 is affected by an $Err_{\%} > 25\%$. All the other magnitudes are confined within the acceptable error region, which is typically tolerated due to the unavoidable intrinsic errors occurring during preliminary design processes like the one illustrated in this work. All the exact values are collected in Table 4.7 and Table 4.8.

- The errors concerning stage 2 are more contained, as predicted also through spider charts. Moreover, the majority of figures resulted in an overestimation with respect to reference values.

- The payload mass of stage 2, being given as an input, is not affected by errors, since the difference between reference and design values is equal to zero.

In general, if all the approximations introduced and the uncertainty about reference data are considered, it is possible to certify a quite robust reliability of the methodology, which is even higher in case only one stage is sized.

Volume budget comments

The computation of volume required deserves a special treatment. In fact, the only instrument of judgment which can be used is physical sense, not being available reference

Name	m.u.	Reference Value	Design Value	Err %	Evaluation
$\frac{T}{W}$	-	0.450	0.611	35.77	CRIT
$\frac{W}{S}$	$\frac{\text{kg}}{\text{m}^2}$	386.40	401.14	3.81	ACC
MTOM	ton	340	418	22.94	ACC
M_{ppl}	ton	100	96	-4	ACC
M_{OE}	ton	149	221	48.32	CRIT
M_{pay}	ton	91	99	8.79	ACC
S_{pln}	m^2	880	1042	18.41	ACC
V	m^3	-	1883.2	-	-
τ	-	-	0.056	-	-

Table 4.7: Final values for stage 1.

Name	m.u.	Reference Value	Design Value	Err %	Evaluation
$\frac{T}{W}$	-	1.680	2.459	46.37	CRIT
$\frac{W}{S}$	$\frac{\text{kg}}{\text{m}^2}$	850.5	999.66	17.53	ACC
MTOM	ton	91	99.88	9.76	ACC
M_{ppl}	ton	65.5	74.37	13.54	ACC
M_{OE}	ton	22.2	21.93	-1.22	ACC
M_{pay}	ton	3.3	3.3	0	ACC
S_{pln}	m^2	108	99.92	-7.48	ACC
V	m^3	-	461.8	-	-
τ	-	-	0.462	-	-

Table 4.8: Final values for stage 2.

data to look at. According to Figure 4.15, the volumes of stage 1 and 2 are 1883.2 m^3 and 461.8 m^3 respectively. These data can be interpreted in terms of length, width and height per each stage, which are available data instead. In other words, the idea for assessing in broad terms the results is to turn the overall volume budget found into an equivalent cylinder: the entire vehicle is assumed to be formed only by the fuselage, with length and diameter equal to those provided by data sheet, and the portion considered in excess is used to account for the rest of the airframe (wing, tail...). In Table 4.9 a summary of the results obtained is reported, for either stage.

Stage	V computed $[m^3]$	Length [m]	Diameter [m]	Eq. diameter cyl. [m]
Stage 1	1883.2	84.50	14.00	5.33
Stage 2	461.8	27.60	5.50	4.61

Table 4.9: Sanger II volume budget data.

The cells indicating the diameter of the equivalent cylinder give an estimation of the real diameter to give the cylinder approximating the vehicle stages so as to guarantee the overall volume found is satisfied. They seem quite reasonable results, also by looking at the visual overlapping between drawing views of both stages and equivalent cylinders reported in proportion (Figure 4.20).

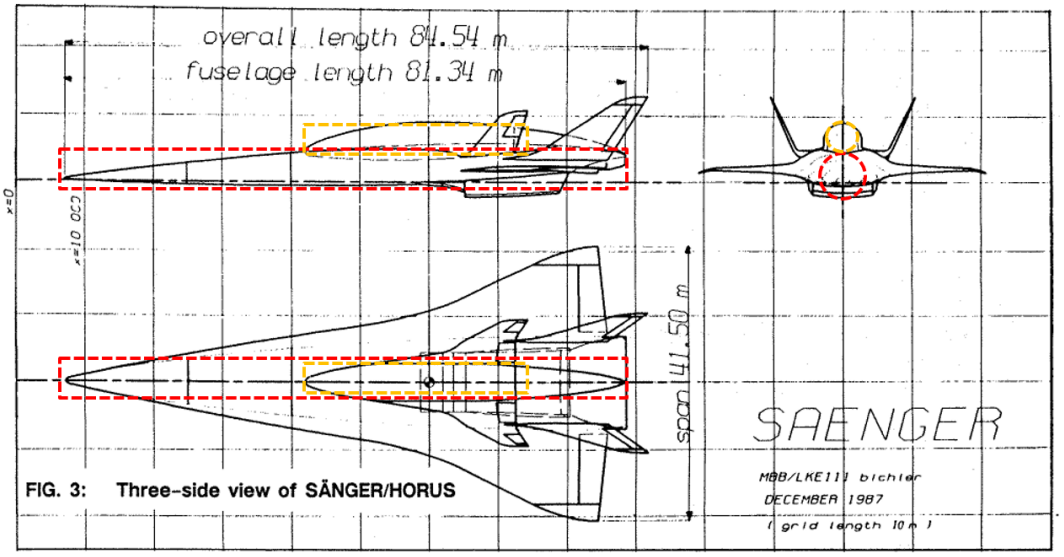

Figure 4.20: Equivalent volume overlapping for stage 1 and 2.

4.4 Comparison with a VLO launcher

Nowadays, multi-stage vertical lift-off (VLO) is the dominant solution for launchers due to multiple reasons, thus a comparison with an equivalent HTHL TSTO in terms of mass requested by keeping fixed the main mission requirements seemed an interesting study to carry out.
The method of Lagrangian Multiplier for sizing a TSTO VLO Launcher is employed here. As consequence of that, before enumerating the assumptions made and presenting the results, a brief theoretical background overview about this method is provided.

4.4.1 The Lagrangian Multiplier Method

The Method of Lagrangian Multiplier is considered an efficient tool to evaluate the mass breakdown of a vertical launcher at a very preliminary stage, provided that the necessary constraints coming from the knowledge of the mission requirements are defined. Therefore, the objective is, given a final orbit and a required payload mass to carry, computing the minimum $m_{G,LO}$ (Gross Mass at Lift Off) and its distribution among the different stages so as to make the mission technically feasible.
In order to understand the mathematical formulation, some quantities have to be introduced and defined, since they will be part of the method. In particular:

- $m_{0,i} \rightarrow$ It is the initial total mass of stage i, before propellant is consumed;
- $m_{f,i} \rightarrow$ It is the final mass of stage i, when the all propellant related to stage i is consumed, just before separation;

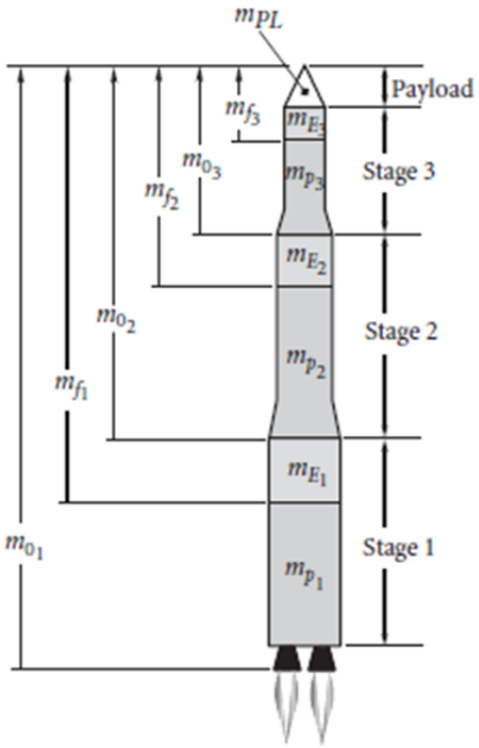

Figure 4.21: Division of VLO launcher in stages (example of 3 stages). p stands for propellant, E for structural.

- $\Lambda_i \rightarrow$ It is the mass ratio of stage i, defined as $\frac{m_{0,i}}{m_{0,i}-m_{ppl,i}}$. In this case there are no intermediate phases, as for a HTHL vehicle, but just 2 segments, each related to the corresponding stage;
- $\lambda_i \rightarrow$ It is the payload ratio of stage i, defined as $\frac{m_{pay,i}}{m_{0,i}}$. According to Figure 4.21, where it is evident that each stage payload is defined as the summation of all the upper stages, the same expression can be written also as $\lambda_i = \frac{m_{0,i+1}}{m_{0,i}}$, with $i = 1, 2$;
- $\phi_i \rightarrow$ It is the propellant ratio, defined as $\frac{m_{ppl,i}}{m_{0,i}}$;
- $\epsilon_i \rightarrow$ It is the structural efficiency, defined as $\frac{m_{OE,i}}{m_{OE,i}+m_{ppl,i}}$. The lower the structural efficiency, the better is the launcher design. In fact, it means that more propellant can be embarked if m_{OE} and m_{pay} are fixed.

The method aims at identifying two functions: an objective function, called f and a constraint function, called g. In the framework of this problem, f is represented by the computation of $m_{G,LO}/m_{pay}$ ratio, indicating the mass required at lift-off. On the other hand, g must contain the information associated to ΔV required for the mission to be accomplished. It is possible to demonstrate that, using the quantities previously

defined, the expressions for f and g are:

$$f = \sum_{i=1}^{N_{st}} ln \left[\frac{(1-\epsilon_i)\Lambda_i}{1-\epsilon_i\Lambda_i} \right] \tag{4.18}$$

$$g = \sum_{i=1}^{N_{st}} [g_0 I_{sp,i} \cdot ln(\Lambda_i)] - \Delta V_{req} \tag{4.19}$$

The optimized values for each quantity are obtained by defining the so-called augmented function f^* and minimizing it. It considers both the effects, through the introduction of the lagrangian multiplier, in this case a number p. The augmented function which has to be minimized through its derivative appears in the form $f + pg$, that is:

$$\sum_{i=1}^{N_{st}} ln \left[\frac{(1-\epsilon_i)\Lambda_i}{1-\epsilon_i\Lambda_i} \right] + p \left[\cdot \sum_{i=1}^{N_{st}} [g_0 I_{sp,i} \cdot ln(\Lambda_i)] - \Delta V_{req} \right] \tag{4.20}$$

Naturally, to solve the problem, some quantities have to be determined before running the code, beyond ΔV_{req}: the structural efficiencies ϵ_i, the number of stages N_{st}, the specific impulse for each stage $I_{sp,i}$ and the lagrangian multiplier p.
Typically, they are all given as inputs, apart from p. The procedure to determine it will not be explained in details, since it is out of the purpose of this work. A performance analysis can be carried out in order to get an initial guess of the value p, consisting of a similar procedure to the one described here, where the aim is to maximize the ΔV available though, given a certain value of payload ratio. Once p is correctly computed, the mass breakdown of the launcher is achieved. In fact, the mass ratio for each stage is:

$$\Lambda_i = \frac{1 + p \cdot g_0 I_{sp,i}}{p \cdot g_0 I_{sp,i} \cdot \epsilon_i} \tag{4.21}$$

Then, the payload ratio per each stage is obtained:

$$\lambda_i = \frac{1 - \Lambda_i \epsilon_i}{(1-\epsilon_i)\Lambda_i} \tag{4.22}$$

After this, the overall payload ratio is determined:

$$\lambda_{tot} = \prod_{i=1}^{N_{st}} \lambda_i \tag{4.23}$$

Finally, the $m_{G,LO}$ is obtained:

$$m_{G,LO} = \frac{m_{0,1}}{m_{pay}} \cdot m_{pay} = \frac{m_{pay}}{\lambda_{tot}}. \tag{4.24}$$

4.4.2 Assumptions

At this point, the mechanism behind the Lagrangian Multiplier Method should be clear, therefore all the assumptions introduced to perform the calculations are now gathered hereafter:

- the vertical launcher is made of two stages, as for Sänger II;
- the payload mass to inject to orbit is equal to 3300 kg, the same provided by Sänger II's official manual;
- the target orbit to achieve is 400 km high, the same used within the function for trajectory computation;
- ΔV losses are considered equal to 2 km/s, since they have to take into account gravity, drag and not adapted nozzle contributions starting from the beginning of lift-off [47];
- a value of $\epsilon_1 = \epsilon_2 = 0.1$ as structural coefficients for each stage is estimated, based on typical values for vertical launchers [47].
- by considering liquid rocket propellant, a specific impulse of 330 s is attributed to both stages.

All the assumptions reported are used to fill in the input fields for the methodology illustrated in the previous paragraph.

4.4.3 Mass breakdown results for a VLO launcher

In Figure 4.22, the results for a vertical lift-off launch vehicle are illustrated as a bar chart, in the same way the mass breakdown for Sanger II is shown in Figure 4.14. Two main considerations are worth being done, by comparing this result with the HTHL TSTO one.

- The overall mass required at lift-off, equal to 172.48 *tons*, is clearly inferior to 418.30 *tons* needed for Sänger II and obtained through the methodology. It represents a mass reduction of approximately 58% with respect to Sänger II, in agreement with what stated in chapter 1, concerning the double mass demand for HTHL vehicles with respect to equivalent-mission VLO launchers. As a matter of fact, this confirms one of the main reasons why vertical lift-off launchers have been preferred over horizontal take-off and landing in the last decades of space exploration.
- The values for ϕ_1 and ϕ_2 are both 0.775, since the two stages are assumed equal in proportions (this information is implicit in the definition of a unique value of structural efficiency for either stage). The amount of propellant is way greater in

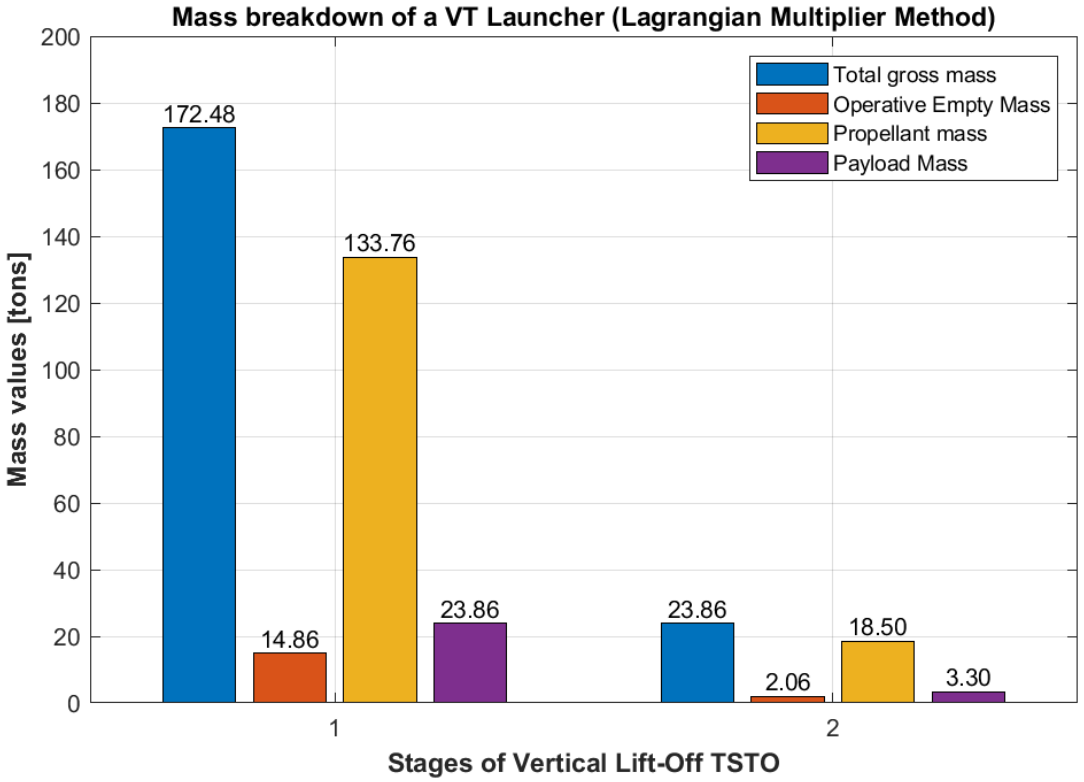

Figure 4.22: Mass breakdown for an equivalent-mission vertical lift-off launcher.

proportion to the overall mass at lift-off with respect to HTHL vehicles, which have a configuration more similar to aircraft. This result is not necessarily an advantage for vertical launchers, or an index of better range performances. As a matter of fact, HTHL airbreathing vehicles need less fuel to be carried on board, because the oxydizer is already available outside, being the air. On the other hand, VLO launchers have to carry both fuel and oxydizer on board, and this can lead to a more demanding propellant mass constraint to fulfill, in order to perform the same mission.

In conclusion, the vertical take-off configuration proves advantageous in terms of lift-off mass requirements, making it a more efficient option for launchers compared to horizontal take-off, if the only mass parameter is taken into account. Nevertheless, on the long run, a heavier reusable TSTO HTHL vehicle may generate more cost savings than a lighter expendable TSTO VLO one, inducing a change of perspective. Indeed, the economical driver is the protagonist of the next and last chapter.

Chapter 5

Cost assessment

5.1 Introduction

Since the access to space capability was gained through the employment of expendable launch vehicles (ELVs), the target of primary concern has become the reduction of the cost to orbit, promoting sustainability, reliability and reusability. To this purpose, worldwide government and private initiatives in the space sector enhanced competitiveness within the launch market [48], consisting of several actors working to foster technological advancement as well as cost savings. Systems reusability has been by far the most attractive means for achieving this goal.

Nevertheless, attaining costs reduction in space access cannot affect negatively in any way the required vehicle effectiveness. Hence, proper cost-effectiveness analyses should be carried out in the framework of conceptual design activities with the aim "to find designs that provide a better combination of the various dimensions of cost and effectiveness [49], implying the need of suitable methodologies for cost estimation and effectiveness assessment. The methodology which is employed in this chapter, the TransCost (TC) model, is based on equations called *Cost Estimation Relationships* (CERs), which express each cost item as a function of sizing and performance parameters (or cost drivers) available since early design stages.

Just for sake of clarity, the TransCost (TC) model can be defined as the most widespread reference in the space cost estimating scene. Progressively updated by D.E. Koelle since its first release in 1971, it is a "launch vehicle-dedicated system model" for the assessment of economic viability of future space transportation systems. It is based on a comprehensive database gathered between 1960 and 2012 and made up of US, European and Japanese space vehicle studies. Even if the most of data refers to expendable vehicles, TC allows for further improvements, it can be re-handled autonomously by the reader and updated with additional data to derive new CERs if required. In this sense, new relationships have been determined for first stages of airbreathing TSTO vehicles, which will be very useful in the next sections [2].

Sanger II concept emerged in the 80s an innovative and totally reusable TSTO vehicle, thus it perfectly fits in with the current rising interests in the space sector. As a matter of fact, after a brief description of the TC cost model relationships, it will be presented as a case study again, but this time for economical assessment.

5.2 The TC Model with upgraded CERs

The overall cost of a generic launch vehicle according to the TC model can be computed by adding three main contributions, divided per LCC stage:

- **Development Cost**, including design, analysis and test activities of breadboards, brass-boards, prototypes, qualification and proto-flight units;
- **Production cost**, consisting of flight units production cost;
- **Ground and Flight Operations Cost**, including the direct operative cost for fuel, crew, maintenance, insurance and other aspects.

The model is built on a macro-division of each contributing cost into a vehicle-related cost and an engine-related cost. However, ground and flight operations cost is the only one not following this rule, thus a whole system approach is used for cost determination. Since this methodology will be used for Sänger II cost assessment, every cost voice shall be calculated for either stage. In other words, the cost breakdown can be summarized as in Table 5.1.

N. stage / Cost	Development		Production		Ground & Operations
	Vehicle	Engine	Vehicle	Engine	
Stage 1: EHTV	$RDTE_{1v}$	$RDTE_{1e}$	TFU_{1v}	TFU_{1e}	$(DOC + RSC + IOC)_1$
Stage 2: Horus	$RDTE_{1v}$	$RDTE_{1e}$	TFU_{1v}	TFU_{1e}	$(DOC + RSC + IOC)_2$

Table 5.1: Cost Breakdown for either stage of Sanger II.

Before delving into the mathematical expressions describing cost trends for each category, it is paramount to stress the fact that several CERs used derive from a re-elaboration of TC methodology from Valeria Vercella work, *Cost-effective and sustainable scenarios for future reusable space transportation and re-entry systems* [2]. Indeed, this upgrade was necessary due to the peculiarity of the vehicle chosen as case study: a TSTO HTOL airbreathing first stage and a rocket-powered HL second stage, which make Sanger II neither a simple HTS (Hypersonic Transportation System) nor a vertical RLV (Reusable Launch Vehicle).
In the following paragraphs, some symbols will be used in cost estimation formulas: the complete explanation of their meaning and the values adopted are discussed in subsection 5.2.4.

5.2.1 Development cost

Development cost accounts for the initial stages of the commercialization of a space vehicle. In fact, also abbreviated through RDTE, standing for Research, Development, Test and Evaluation, it represents the first milestone into the cost assessment process. By referring to [2], the following formulation for a HTHL airbreathing first stage (no engine included), based on TC model has been derived:

$$RDTE_{1v} = 0.68 + 922.56 \cdot m_{v,dry}^{0.12} \cdot M^{1.39} \quad [WYr] \tag{5.1}$$

Its utilization is suggested since it considers both the effect of staging Mach and dry mass, and it shows the lowest sample standard error among all the interpolation possibilities. As far as the engine is concerned, the CER hereafter must be employed, due to the turbo-ramjet combined cycle propulsive architecture:

$$RDTE_{1e} = 364.47 \cdot m_{e,dry}^{0.48} \quad [WYr] \tag{5.2}$$

A different set of equations must be used for the second stage Horus, since it is categorized as a liquid rocket-propelled HL second stage. The results in terms of CERS derived show that using a power function, depending on staging Mach and dry mass as in the first stage is the most convenient choice to reduce the sample standard error. For the vehicle with no engines considered the relationship found is:

$$RDTE_{2v} = 32.82 \cdot m_{v,dry}^{0.68} \cdot M^{0.064} \quad [WYr] \tag{5.3}$$

To include the effect of the engine, the classical TC model formulation for liquid propellant rockets will be used, in spite of the aircraft configuration. This choice is due to the fact that Horus is far more similar to a rocket in functioning than to an aircraft. It is found:

$$RDTE_{2e} = 277 \cdot m_{e,dry}^{0.48} \cdot f_1 f_2 f_3 f_8 f_9 f_{10} f_{11} \quad [WYr] \tag{5.4}$$

All the coefficients appearing are described and collected in subsection 5.2.4.

5.2.2 Production cost

The production cost encompasses the cost for flight units manufacturing, thus it represents the successive step towards the commercialization of a new vehicle. By referring to [2], the following formulation for a HTHL airbreathing first stage (no engine included), based on TC model and appropriately adjusted, has been derived:

$$TFU_{1v} = 1.55 \cdot m_{v,dry}^{0.54} \cdot M^{0.67} \quad [WYr] \tag{5.5}$$

Its utilization is suggested since it considers both the effect of staging Mach and dry mass, and it shows the lowest sample standard error among all the interpolation possibilities. About the engine production cost for the first stage, no specific relations were available, thus it was opted for a weighted average between turbojet and ramjet engine production cost, taken singularly. The weight is altitude-based, meaning that the cost of either turbojet or ramjet production is multiplied by the respective fraction of vertical altitude to gain with respect to the overall altitude for separation. In formula:

$$TFU_{1e} = \frac{19.5}{31} \cdot 2.29 \cdot m_{e,dry}^{0.545} \cdot f_4 f_8 f'_{10} f'_{11} + \frac{31 - 19.5}{31} \cdot 5.63 \cdot T^{0.35} \cdot f_4 f_8 f'_{10} f'_{11} \quad [WYr] \tag{5.6}$$

As regards the second stage, powered by liquid propellant, another formula seems more adapt, where the effect of engines is still excluded:

$$TFU_{2v} = 0.212 \cdot m_{v,dry}^{0.978} \quad [WYr] \tag{5.7}$$

It is to be noticed that, due to the poor amount of data available, the dependency on Staging Mach as additional driver is not present in this case. The production cost for the second stage rocket engine can be computed as follows instead:

$$TFU_{2e} = 3.15 \cdot m_{e,dry}^{0.535} \cdot f_4 f_8 f'_{10} f'_{11} \quad [WYr] \tag{5.8}$$

All the coefficients appearing are described and collected in subsection 5.2.4.

5.2.3 Ground & Operations cost

Ground and Operations refer to a very great number of sub-activities and processes related to what comes between the end of manufacturing phase and the end of the vehicle's life. Therefore, cost associated to launch events, maintenance, insurance and transportation have to be taken into account, as better illustrated in Figure 5.1. To be more precise, the overall cost is given by the summation of three major contributions:

- Direct Operating Cost (DOC). It includes:
  - Ground Operations Cost, with assembly integration and checkout and launch preparation as main activities performed;
  - Materials and Propellant Cost, including the cost of fuel, oxidizer, gases and other consumables;
  - Flight and Mission Operations Cost, i.e., mission planning and preparation, launch and flight operations;
  - Transport & Recovery Cost, with the cost of transportation to launch site;
  - Fees and Insurance, encompassing launch site user fees per launch (for commercial launch providers), Public Damage Insurance, vehicle Loss Charge and

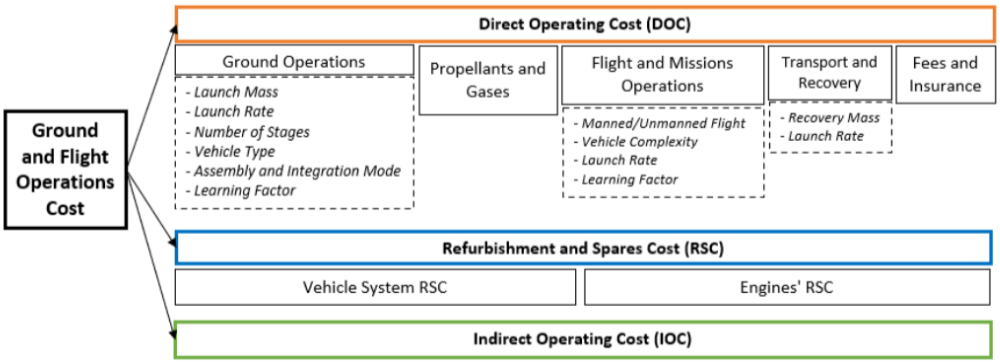

Figure 5.1: Overview of Ground & Operations cost.

Mission Abort Charge.

- Refurbishment and Spares Cost (RSC). It is mainly associated with maintenance interventions to ensure safety and reliability of operations and systems. It could be compared to aircraft "major overhaul" since it deals with all off-line activities (i.e., detailed vehicle system inspection, exchange of critical elements like TPS panels, replacement of rocket engine, etc.).

- Indirect Operating Cost (IOC). It includes all activities not strictly related to flight operations, such as program administration and system management, marketing, and contracts (labelled as Commercialization Cost) as well as launch site infrastructure Operations & Support [2].

Updated formulations for TSTO vehicles like for development and production cost are not available, thus only a rough estimation can be provided as regards this last contribution. Secondly, the high number of items composing the overall cost makes the computation of Ground & Operations cost extremely difficult to assess in a quite reliable way. In addition to that, Sänger II is a design concept, characterized by a very narrow range of figures and numbers available, especially under the economical perspective.
For all these reasons, Ground & Operations cost will not be assessed numerically, but a general breakdown is shown anyway. Furthermore, a division between stage 1 and stage 2 does not exist in this case, therefore DOC_1 and DOC_2 will not be computed separately, but as a unique term, called DOC. The same reasoning applies to IOC and RSC/Maintenance.

In Table 5.2 the formulas applied are gathered. Wherever "not considered" appears, it means a specific mathematical formulation for the assessment of that part of cost either was not found in literature or the available models weren't applicable to TSTO HTHL vehicles.
The computation of Ground & Operation cost would be a crucial value to assess in case the interest was delved into the operating life of Sänger II. Since it never appeared as

DOC	Symbol	Formula
Ground Operations	C_g	$8 \cdot MTOM^{0.67} L^{-0.9} N^{0.7} f_v f_c f_4 f_8 f'_{11}$
Propellant	C_p	$c_{s,ppl} \cdot m_{ppl} \cdot L$
Flight & Mission Ops.	C_{fm}	$20 \cdot \left(\sum_{i=1}^{N} Q_i\right) \cdot L^{-0.65} f_4 f_8$
Transport	C_t	not considered
Fees/Insurance	C_{fi}	not considered
RSC/Maintenance	**Symbol**	**Formula**
Vehicle System	C_{vs}	$f_{5,1} \cdot TFU_{1v} + f_{5,2} \cdot TFU_{2v}$
Maintenance Labour (TJ & RJ)	C_{ml}	eqs. (69) and (71) [2]
Maintenance Material (TJ & RJ)	C_{mm}	eqs. (70) and (72) [2]
IOC	**Symbol**	**Formula**
Commercialization	C_{co}	not considered

Table 5.2: DOC, RSC and IOC summary. The unit of measurement is WYr.

a concrete vehicle in reality, what really matters for this preliminary cost assessment is confined to only the first two stages of the Life Cycle Assessment, namely development and production. This is another justification of the approach used in this chapter, even though a detailed analysis could be carried out to obtain a quantitative estimation of operational cost.

5.2.4 Cost computation and comments

As previously stated, only $RDTE$ and TFU are computed numerically for Sanger II. Before delving into the mathematical results, it is essential to define all the variables and coefficients appearing in the equations of the previous paragraphs and attribute to them appropriate numerical values. A summary is provided in Table 5.3.
The following assumptions are made:

- Since the CERs illustrated require a high-level mass breakdown concerning vehicle and engine for each stage and no reliable data are available for Sanger II, the proportions suggested in [2] for Stratofly TSTO are taken as reference. Thus:
  1. Engine of stage 1 $\rightarrow 20\% \cdot m_{OE,1} = 20\% \cdot 149 = 29.8\ ton$;
  2. Engine of stage 2: $\rightarrow 20\% \cdot m_{OE,2} = 20\% \cdot 22.2 = 4.44\ ton$;
- In this chapter, it is assumed that $m_{OE} \approx m_{dry}$.
- All the coefficients not affecting either $RDTE$ or TFU cost are not given a numerical estimation, thus they appear in the table as "not necessary".

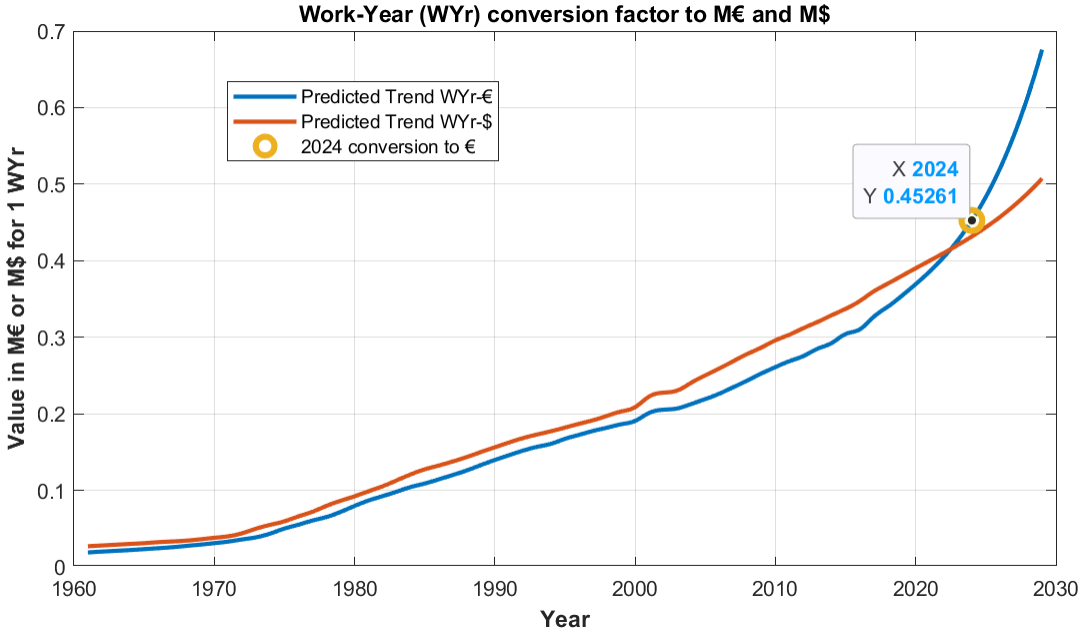

Figure 5.2: Conversion 1 WYr to M€ and to M$ trend.

- The geographical region of development and production is Europe, since Sänger II is a German project, thus the value for f_8 is picked accordingly.
- All the other values are chosen in conformity to Stratofly TSTO project data, provided in [2], due to the similar overall architecture between the two vehicles.
- The computation of both $RDTE$ and TFU is first expressed in WYr (Work-Year) and then converted into €. For sake of clarity, TC provides WYr Conversion Factors between 1961 to 2016, remaining values up to 2024 are estimated by interpolation (see Figure 5.2).
- The final values refer to the summation of development and production cost for one single prototype. The economical impact analysis based on a scale production and commercialization of Sänger II is out of the aim of this work. The only purpose is to assess the project cost, from the conceptual design phase to the complete construction of a prototype, in order to establish a comparison with other notorious vehicle systems used to reach LEO orbit.

The final result in terms of WYr and € required to both development and production of a unit is gathered in Table 5.4. It is compared with the estimations provided by old online articles concerning the project cost of Sanger II [51], which, dating back to 1985, have been appropriately adjusted to the actual money value and inflation.
It seems clear that the procedure applied demonstrates quite good concordance with real estimations: the deviation from CERs to real values expressed as relative error in percentage is equal to 11.45%, falling into an acceptable range of uncertainty.

Variable	m.u.	Explanation	Value
$m_{v,dry}$	kg	Dry mass of vehicle (no engines)	St.1: 119200 kg St.2: 17760 kg
$m_{e,dry}$	kg	Dry mass of engines	St.1: 29800 kg St.2: 4440 kg
T	kN	Thrust provided by ramjet	1250
f_1	-	Development standard factor	0.8
f_2	-	Technical quality factor	1.436
f_3	-	Team experience factor	0.9
f_4	-	Learning Curve factor	0.7
f_5	-	Refurbishment factor	Not necessary
f_8	-	Productivity of region	0.86 [50]
f_9	-	Impact of subcontractor	0.86
f_{10}	-	Reduction factor due to experience	0.75
f_{11}	-	Reduction factor for absence of gov. contracts	0.45
f'_{10}	-	Production cost improvements factor	0.7
f'_{11}	-	Government contracts factor for production	0.5
L	$year^{-1}$	Launch per Annum	Not necessary
N	-	Number of stages	Not necessary
f_v	-	Impact of launch vehicle type	Not necessary
f_c	-	Impact of assembly and integration mode	Not necessary
Q_i	-	Flight Operation coefficient of stage i	Not necessary
$c_{s,ppl}$	$\$/kg$	Propellant cost per unit of mass	Not necessary

Table 5.3: Cost coefficients summary.

Finally, a vehicle-based comparison among similar launch systems to reach space orbits can be made to provide a very brief overview of the feasibility of the project. In Figure 5.3 a bar chart illustrates the overall $RDTE + TFU$ cost for 4 different types of vehicles: Sanger II, Stratofly TSTO, SuperHeavy/Starship X and Ariane V. They are characterized by different properties:

- Sanger II $\implies$ HTHL TSTO, totally reusable, only for LEO orbit and High Speed Transportation;
- Stratofly TSTO $\implies$ HTHL TSTO, totally reusable, only for LEO orbit and High Speed Transportation;
- SuperHeavy/Starship X $\implies$ VTVL first stage and HL second stage, totally

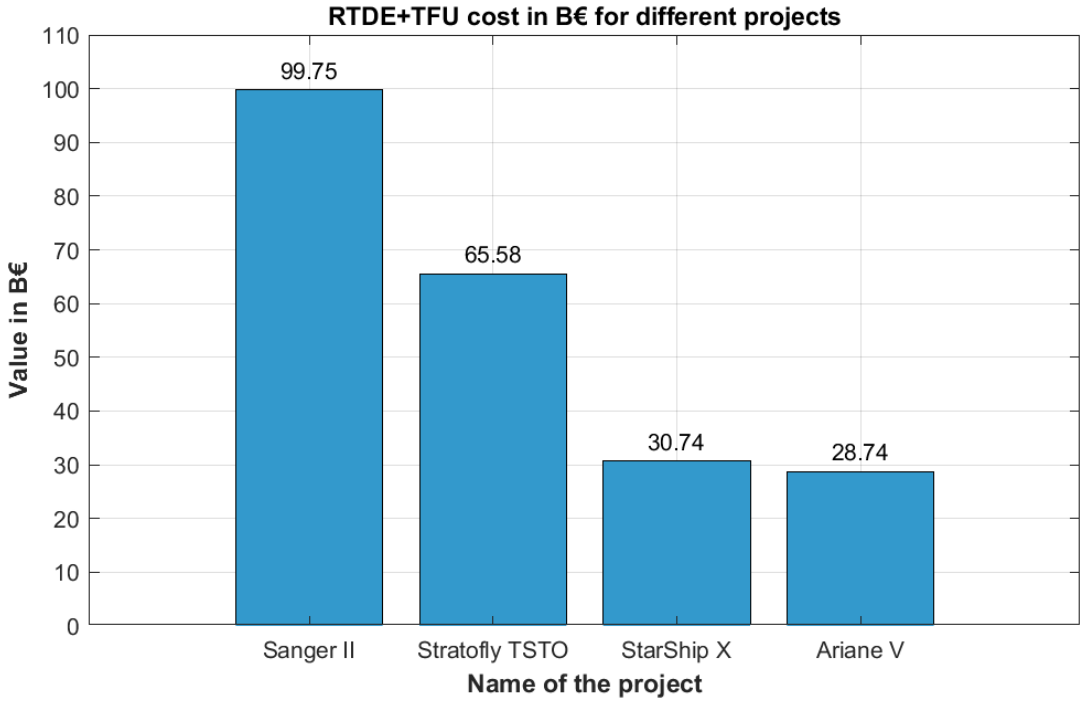

Figure 5.3: $RTDE + TFU$ cost for different space access projects in billion euros ([2], [51], [52].)

reusable, also for planetary missions;

- Ariane V $\implies$ VT TSTO, expendable, for LEO orbit.

The analysis is limited to development and production cost for a single unit. All the cost computed are referred to 2024. As expected, vertical take off and landing configurations are characterized by the lower cost, as illustrated in Figure 5.3. This certifies the consistent effort to make at preliminary stages to impose such a HTHL TSTO disruptive design for space access.
Even though Starship claims to be a totally reusable launch system, only 12 reuses for each second stage vehicle are foreseen before replacement, thus it can be considered as a partially reusable system if compared to horizontal take off and landing configurations [2]. Therefore, on the long period, operative life reveals to be crucial for the sustainability of the projects, since over time cost savings concerning HTHL configurations could overweigh VTVL. Nevertheless, lots of other factors should be taken into account, from ease of maintenance to governmental acceptance, to the technology maturity level required to achieve specific performances and safety standards.

5.3 Further work

The results presented in this Master Thesis provided valuable insights concerning design aspects of hypersonic HTHL TSTO vehicles. Nevertheless, they also highlighted

Data	Value in WYr	Value in $ or €
Total Cost (from CERs) in 2024 (EUR)	220390	99.75 B€
Total Cost (Ref. article) in 1985 (USD)	Not available	28.00 B$
Total Cost (Ref. article) ref. to 2024 (USD)	Not available	94.87 B$
Total Cost (Ref. article) ref. to 2024 (EUR)	Not available	89.50 B€
Relative error in %	-	+11.45 %

Table 5.4: $RDTE$ and TFU cost results for Sänger II.

opportunities for further exploration. Future work will aim to expand and refine on these findings, by addressing the limitations encountered, exploring new scenarios and applying the methodology to broader or more complex contexts. As a matter of fact, the application of this methodology to other case studies can be done, so as to verify its compliance with further examples of TSTO HTHL vehicles.
Moreover, the methodology itself may be deeply investigated with the aim of increasing the accuracy of models used (e.g. the aerodynamic or the propulsive strategies model) by acting on the dedicated functions. Secondly, it could be possible and presumably more efficient to embed the MMCs tool inside the iterative convergence loop instead of using it in series, after all the potential design point are determined. More customization of the tool is another aspect to focus on, for instance by extending the methodology to a whichever desired number of stages as input or by giving the chance to select different numbers of τ samples for different stages, for a more selective refinement of the design procedure.
Finally, coding the entire methodology into *Python* would be advantageous, due to the fact it is the official programming language used by ESA (European Space Agency) experts within the framework of this project.
By pursuing these paths, subsequent research can contribute to a more comprehensive understanding of the matter and potentially uncover new perspectives that are beyond the scope of the present study.

Bibliography

[1] D'ambrosio D., "Aerotermodinamica Ipersonica". In: *University lectures*. 2024.

[2] Vercella V., "Cost-effective and sustainable scenarios for future reusable space transportation and re-entry systems". PhD thesis. Politecnico di Torino, 2023.

[3] Bartolotta P., *Horizontal Launch: A Versatile Concept for Assured Space Access*. Tech. rep. 2011.

[4] Czysz P., *Future Spacecraft Propulsion Systems and Integration*. Springer, 2018.

[5] Penn J. P., "SSTO vs TSTO design considerations: an assessment of the overall performance, design considerations, technologies, costs, and sensitivities of SSTO and TSTO designs using modern technologies". In: *Space technology and Applications International forum: 1st Conference on commercial development of space.* (1996).

[6] Koelle D. E., "Economics of small fully reusable launch systems (SSTO vs. TSTO)". In: *Acta Astronautica* (1997).

[7] Clark C., "The History and Promise of Combined Cycle Engines for Access to Space Applications". In: *NASA Dryden Flight Research Center* (2010).

[8] B52 aircraft overview. Website: www.boeing.com/defense/b-52overview.

[9] Donald D., *The Encyclopedia of World Aircraft*. Prospero Books, 1997.

[10] "Boeing B-52 Stratofortress Airplane Videos and Airplane Pictures". In: (2022).

[11] X15 aircraft overview. Website: www.nasa.gov/reference/x-15/hds-sidebar-nav-1.

[12] Dorr R. F., *Stratofortress...The Big One from Boeing*. Air Enthusiast.

[13] Pegasus rocket overview. Website: www.northropgrumman.com/space/pegasus-rocket.

[14] Pegasus rocket overview. Website: www.nasa.gov/image-article/pegasus-rocket-booster-close-up.

[15] Pegasus rocket overview. Website: www.nasa.gov/reference/x-43a/.

[16] Collins. 1990.

[17] "Saenger II". In: *Encyclopedia Astronautica* (2002).

[18] Koelle E., "Sanger II, a hypersonic Flight and Space Transportation System". In: *ICAS-88-1.5.1.* (1988).

[19] Sanger II overview. Website: www.secretprojects.co.uk/aerospaceplane-project.

[20] White Knight I overview. Website: scaled.com/portfolio/white-knight/.

[21] SpaceShipOne overview. Website: airandspace.si.edu/collection-objects/spaceshipone.

[22] White Knight I flight tests overview.
Website: web.archive.org/web/20100822194232/http://www.scaled.com/projects/tierone/combined_white_knight_spaceshipone_flight_tests.

[23] White Knight II overview. Website: www.aerospace-technology.com/projects/virgin-spaceship/.

[24] SpaceShipTwo overview.
Website: web.archive.org/web/20130816140953/http://www.scaled.com/projects/test_logs/35/model_339_spaceshiptwo.

[25] SpaceShipTwo overview. Website: www.bbc.com/news/science-environment-47336617.

[26] Press Release, "Generation Orbit Partners With Space Propulsion Group". In: *Citizens In Space* (2012).

[27] Messier D., "Generation Orbit, SPG Team Up for Smallsat Launcher at Parabolic Arc". In: (2012).

[28] ARCA Space, "IAR-111 Supersonic Aircraft".

[29] ARCA Space, "Venator Rocket Engine".

[30] The second stage of Haas 2C rocket. Website: www.googlelunarxprize.org/teams/arca/blog/second-stage-haas-2c-rocket-0.

[31] "Cabin of the first Romanian supersonic IAR-111, successfully tested in flight. Preparing for space tourism?" In: *Adevarul* (2012).

[32] Scott W.B., "Two-Stage-to-Orbit 'Blackstar' System Shelved at Groom Lake?" In: *Aviation Week Space Technology* (2021).

[33] Chudoba B., *Solution-Space Screening of a Hypersonic Endurance Demonstrator.* Tech. rep. 2012.

[34] Torenbeek E., *Advanced Aircraft Design, Appendix A: Volumes Surface and Wetted Areas.* Wiley and Sons, 2013.

[35] Roskam J., *Airplane Design Part III.* DARcorporation, 1985.

[36] Cau R., "Characterisation and Simulation of Reusable Single-Stage-To-Orbit Vehicles Ascent Phase during Conceptual Design". MA thesis. Politecnico di Torino, 2024.

[37] Sziroczak D., *A review of design issues specific to hypersonic flight vehicles*. Tech. rep. Cranfield University, United Kingdom, 2016.

[38] Ramjet/Scramjet Thrust.
Website: www.grc.nasa.gov/WWW/k-12/airplane/ramth.html.

[39] Boretti A., *Hydrogen hypersonic combined cycle propulsion: advancements, challenges and applications*. Tech. rep. Melbourne Institute of Technology, Australia, 2024.

[40] Nicolai L.M., *Fundamentals of Aircraft and Airship Design*. American Institute of Aeronautics and Astronautics, 2010.

[41] Viola N. Ferretto D. Fusaro R., *Innovative Multiple Matching Charts approach to support the conceptual design of hypersonic vehicles*. Tech. rep. Politecnico di Torino, Italy, 2024.

[42] Fusaro R., *Innovative Multiple Matching Charts approach to support the conceptual design of hypersonic vehicles (Original Article)*. Tech. rep. Politecnico di Torino, 2020.

[43] Raymer D., "Aircraft Design: A Conceptual Approach, Sixth Edition". In: American Institution of Aeronautics and Astronautics, 2018. Chap. V: Thrust-to-Weight Ratio and Wing Loading.

[44] Gili P., "Fondamenti di Meccanica del Volo". In: *University lectures*. 2022.

[45] Molinari T., "Conceptual design methodology and tool for reusable single-stage-to-orbit vehicles with horizontal take-off and landing". MA thesis. Politecnico di Torino, 2024.

[46] Tjonneland E., "Short Course on Engine-Airframe Integration". In: *Survey of Integration Problems, Methods of Solutions, and Applications*. 1988.

[47] Di Sotto E., "Launchers and Reentry". In: *University lectures*. 2023.

[48] Heald D.A., "31st AIAA/ASME/SAE/ASEE Joint Propulsion Conference and Exhibit". In: *Should Commercial Launch Vehicles Be Reusable?* 1995.

[49] Hammond W., "Space Transportation: A Systems Approach to Analysis and Design." In: *Space Transportation: A Systems Approach to Analysis and Design* (1999).

[50] Koelle D.E., *Handbook of cost engineering and design of space transportation systems*. TRANSCOST Systems, 2013.

[51] "Saenger II". In: *Encyclopedia Astronautica* (2002).

[52] Wade M., "Ariane V". In: *www.astronautix.com* (2019).